On the Equilibrium Diagram of Ternary Alloy System of Iron, Manganese and Carbon

On the Equilibrium Diagram of Ternary Alloy System of Iron, Manganese and Carbon*

Mitsutake ISOBE

The Research Institute for Iron, Steel and Other Metals

(Received July 23, 1951)

Synopsis

The diagram of the ternary alloy system of iron, manganese and carbon was determined by thermal analysis, thermal dilatation, magnetic analysis, microscopic examination and X-ray analysis, with alloying materials of electrolytic iron, distilled manganese and sugar charcoal.

As for primary crystal surfaces, there were the following seven kinds of primary crystal surfaces: (1) δ iron ternary solid solution: ternary solid solution of δ iron in which a small amount of manganese and carbon are dissolved, (2) γ iron ternary solid solution: ternary solid solution of γ iron in which manganese and carbon are dissolved, (3) C ternary solid solution: ternary solid solution of carbide $(Fe, Mn)_3C$ consisting of Fe_3C which contains manganese, (4) δ manganese ternary solid solution: ternary solid solution of δ manganese in which a small amount of iron and carbon are dissolved, (5) γ manganese ternary solid solution: ternary solid solution of γ manganese in which iron and carbon are dissolved, (6) βC ternary solid solution, in which iron is dissolved in βC solid solution of manganese and carbon binary alloy, (7) αC ternary solid solution, in which iron is dissolved in αC binary solid solution of manganese and carbon. Intersecting one another, these surfaces gave six kinds of peritectic lines, four kinds of eutectic lines, two peritecto-eutectic points and one ternary eutectic point.

In the solid state, three kinds of peritecto-eutectoid reactions and four kinds of eutectoid reactions were observed. Moreover, fifteen eutectoid lines, three peritectoid lines, three peritecto-eutectoid points, four ternary eutectoid points and forty six solubility surfaces were confirmed.

The cause of the weathering of iron alloys of high manganese and high carbon was plainly understood from the complete diagram of the system. In other words, it was shown that the weathering could be attributed to the disintegration of αC solid solution or of γC solid solution or of both owing to the moisture in atmosphere, and accordingly some appropriate means to prevent the alloy from being weathered could be devised.

I. Introduction

A number of studies of the iron-manganese-carbon ternary alloy system has been reported, but the most of them gave no satisfactory diagram owing to the deficiency in basic study. In 1935, R. Vogel and W. Doring[1] reported a part of the ternary diagram, but it cannot be said to be a satisfactory one, because it did not extend to the points on the diagram of iron-manganese and manganese-carbon binary alloys.

The present writer studied manganese and its alloys for several years and the diagrams of the binary alloys which are the foundation of the ternary system were

* The 650th report of the Research Institute for Iron, Steel and Other Metals.

(1) R. Vogel and W. Doring, Archiv. Eisenhüttenw., 9 (1935), 247.

already determined all based on the author's own investigations.(2)(3)(4)(5) Hence, in this paper, the ternary diagram will be reported.

II. Preparation of specimens

Electrolytic iron, distilled manganese and sugar charcoal were always used as alloying materials, the chemical analyses of which are shown in Table 1.

Table 1. Chemical analysis of component metals.

Electrolytic iron

Fe %	C %	Mn %	Si %	P %	S %	Al %	Zn %	Sn %
99.88	0.03	0.01	0.02	0.04	0.00	0.02	none	none

Distilled manganese

Mn %	C %	Al %	Fe %	Si %
99.9	0.01	0.029	0.045	trace

Samples of desired compositions were made with mother alloys, for example, with iron and iron alloys, each containing 20, 40, 60, 80 and 90 per cent of manganese, and these iron alloys containing a suitable amount of carbon. As the contents both of manganese and carbon changed during melting because of distillation or of other influences, the compositions of all the alloys were chemically checked.

Fig. 1 is the plot of the compositions of the alloys prepared in the present work.

Thermal analysis was carried out in vacuum, and the samples for thermal dilatation, heat treatment and others were melted in hydrogen atmosphere with the use of magnesia crucible,

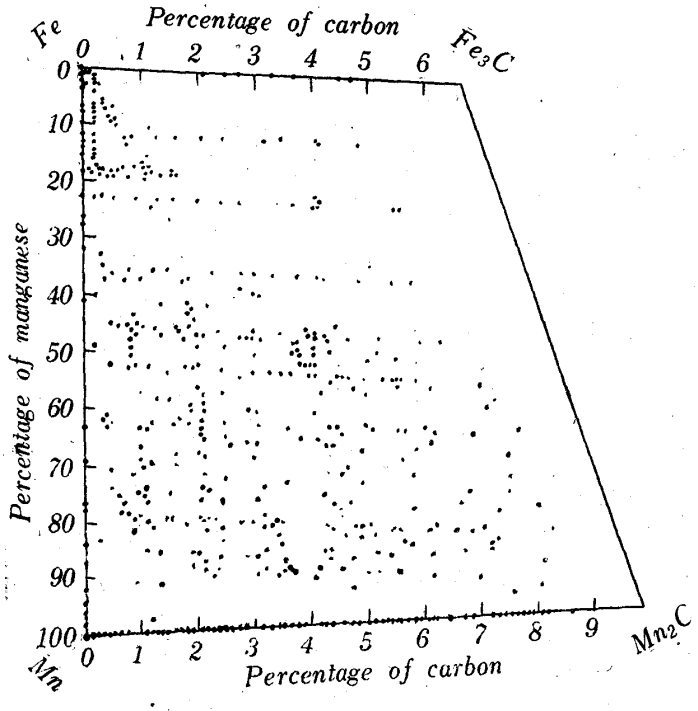

Fig. 1. Plot of compositions of alloys studied.

(2) H. Endo and M. Isobe, Kinzoku no Kenkyu, 4 (1927), 150.
(3) M. Isobe, Sci. Rep., RITU, 3 (1951), 78.
(4) M. Isobe, Sci. Rep., RITU, 3 (1951), 151.
(5) M. Isobe, Sci. Rep., RITU, 3 (1951), 468.

and some samples were made by furnace-cooling or by sand casting, and those containing a small amount of manganese and carbon were forged after cooled in furnace or in air.

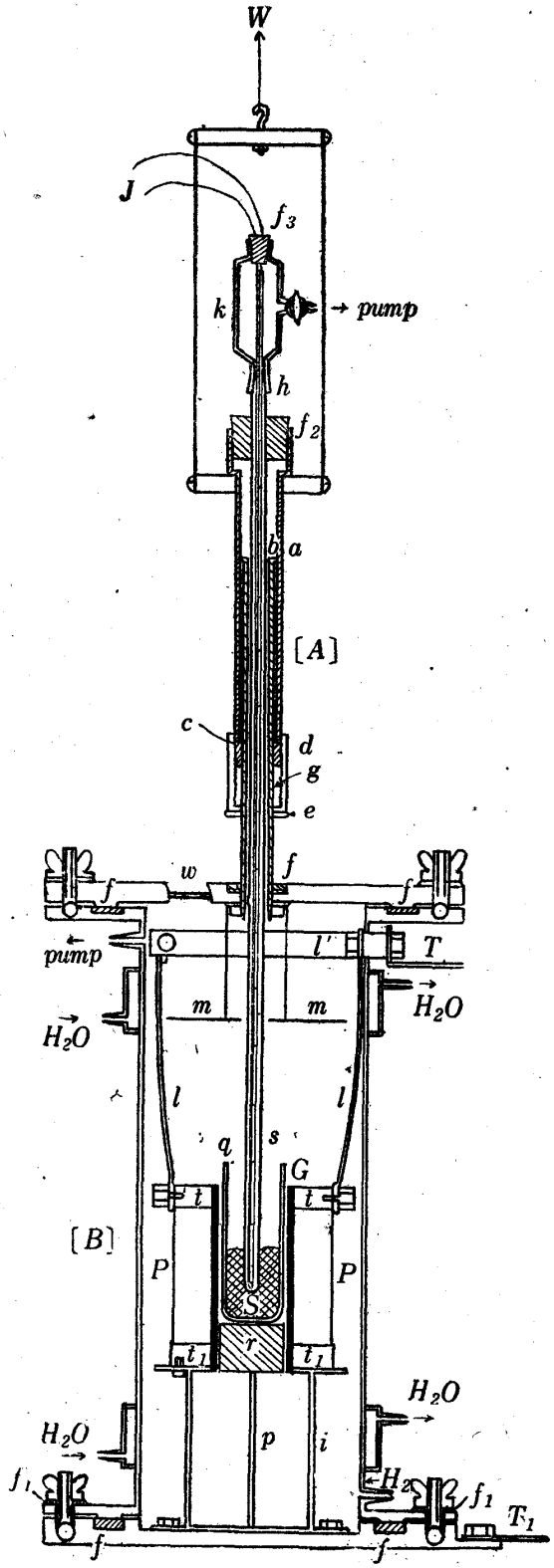

Fig. 2. Apparatus for in vacuum thermal analysis.

III. Thermal analysis

Thermal analysis was carried out by the vacuum furnace of Tammann's type with special apparatus devised by Dr. T. Ishiwara. A pot, 25 mm in inside diameter, 33 mm in outside diameter, 125 mm in depth, 131 mm in height, made of well-burned magnesia, was used for melting the samples.

Fig. 2 shows the vacuum furnace and the apparatus for thermal analysis, a brief explanation of which is given below.

The lower half [B] of the figure is the melting furnace, outer wall of which is made of an iron cylinder, about 200 mm in diameter and 800 mm in height, and can be evacuated or filled with dry hydrogen gas. f is the packing made of fibre, rubber, etc., and f_1 the fibre isolator which will be used in the case of combining the cylinder with the lid of bottom. The furnace is placed in the center of the cylinder. To prevent these fibres from being over-heated, water jackets were set on the cylinder at the positions near both ends.

$TltGt_1iT_1$ is the circuit of electric current. T is a brass terminal and l' is a semi-circular copper plate curved along the inside wall of the cylinder and leads the terminal to the opposite side of the cylinder. l is a pile of thin copper plates. tGt_1 is a furnace almost the same as ordinary Tammann's type, t and t_1 being iron checks, and G being the tube furnace made of graphite or of carborundum. A special screw device with a conical top, though not shown in the figure, is fixed to adjust the contact

between G and t, and accordingly even a thin furnace may by used. i is an iron stock, the height of which is adjustable. The specimen S is put in the crucible q which is placed on the fire-proof block r supported by the porcelain rod p. p is a porcelain tube, which protects the heating element G from heat loss. Granular fire-proof stuff is, generally, packed between G and P for thermal protection, but nothing was used in the present experiment. w is a glass window fixed to the lid, and m is a mica plate suspended in the middle space so that the lid may not be exposed directly to the furnace heat. In case the lid is too much heated, the upper water jacket may also be used.

The upper half [A] of the figure is the apparatus supporting silica protection tube s in which a thermojunction J is put, with a device of moving the tube easily up and down. [A] consists of double brass pipes, a and b. The inner pipe b is fixed to the lid by means of packing screws which connect [B] with the lower part [A]. Two pipes a and b are rubbed on and fitted to each other at c, where there is a device for moving the outer tube a up and down about 200 mm. The device d together with c makes the inner part more air-tight; the lower end of d, contacts with the inner tube b, while its upper part is fixed to the outer tube a by a screw and consequently a pocket g is formed between b and d. In this pocket vacuum grease is filled and the screwing of d makes grease fill up the connecting parts through a, b and d, and thus the apparatus becomes well air-tight. e is a flat nut on the tube b for setting the tube a in any desired position. f_2 is a rubber stopper by which the protection tube of thermojunction is fixed to a and thus the thermojunction is kept in an appropriate place by vertical motion of a. k is a glass tube which is rubbed on the silica tube at h, and the thermojunction is sealed at the rubber stopper f_3. Connecting k with pump, vacuum can be obtained in the silica protection tube independently of the furnace.

The upper part of a can be kept at desired position by a counter weight W, and thus the protection tube in which thermojunction is inserted can be moved up and down lightly and promptly. This device can also be used for stirring alloy during melting.

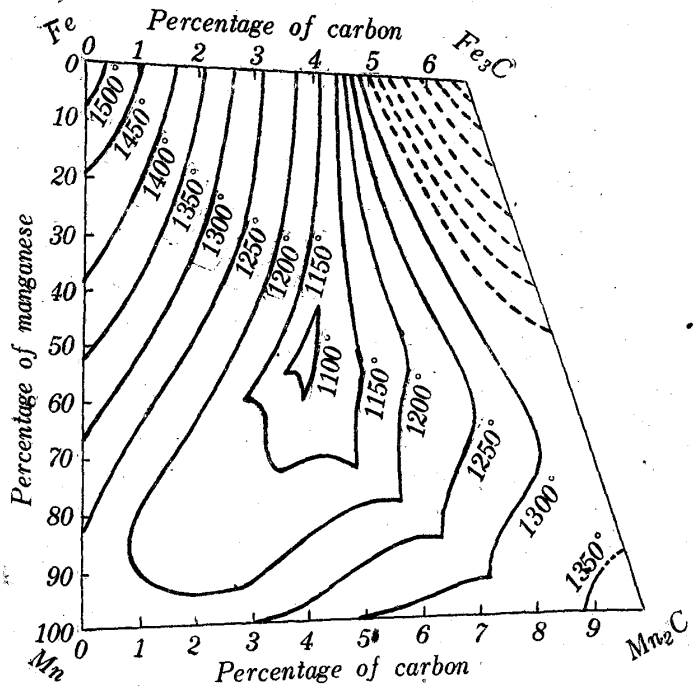

Fig. 3. Isothermal lines on the primary surface of iron-manganese-carbon ternary diagram.

Table 2. Transition points obtained by cooling curves of iron, manganese and carbon ternary alloys.

Specimen number	Chemical composition		Transition point, °C						
	Mn %	C %							
15050	11.50	0.05	1502						
15100	11.70	1.00	1421						
15150	11.55	1.41	1390						
15200	12.00	1.75	1356						
15250	11.85	2.16	1378,	1115					
15300	11.70	2.51	1302,	1125					
15350	11.51	2.85	1272,	1127					
15400	11.50	3.20	1245,	1133					
15450	11.52	3.81	1187,	1134					
15500	11.45	3.95	1171,	1135					
15550	11.40	4.50	1167,	1132					
30050	21.75	0.35	1431						
30100	22.80	0.76	1401						
30150	22.01	1.90	1366						
30200	22.50	1.80	1382						
30250	22.00	2.27	1307,	1100					
30300	22.97	2.65	1270,	1111					
30350	22.87	3.26	1221,	1129					
30400	22.95	3.51	1197,	1130					
30450	22.10	3.90	1145,	1130					
30500	22.10	4.45	1145,	1130					
30550	22.41	5.40	1256,	1130					
40050	35.00	0.60	1380						
40100	34.95	1.02	1355						
40150	34.80	1.57	1321						
40200	35.25	2.11	1286						
40250	35.05	2.77	1239,	1098					
40300	35.10	3.16	1211,	1103					
40350	35.17	3.62	1170,	1105					
40400	35.20	4.07	1120,	1105					
40450	35.25	4.63	1153,	1105					
40500	34.87	5.28	1263,	1104					
40550	35.45	5.62	1284,	1103					
50050	45.25	0.40	1356						
50100	45.50	0.70	1337						
50150	44.80	1.45	1304						
50200	45.05	2.20	1253						
50250	45.10	2.81	1211,	1088					
50300	45.07	3.31	1172,	1095					
50350	45.20	3.85	1116,	1095					
50400	45.05	4.52	1127,	1096					
50450	45.10	5.01	1163,	1095					
50500	44.75	5.75	1212,	1090					
50550	45.17	6.11	1289,	1090					
60050	52.52	0.45	1326						
60100	52.05	1.15	1290						

(continued 1)

Specimen number	Chemical composition		Transition point, °C						
	Mn %	C %							
60150	52.00	1.80	1251						
60200	52.32	2.47	1208						
60250	52.43	3.01	1169						
60300	51.95	3.31	1144						
60350	51.74	3.49	1123						
60400	52.05	4.01	1101						
60420	52.41	4.11	1107						
60450	52.35	4.42	1123						
60470	52.01	4.93	1153						
60500	52.05	5.10	1113						
60520	52.50	5.45	1184						
60550	52.57	5.77	1203						
60570	51.85	5.95	1217						
60600	52.54	6.32	1231						
50051	46.41	0.92	1312,		780				
55050	52.10	0.93	1301,		860				
60051	56.67	1.02	1283,	1113,	880				
65050	62.02	1.11	1264,		895,	855			
70050	62.50	1.01	1250,		920,	850			
75050	68.53	1.18	1239,	1200,	930,	850			
80050	72.97	1.12	1226,		940,	850			
85050	79.32	1.14	1201,		925,	853			
90050	84.66	1.36	1215,		910,	852,		790	
95050	89.87	0.92	1223,		890,	853,		700	
97050	90.33	1.34	1214,		870,	850,		740	
50101	46.61	1.42	1285,	1130,	1020,		765,	720	
55100	52.95	1.52	1270,	1130,			800,	715	
60101	57.43	1.53	1254,	1125,		850,		726	
65100	61.58	1.57	1225,	1160,		860,		730	
70100	66.61	1.65	1211,	1165,	905	855,		725	
75100	68.22	1.65	1205,	1165,	1085,	890,	850,	733	
80100	75.79	1.78	1200,	1165,		895,	855,	780	
85100	78.99	1.87	1180,			895,	855,	780	
90100	84.11	1.92	1182,				855,	785	
95100	87.16	1.93	1186,				850,	800	
50151	48.45	2.01	1255,	1090,					727
55150	51.95	1.94	1241,	1110,	1090,				727
60151	58.30	1.88	1213,	1150,	1103,			810,	725
65150	62.20	2.03	1207,	1165,	1125,				730
70150	65.83	2.05	1202,	1155,	1135,			810,	725
75150	70.52	2.07	1203,	1148,		952,	855,		730
80150	73.25	2.26	1194,	1140,			860,	760	
85150	82.47	2.21	1183,	1166,		975,	915,	810	
90150	84.75	2.40	1192,	1172,		968,	930,	810,	780
95150	87.30	2.38	1184,			990,	950,		800
50201	46.24	2.08	1246,	1092,	1070,				690
55200	55.32	2.45	1203,	1035,	1070,				710
60201	57.88	2.09	1210,	1150,	1105,				713
65200	63.36	2.54	1174,	1150,	1093,				715
70200	64.66	2.58	1170,	1135,	1090,				730
75200	70.65	2.56	1169,		1100,	1013,	875,		717

(continued 2)

Specimen number	Chemical composition Mn %	C %	Transition point, ℃						
80200	75.07	2.46	1174,		1130,		860,	760	
85200	79.43	2.49	1167,		1155,	994,	860,	775	
90200	83.72	2.87	1175,		1160,	1000,	860,	775	
94200	87.41	2.80	1191,		1080,	990,	945,	805,	780
50251	49.08	3.02	1189,		1090,				700
55250	52.77	2.82	1182,		1089,				702
60251	58.49	2.90	1163,	1105,					710
65250	64.12	2.88	1155,	1100,					740
70250	66.33	2.96	1155,	1100,					705
75250	71.29	3.17	1164,	1100			920,		715
80250	74.66	3.10	1168,	1120	1015,		923,	775	
85250	78.79	3.16	1168,	1132	1020,		920,	780	
90250	84.25	3.06	1181,	1170	1105,	1020,	880,	785	
93250	87.26	3.15	1195,	1160			874,	800	
45300	38.56	3.80	1135,	1100					
50301	48.29	3.72	1113,	1095					
55300	52.20	3.66	1120,	1105,	1090				
60301	58.63	3.06	1138,	1110,	1090,				700
65300	63.99	3.05	1170,		1085,				720
70300	70.95	3.58	1153,	1138,	1102,	1040,		761	
75300	76.70	3.18	1164,	1130,		1060,	940,	770	
80300	80.53	3.47	1179,	1164,	1141,		940,	780	
83300	81.87	3.51	1190,	1161,			939,	777	
85300	84.23	3.57	1198,	1165,			940,	810	
88300	87.88	3.44	1204,	1195,		1027,	913,	805	
90300	85.98	3.65	1214,			1020,	927,	820	
93300	87.16	3.74	1222,	1203,			927		
48330	46.58	3.71	1095,		1090,				730
50330	46.31	3.77	1111,		1095,				720
51330	48.34	3.84	1103,		1090,				725
52330	50.29	3.85	1105,		1090,				735
45350	45.47	4.30	1130,		1095				
48350	47.04	3.79	1120,		1090				
50351	48.54	4.03	1092,		1090				
52350	50.51	3.93	1100,		1090				
55350	54.83	4.19	1107,		1094				
60351	58.52	4.04	1112,		1090				
65350	64.20	4.28	1129,		1098				
70350	68.55	4.35	1154,		1090,		920		
75350	72.73	4.24	1174,		1089,	983,	925		
80350	78.34	4.40	1190,	1130,	1067,	978,	950		
83350	82.89	3.30	1183,	1152,	1062,		920		
85350	82.28	4.41	1198,		1073,	958			
87350	86.64	3.65	1113,	1194,		947			
90350	86.16	4.17	1223,	1189,		965,	934		
92350	87.86	4.03	1233,	1208,			931		
48370	47.40	4.04	1100,	1090					
50370	50.43	3.98	1098,	1090					
52370	50.44	4.02	1110,	1090					
45400	49.31	3.88	1109,	1092					
50401	47.74	4.33	1120,	1100					

(Continued 3)

Specimen number	Chemical composition		Transition point, °C						
	Mn %	C %							
55400	52.67	4.36	1122,	1092					
60401	55.89	4.37	1132,	1090					
65400	62.10	4.55	1148						
70400	67.31	4.66	1158,	1080					
75400	73.32	4.70	1185,	1098					
80400	77.36	5.03	1206,	1155					
83400	82.53	4.28	1212,	1170,		973,	925		
85400	83.98	4.35	1214,	1188,		977,	922		
90400	89.59	4.74	1241,	1225,	1010,	991,	940		
91400	86.23	4.56	1242,	1200,		990,	925,	794	
50450	49.56	4.49	1129,	1094,					725
55450	54.26	4.74	1140,	1093,					727
60450	60.99	4.51	1145,	1094					
65450	64.22	4.42	1145,	1084					
70450	69.09	4.55	1161,	1086,			925		
75450	74.84	4.54	1191,	1112,			925		
80450	79.72	4.63	1208,	1155,		945,	915		
84450	83.36	4.74	1231,	1200					
85450	79.89	4.91	1235,	1197,			925		
90450	86.32	5.03	1254,	1222,	1077,	1030,	910		
50501	47.48	5.17	1165,	1110					
55500	54.78	4.95	1160,	1082,					735
60501	60.35	4.95	1180,	1100,					750
65500	64.61	4.85	1187,	1137,	1091,			880	
70500	70.58	4.92	1186,	1127,	1100,	1040,	926		
75500	74.43	4.44	1190,		1100,		925		
80500	79.41	5.14	1227,	1181,	1099,	992,	923		
83500	82.34	5.21	1239,	1200,	1098,	1000,	920		
85500	83.13	5.39	1250,	1204,	1094,	1032,	956		
89500	86.21	5.24	1268,	1232,	1085,		986		
50551	48.54	5.48	1198,		1100				
55550	53.04	5.50	1200,		1094				
60551	55.85	5.43	1205,		1096				
65550	61.07	5.61	1200,	1100,	1080				
70550	65.74	5.58	1208,		1082				
75550	70.88	5.61	1205,	1170					
80550	77.85	5.59	1241,	1195					
82550	79.90	5.68	1243,	1185					
85550	80.52	5.83	1253,	1188					
88550	85.98	5.67	1273,	1237					
50600	48.79	5.90	1222,		1110				
55600	53.27	6.13	1228,		1091				
60601	59.77	6.00	1231,		1086				
65600	64.26	5.89	1228,		1088				
70600	68.48	5.85	1239,	1125					
75600	74.56	5.91	1243,	1175					
80600	78.35	6.10	1245,	1225,	1196				
85600	82.75	6.14	1263,	1222,	1160				
88600	86.07	6.20	1296,	1225,	1163				

With this apparatus or with suitable utilization of its upper half, heating, melting and thermal analysis could easily be carried out in vacuum without any difficulty.

To avoid oxidation, the measurements were made in hydrogen atmosphere, and the furnace was so controlled as the cooling velocity might be almost the same in every measurement. Table 2 shows the transition points obtained from the cooling curves.

Fig. 3 shows the isothermal lines on the primary surface of iron-manganese-carbon ternary system obtained by plotting the results of thermal analyses.

To determine the range of δ iron ternary solid solution crystallized as a primary crystal, thermal analyses were carried out by vacuum high frequency induction furnace with samples containing 1.25~30 per cent of manganese and 0.05~1.2 per cent of carbon. Table 3 shows the results.

Table 3. Transition points obtained by cooling curves of iron, manganese and carbon ternary alloys.

Specimen number	Chemical composition of alloys %				Transition point, °C		
	Preparated		Analysed				
	Mn	C	Mn	C			
5	1.25	0.05	0.43	0.08	1521,	1478,	1450
55	1.25	0.05	0.46	0.07	1521		
333	2.50	0.10	0.78	0.13	1521,	1487,	1430
3	2.50	0.10	0.93	0.02	1520		
6	3.75	0.15	3.01	0.21	1502,	1480,	1460
22	5.00	0.20	3.95	0.25	1495,	1480,	1460
7	6.25	0.25	4.54	0.29	1491,	1480,	1420
4	7.50	0.30	6.63	0.37	1480		
1212	8.75	0.35	7.80	0.47	1470		
1	10.00	0.40	7.52	0.21	1480		
111	10.00	0.40	8.94	0.44	1460		
13	12.50	0.50	9.95	0.59	1460		
88	15.00	0.60	13.00	0.75	1450		
888	15.00	0.60	13.32	0.79	1443		
9	20.00	0.80	17.12	1.03	1413		
11	30.00	1.20	26.56	1.54	1350		

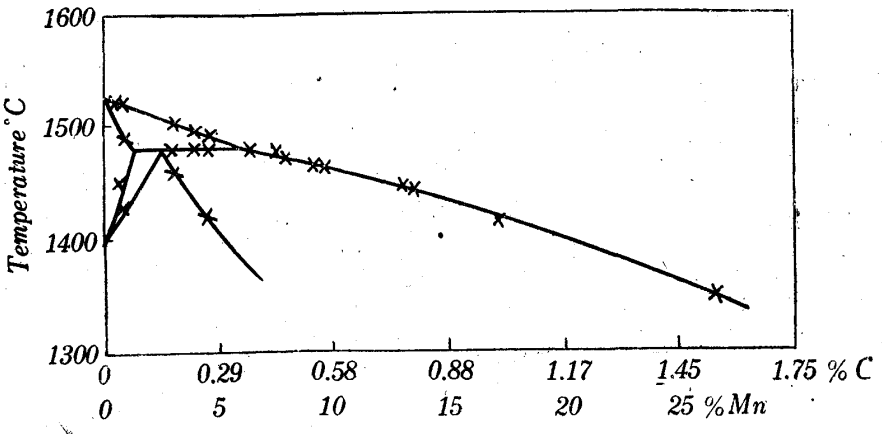

Fig. 4. Sectional diagram of iron-manganese-carbon alloy at iron rich corner where δ iron crystallized as primary crystals.

Some typical results are shown in Fig. 4. From the results, the temperature and composition concerning the reaction, liquid + δ iron ternary solid solution → γ iron ternary solid solution, were determined. Fig. 5 shows the ternary diagram thus obtained with iron-rich alloys at high temperatures.

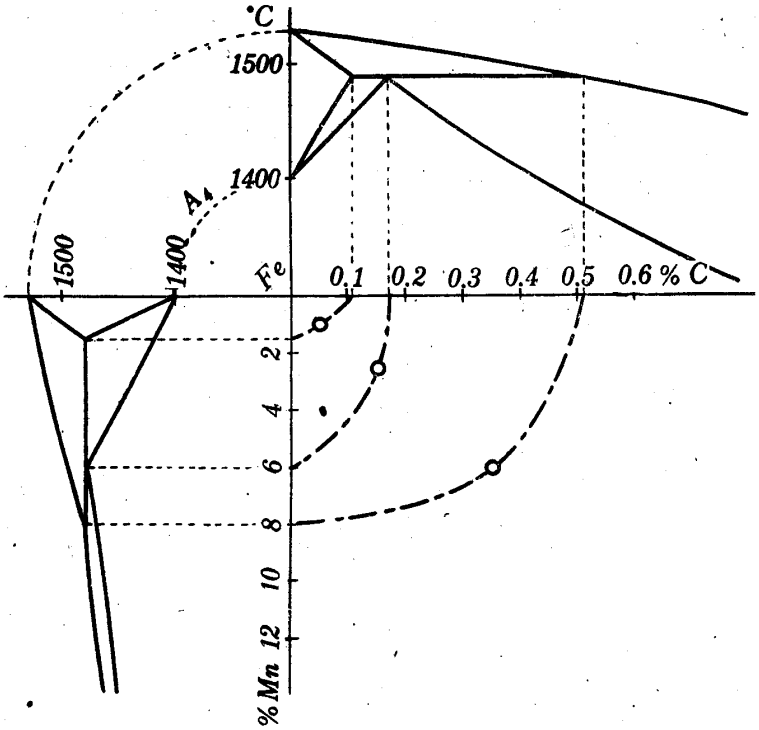

Fig. 5. Ternary diagram of iron-manganese-carbon alloy at iron rich corner, which shows the composition of the region of δ iron ternary solid solution and of the reaction concerning it.

IV. Microscopic examination

The microscopic investigation showed the following seven kinds of primary crystals. Primary crystals both of δ iron and δ manganese ternary solid solution were hardly seen under microscope because of the narrowness of their crystallization range, and yet they could be confirmed by other experiments, which will be shown later.

δFe, ternary solid solution of δ iron in iron corner.

γFe (A), ternary solid solution of γ iron in which manganese and carbon are dissolved.

C, $(Fe, Mn)_3C$ ternary solid solution of iron carbide Fe_3C in which manganese is dissolved.

γMn, ternary solid solution of γ manganese in which iron and carbon are dissolved.

δMn, ternary solid solution of δ manganese in which iron and carbon are dissolved.

βC, ternary solid solution of βC binary solid solution of manganese and carbon in which iron is dissolved.

αC, ternary solid solution of αC binary solid solution of manganese and carbon in which iron is dissolved.

Fig. 6 shows ranges of composition of respective phases.

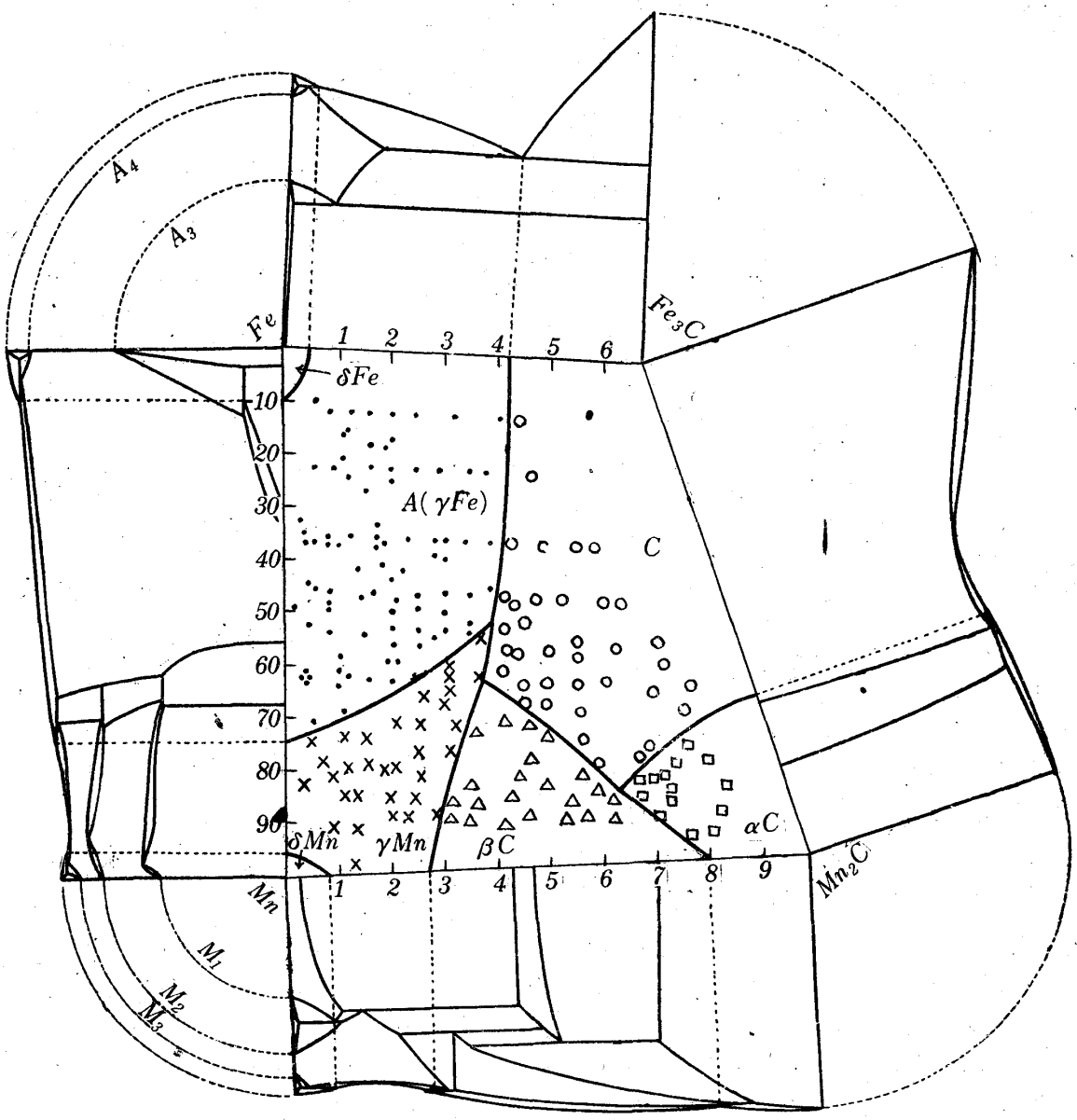

Fig. 6. Seven kinds of primary crystals appeared in iron-manganese-carbon ternary alloy.

δFe	: δ iron ternary solid solution	αC	: αC ternary solid solution
$A(\gamma$Fe)	: γ iron ternary solid solution	βC	: βC ternary solid solution
δMn	: δ manganese ternary solid solution	C	: C ternary solid solution
γMn	: γ manganese ternary solid solution		

From isothermal lines (Fig. 3) and microscopic structures (Fig. 6) the primary surfaces of iron-manganese-carbon ternary system could be obtained. Fig. 7 is the result and the explanations of respective surfaces, lines and points are given in Table 4.

Next, some explanations about microscopic photographs will be given below.

The primary crystals of ternary solid solution of γ iron (A), ternary solid solu-

tion C, γ manganese, βC and αC ternary solid solutions are shown in Photos. 1 and 2, 3, 4, 5 and 6, and 7 respectively. The primary crystals of δ manganese ternary solid solution and δ iron ternary solid solution are hardly observable as above stated.

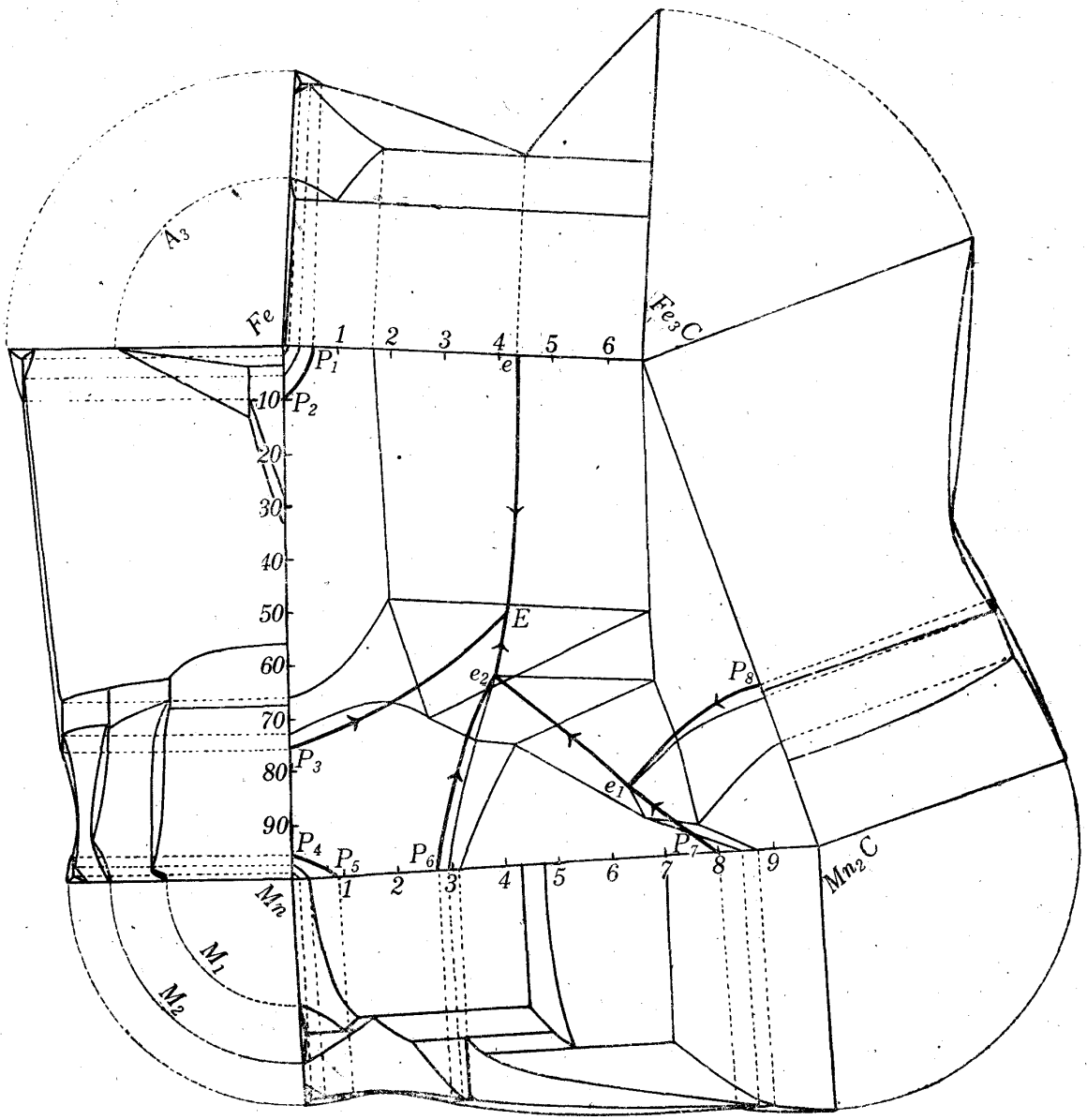

Fig. 7 Primary surface of iron-manganese-carbon ternary alloy. Meanings of respective primary surfaces, curves and points are shown in Table 4.

The eutectic structure precipitated along the line eE in Fig. 7 is seen in Photo. 1, which is the structure of the specimen containing 38.56 per cent of manganese and 3.10 per cent of carbon. In this specimen γ iron ternary solid solution first crystallizes as primary crystal and then the eutectic of γ iron ternary solid solution and C ternary solid solution precipitates. The eutectic produced along the line eE is almost of the same appearance as that in iron-carbon binary alloy.

The eutectic produced along the line P_3E is shown in Photos. 2, 8, 9 and 10.

In the specimen in Photo. 2, after the crystallization of γ iron ternary solid solution as primary crystal, the binary eutectic of γ iron ternary solid solution and γ manganese ternary solid solution is produced. But in case of alloys contains almost the same amount of carbon but different amount of manganese, the more they contain manganese, the less they crystallize γ iron ternary solid solution

Table 4. Explanation of the meaning of respective primary surfaces, curves and points in figure 7.

Primary surfaces

Primary surfaces	Mark	Meaning of the each primary surfaces
FeP_1P_2Fe	δFe	Ternary solid solution of δ iron in which a small amount of manganese and carbon are dissolved.
$P_1P_2P_3EeP_1$	γFe(A)	Ternary solid solution of γ iron in which manganese and carbon are dissolved.
$Fe_3CeEe_2e_1P_8Fe_3C$	C	Ternary solid solution of carbide $(Fe, Mn)_3C$ consisting of Fe_3C which contains manganese.
$P_3P_4P_5P_6e_2EP_3$	γMn	Ternary solid solution of γ manganese in which iron and carbon are dissolved.
MnP_4P_5Mn	δMn	Ternary solid solution of δ manganese in which a small amount of iron and carbon are dissolved.
$P_6P_7e_1e_2P_6$	βC	βC ternary solid solution, in which iron is dissolved in βC solid solution of manganese and carbon binary alloy.
$P_7Mn_2CP_8e_1P_7$	αC	αC ternary solid solution, in which iron is dissolved in αC solid solution of manganese and carbon binary alloy.

Eutectic lines

Eutectic lines	Reactions
eE	liquid $\rightarrow$ γ iron ternary solid solution + C ternary solid solution
P_3E (a part)	liquid $\rightarrow$ γ iron ternary solid solution + γ manganese ternary solid solution
e_2E	liquid $\rightarrow$ γ manganese ternary solid solution + C ternary solid solution
e_1e_2	liquid $\rightarrow$ βC ternary solid solution + C ternary solid solution
P_7e_1 (a part)	liquid $\rightarrow$ αC ternary solid solution + βC ternary solid solution

Peritectic lines

Peritectic lines	Reactions
P_1P_2	liquid + δ iron ternary solid solution $\rightarrow$ γ iron ternary solid solution
P_3E (a part)	liquid + γ iron ternary solid solution $\rightarrow$ γ manganese ternary solid solution
P_4P_5	liquid + δ manganese ternary solid solution $\rightarrow$ γ manganese ternary solid solution
P_6e_2	liquid + βC ternary solid solution $\rightarrow$ γ manganese ternary solid solution
P_7e_1 (a part)	liquid + αC ternary solid solution $\rightarrow$ βC ternary solid solution
P_8e_1	liquid + αC ternary solid solution $\rightarrow$ C ternary solid solution

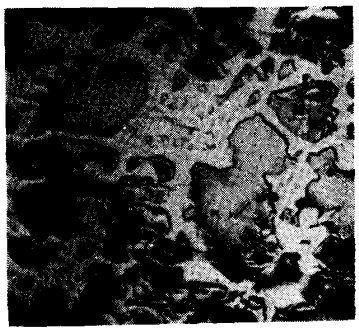

Photo. 1. ×200
38.56%Mn, 3.10%C, showly cooled from melt; primary crystal of γ iron ternary solid solution and eutectic of γ iron ternary solid solution and of C ternary solid solution.

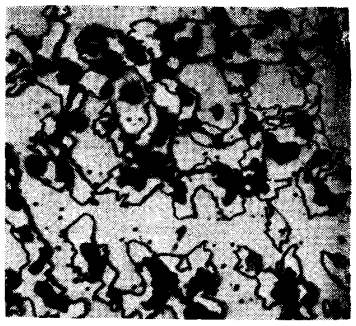

Photo. 2. ×100
58.30%Mn, 1.88%C; slowly cooled from melt; primary crystal of γ iron ternary solid solution and eutectic of γ iron ternary solid solution and of γ manganese ternary solid solution.

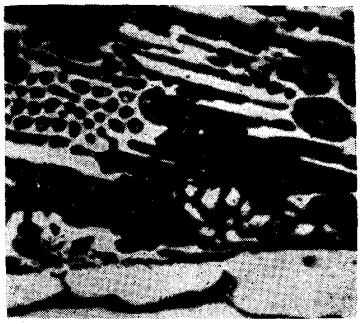

Photo. 3. ×200
55.89%Mn, 4.37%C, slowly cooled from melt; primary crystal of C ternary solid solution and binary eutectic of γ manganese ternary solid solution and of C ternary solid solution, and ternary eutectic of C ternary solid solution, γ manganese ternary solid solution and γ iron ternary solid solution.

Photo. 4. ×100
63.99%Mn, 3.05%C; slowly cooled from melt; primary crystal of γ manganese ternary solid solution and binary eutectic and a small amount of ternary eutectic.

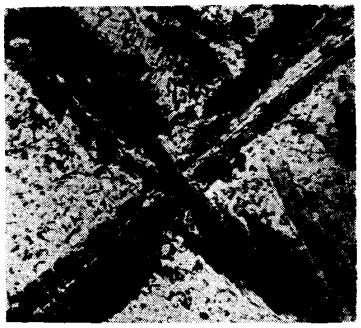

Photo. 5. ×50
78.79%Mn, 3.16%C; slowly cooled from melt; primary crystal of βC ternary solid solution.

Photo. 6. ×70
80.53%Mn, 3.47%C; slowly cooled from melt; primary crystal of βC ternary solid solution.

Photo. 7. ×100
77.22%Mn, 8.29%C ; quenched at 1100℃ in ice brine water ; primary crystal of αC ternary solid solution and the white part is C ternary solid solution.

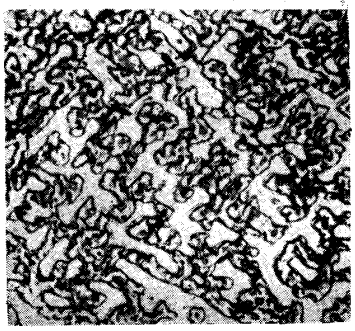

Photo. 8. ×50
58.30%Mn, 1.88%C ; slowly cooled from melt ;eutectic structure of γ iron ternary solid solution and of γ manganese ternary solid solution.

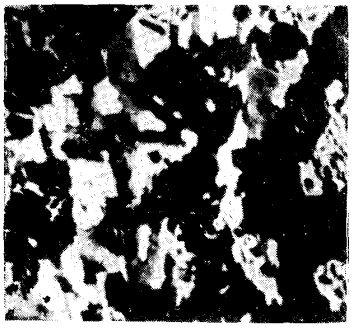

Photo. 9. ×200
58.63%Mn, 3.06%C ; slowly cooled from melt ; primary crystal, binary eutectic and ternary eutectic.

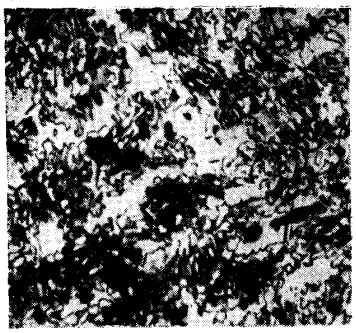

Photo. 10. ×100
63.36%Mn, 2.54%C ; slowly cooled from melt ; primary crystal of γ manganese ternary solid solution and binary eutectic.

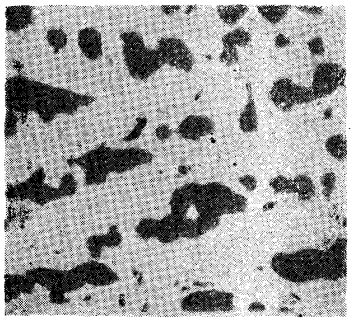

Photo. 11. ×100
89.87%Mn, 0.92%C ; slowly cooled from melt ; uniform γ manganese ternary solid solution.

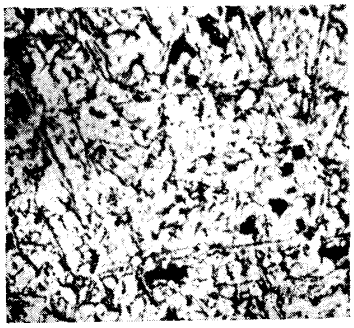

Photo. 12. ×70
84.75%Mn, 2.40%C ; slowly cooled from melt ; γ manganese ternary solid solution.

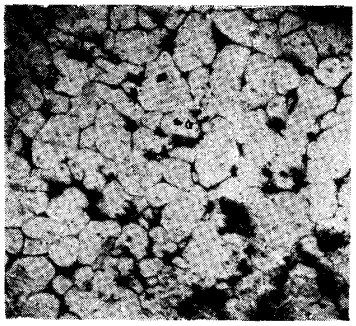

Photo. 13. ×50
84.75%Mn, 2.40%C; quenched at 1100°C in ice brine water; γ manganese ternary solid solution.

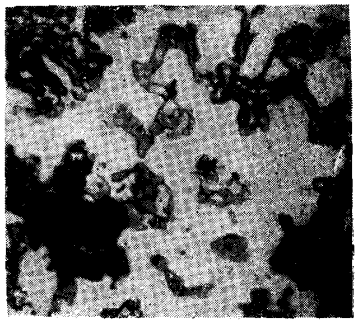

Photo. 14. ×200
78.79%Mn, 3.16%C; quenched at 1000°C in ice brine water; γ manganese ternary solid solution and βC ternary solid solution.

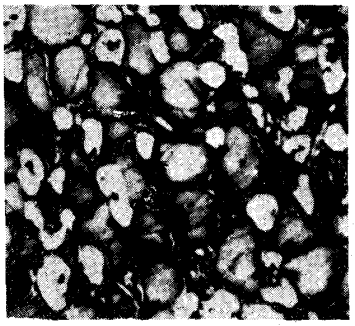

Photo. 15. ×100
80.53%Mn, 3.47%C; quenched at 1100°C in ice brine water; γ manganese ternary solid solution and βC ternary solid solution.

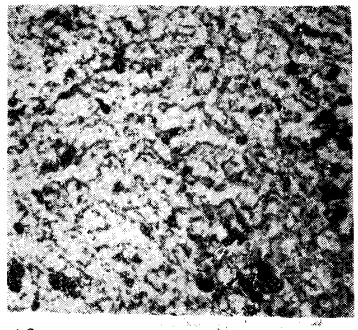

Photo. 16. ×70
82.28%Mn, 4.41%C; as cast structure, βC ternary solid solution.

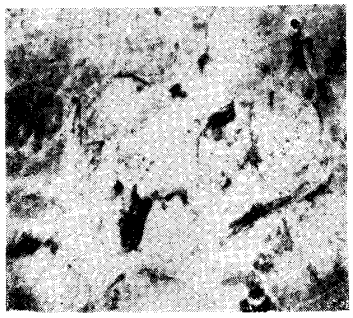

Photo. 17. ×350
82.28%Mn, 4.41%C; quenched at 1100°C in ice brine water; uniform βC ternary solid solution.

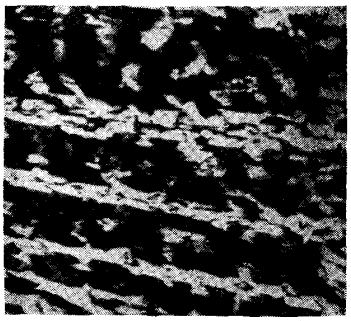

Photo. 18. ×100
74.84%Mn, 4.54%C; as cast structure; primary crystal of βC ternary solid solution, and binary eutectic of βC ternary solid solution and of C ternary solid solution.

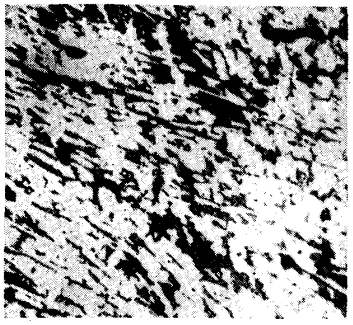

Photo. 19. ×50
78.35%Mn, 6.10%C ; slowly cooled from melt ; the eutectic structure of βC ternary solid solution and of C ternary solid solution.

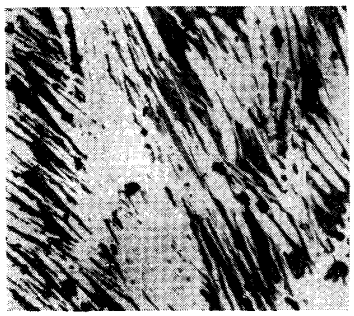

Photo. 20. ×50
64.26%Mn, 5.89%C ; slowly cooled from melt ; the eutectic structure of βC ternary solid solution and of C ternary solid solution.

Photo. 21. ×200
74.84%Mn, 4.54%C ; quenched at 1100°C in ice brine water ; βC ternary solid solution is martensitic and a small amount of C ternary solid solution is white.

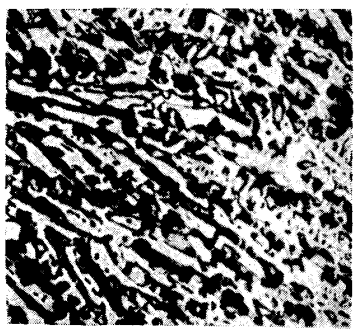

Photo. 22. ×100
48.54%Mn, 4.03%C ; slowly cooled from melt ; ternary eutectic structure.

Photo. 23. ×1000
48.54%Mn, 4.03%C ; slowly cooled from melt ; same as Photo. 22, but high magnification ; ternary eutectic structure.

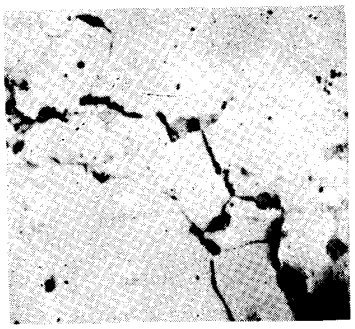

Photo. 24. ×100
78.99%Mn, 1.87%C ; quenched at 1000°C in ice brine water ; uniform γ manganese ternary solid solution.

Peritecto-eutectic points

Peritecto-eutectic points	Temperature °C	Reactions	Fe %	Mn %	C %
e_1	1260	liquid + αC → βC + C	13.70	80.00	6.30
e_2	1105	liquid + βC → γMn + C	35.20	61.00	3.80

Ternary eutectic point

Eutectic point	Temperature °C	Reaction	Fe %	Mn %	C %
E	1090	liquid → γFe + γMn + C	47.50	48.50	4.00

as primary crystal and the more they produce eutectic structure. In Photo. 10 the primary crystal is γ manganese ternary solid solution, the binary eutectic being the same as before. In Photo. 9 the specimen is almost of the same composition as that on the line P_3E, and it produces neither γ iron ternary solid solution nor γ manganese ternary solid solution as primary crystal, but ternary eutectic after crystallizing the binary eutectic of γ iron ternary solid solution and γ manganese ternary solid solution. It was rather difficult to distinguish γ manganese ternary solid solution from C ternary solid solution by ordinary etching, but as the latter had more resistance to strong etching than the former, the distinction between them was possible by severe etching. In this case, however, γ iron solid solution was etched so intensely that it became more difficult to distinguish γ iron ternary solid solution from the very fine mixture of γ iron ternary solid solution and γ manganese ternary solid solution.

The alloy in Photo. 4 solidifies on crystallizing γ manganese ternary solid solution as primary crystal and the binary eutectic of γ manganese ternary solid solution and C ternary solid solution on the line e_2E. The alloy in Photo. 11 containing 89.87 per cent of manganese and 0.92 per cent of carbon is made of the uniform solid solution of γ manganese. The same is also said for the alloy containing 84.75 per cent of manganese and 2.40 per cent of carbon as shown in Photo. 12. When this specimen is quenched in brine ice water immediately after the solidification, the structure is made of uniform solid solution as shown in Photo. 13. When the alloy with the same composition as that in Photo. 5 is quenched at 1000°C in brine ice water, the structure consists of γ manganese ternary solid solution and βC ternary solid solution as shown in Photo. 14. The same will be seen in Photo. 15, which is the structure of the alloy in Photo. 6 quenched at 1100°C. Photo. 16 is the cast structure of the alloy containing 82.28 per cent of manganese and 4.41 per cent of carbon and Photo. 17 is the structure of the alloy heated at 1100°C and then rapidly cooled, both consisting of uniform βC ternary solid solution.

Photo. 18 shows that, in the alloy containing 74.84 per cent of manganese and 4.54 per cent of carbon, ternary solid solution βC crystallizes as primary crystal

and then the eutectic of βC ternary solid solution and C ternary solid solution on the line e_1e_2 is precipitated. Photo. 7 shows the structure after the peritectic reaction along the line P_8e_1.

The alloy shown in Photo. 19 is almost of the same structure as that on the line e_1e_2 and is made mostly of the eutectic of βC ternary solid solution and C ternary solid solution. In Photo. 20 the structure is made of the eutectic of βC ternary solid solution and C ternary solid solution, primary crystal being C ternary solid solution. Photo. 21 shows the structure of alloy quenched at 1100°C in brine ice water. The martensitic structure appears in quenched βC ternary solid solution, in which white fine particles are C ternary solid solution and this is the structure in the vicinity of the limiting region of βC ternary solid solution. Photo. 3 shows that in the alloy containing 55.89 per cent of manganese and 4.37 per cent of carbon, C ternary solid solution first and then binary eutectic along the line e_3E crystallizes and lastly ternary eutectic at the point E is formed. Photos. 22 and 23 show that the alloy containing 48.54 per cent of manganese and 4.03 per cent of carbon is of the ternary eutectic structure, corresponding just to the composition of the point E. In these photographs, the black coloured part is γ iron ternary solid solution, namely, austenite of ternary alloy and the middle coloured part is γ manganese ternary solid solution and unattacked white coloured part is C ternary solid solution. Photo. 23 clearly shows the differences among them in high magnification.

V. Changes in solid phase

(A) A_3 surface

It has been known that A_3 point of pure iron falls gradually with the addition of carbon, but this change was not obvious in the case of the addition of manga-

Table 5. Transformation points obtained by thermal dilatation curves of iron, manganese and carbon ternary alloys rich in iron.

Specimen number	C %	Mn %	Ac_3	Ar_3	Ac_1	Ar_1					
0002	0.20	0.00	862	842	725	700					
0202	0.18	1.43	820	745	720	630					
0402	0.20	3.04	795	495							
0602	0.17	4.85	765	300							
1002	0.18	7.90	712	135							
1202	0.21	10.32	700	85							
1302	0.21	11.68	680	60							
1502	0.22	13.00	646								
				Ah lower			Ah upper				
				Ahc	Ahr	Mean	Ahc	Ahr	Mean		
1602	0.19	13.07	630	220			270				
1802	0.21	15.54	620	215	15	115	275	70	172		
1902	0.21	16.45		195	15	105	250	60	155		
4002	0.22	21.94		190	−35	77	245	10	127		
3002	0.35	34.90									

nese. In order to clarify this point, the following experiments were first made. Twenty specimens containing about 0.2 per cent of carbon and 0~40 per cent of manganese were melted in vacuum furnace and cooled in it. Then, they were forged into rods, 7 mm in diameter, out of which specimens for microscopic examination, dilatometric examination and heat treatment were made.

Dilatometric observations were carried out in vacuum, the specimens, 50 mm in length, being annealed at 1200°C. The results are shown in Fig. 8. From the figure it will be seen that, as the content of manganese increases, Ac_3 point falls gradually to 620°C, at which manganese content is 15.5 per cent, and that Ar_3 point rapidly falls to 60°C at which manganese content is 11.68 per cent. Namely, the irreversibility of A_3 transformation increases in proportion to the content of manganese. In the alloys containing 11.68~34 per cent of manganese, the change at A_3 point becomes no more observable, whereas the change showing the reversible transformation, γ iron ternary solid solution $\rightleftarrows$ h ternary solid solution, becomes noticeable below 200°C. But the temperature falls gradually as the content of manganese increases and the transformation disappears at 34 per cent of manganese.

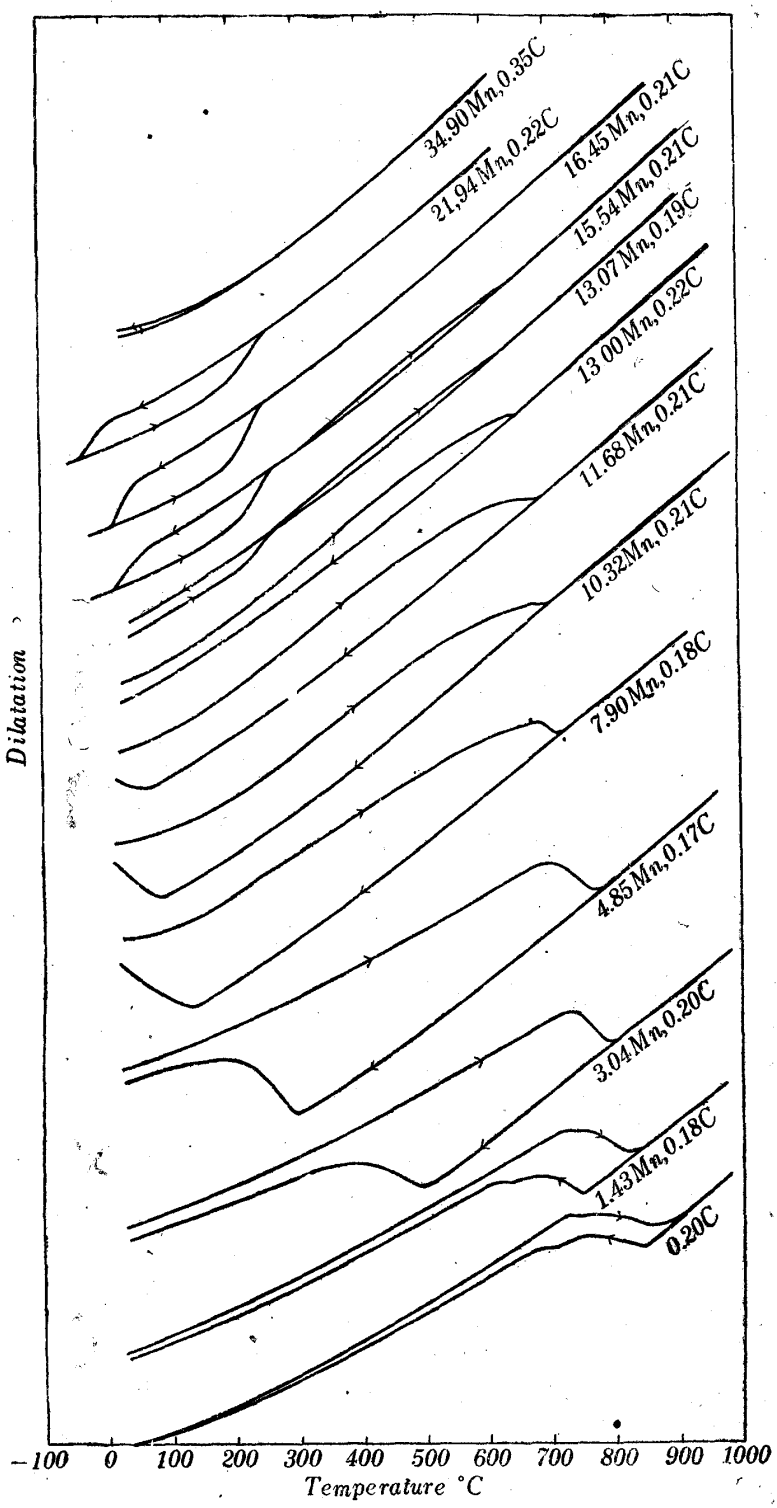

Fig. 8. Dilatation curves of iron rich ternary alloys showing A_3 and h transformations.

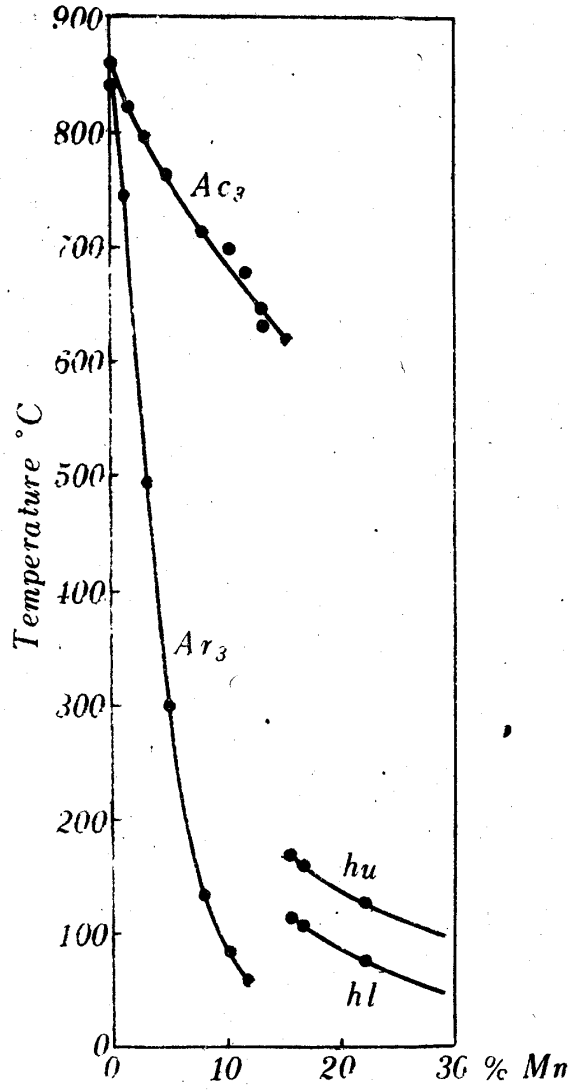

Fig. 9. Sectional diagram of iron-manganese-carbon ternary alloy at iron rich corner containing 0.2 per cent of carbon.

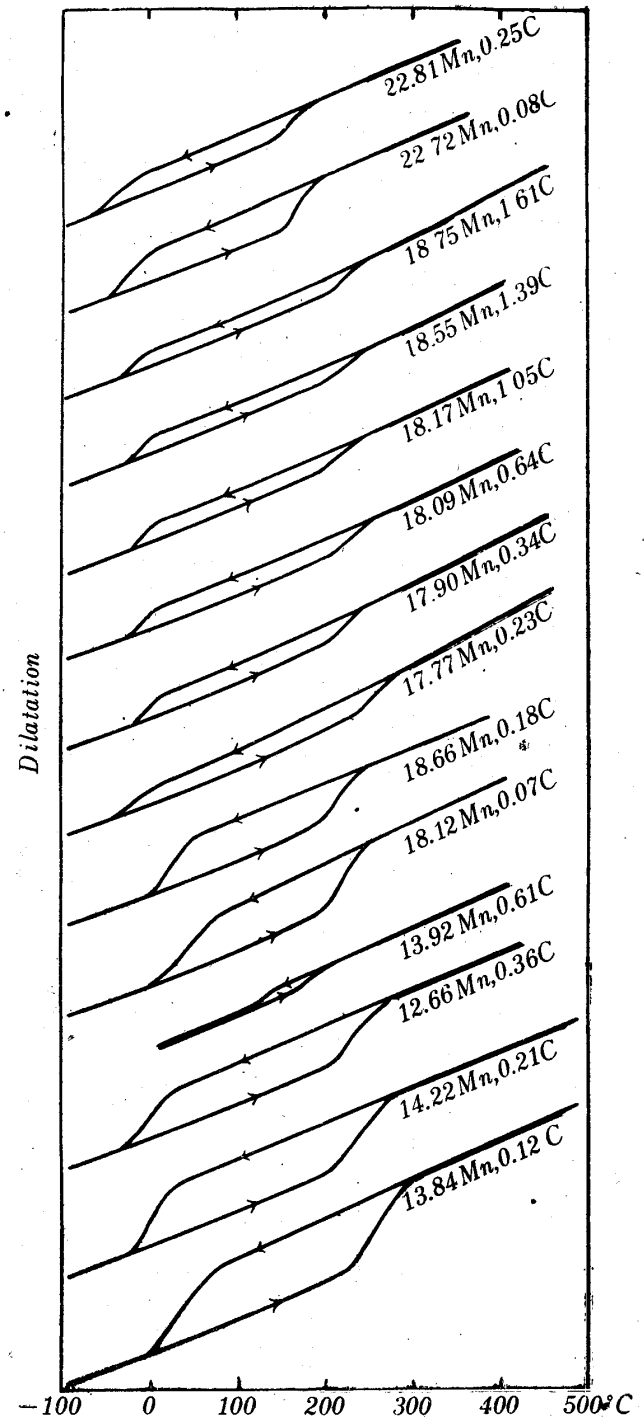

Fig. 10. Dilatation curves of three alloy series containing about 14, 18 and 35 per cent of manganese, respectively and different amounts of carbon in iron-manganese-carbon ternary system.

Fig. 9 shows the sectional diagram at an alloy of iron rich corner containing 0.2 per cent of carbon in iron-manganese-carbon ternary system, from which the influence of manganese upon the A_3 and h transformations can be clearly seen.

Ac_3, Ar_3, Ac_1, Ar_1, Ahc and Ahr transformation points in ternary alloys containing 0.18~0.35 per cent of carbon and 1.43~34.90 per cent of manganese are shown in Table 5.

(B) Hexagonal surface

Next, influence of carbon upon the $h \rightleftarrows \gamma$ transformation in iron-manganese binary

system was examined with the alloys containing 14, 18 and 35 per cent of manganese and 0~2.0 per cent of carbon. The results of dilatometric measurements are shown in Fig. 10. Table 6 shows the transformation points of respective alloys.

Table 6. Transformation points obtained by thermal dilatation curves of iron, manganese and carbon ternary alloys.

Specimen number	C %	Mn %	Ah lower			Ah upper		
			Ahc	Ahr	Mean	Ahc	Ahr	Mean
2000	0.07	18.12	190	0	95	240	80	160
2002	0.18	18.16	180	0	90	240	45	142
2001	0.23	17.77	250	−75	88	280	5	142
2003	0.34	17.90	190	−20	85	250	15	132
2005	0.64	18.09	190	−25	82	250	10	130
2010	1.05	18.17	190	−25	82	250	5	127
2014	1.39	18.55	195	−30	82	250	5	127
2018	1.61	18.75	200	−30	85	250	0	125
1500	0.12	13.84	230	0	115	300	80	190
1502	0.21	14.22	210	−20	95	270	30	150
1504	0.36	12.66	210	−20	95	270	30	150
1506	0.61	13.92				170	130	150
2500	0.08	22.72	150	−50	50	200	10	105
2502	0.25	22.81	140	−70	35	200	0	100

As seen from the above results, the transformation point falls first as the carbon content increases up to 0.20 per cent and then becomes almost constant for the further increase of carbon content. In every case the amount of transformation is the largest at the binary alloys and as the content of carbon increases it de-

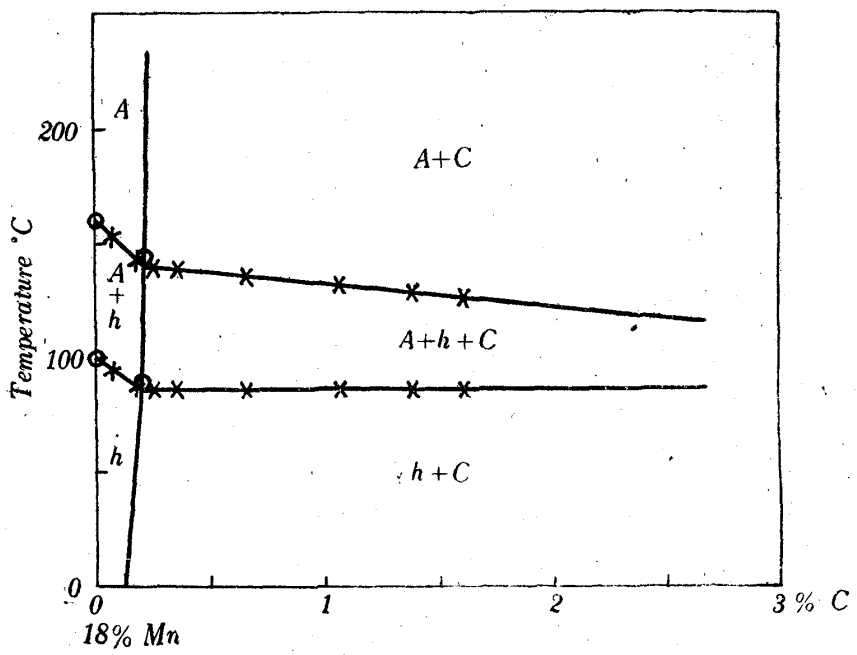

Fig. 11. Sectional diagram of iron-manganese-carbon ternary alloy at iron-manganese side containing 18 per cent of manganese and different amounts of carbon at low temperatures.

A : γ iron ternary solid solution
h : *h* ternary solid solution
C : *C* ternary solid solution

creases comparatively rapidly until 0.2 per cent of carbon, showing the range of transformation of γ iron ternary solid solution and h ternary solid solution. As the content of carbon further increases, the amount of transformation becomes small and gradually decreases, the structure consisting of three phases of γ iron, h and C ternary solid solutions. Fig. 11 is the sectional diagram at iron-manganese side containing 18 per cent of manganese in low temperature ranges.

(C) Acm surface

The change of Acm line with the addition of manganese in iron-carbon system, namely, the change of Acm surface of iron-manganese-carbon ternary alloy was examined with the alloys, each containing about 18, 36 and 45 per cent of manganese and various amounts of carbon, the specimens being quenched at suitable temperatures in brine ice water, and the structure was examined microscopically. The results are shown in Tables 7, 8 and 9, respectively.

From the results of microscopic examinations, solubilities of C ternary solid solution and other phases in γ iron ternary solid solution were determined, and

Table 7. Microscopic structure of alloys containing almost the same amount of manganese and different amounts of carbon, and quenched from respective temperatures.

Specimen number	Mn %	C %	Quenching temperature °C and microscopic structure								
			1300	1200	1150	1100	1050	1000	975	925	875
20001	17.77	0.23	A	A							
20002	17.90	0.34	A	A							
20003	19.05	0.50	A	A							
20004	18.70	0.55	A	A							
20005	18.09	0.64	M	A							A
20006	17.30	0.74	M	A						A	A
20007	19.54	0.82	M	A						A	A
20008	17.52	0.92	M	A					A	A	A+C
20010	18.17	1.05		A	A			A	A	A	A+C
20012	17.95	1.23		M	A	A	A	A	A+C	A+C	A+C
20014	18.55	1.39		M	M	A	A	A+C	A+C	A+C	A+C
20016	18.00	1.62			M	A	A+C	A+C	A+C	A+C	A+C
20018	18.75	1.61			M	A	A+C	A+C	A+C	A+C	A+C
20020	17.08	2.01				A+C	A+C	A+C	A+C	A+C	A+C

Specimen number	Mn %	C %	Quenching temperature °C and microscopic structure							
			850	775	750	725	690	665	645	615
20001	17.77	0.23			A	A	A	A	A	A
20002	17.90	0.34			A	A	A			
20003	19.05	0.50	A	A	A	A	A+C	A+C	A+C	A+C
20004	18.70	0.55	A	A	A					
20005	18.09	0.64	A	A	A+C	A+C	A+C			
20006	17.30	0.74	A	A+C	A+C					
20007	19.54	0.82	A+C	A+C	A+C					
20008	17.52	0.92	A+C	A+C						
20010	18.17	1.05	A+C	A+C						
20012	17.95	1.23	A+C	A+C						

Note: M=Partially melted
A=Austenite, γ iron ternary solid solution
C=Carbide, C ternary solid solution

Table 8. Microscopic structure of quenched alloys containing almost the same amount of manganese and different amounts of carbon.

Specimen number	Mn %	C %	Quenching temperature °C and microscopic structure								
			1000	950	900	850	800	750	700	650	600
40000	41.15	0.05	A	A	A	A	A	A	A	A	A
40001	48.88	0.21	A	A	A	A	A	A	A	A	A
40002	41.39	0.35	A	A	A	A	A	A	A	A	A
40003	36.96	0.42	A	A	A	A	A	A	A	A	A
40004	36.22	0.53	A	A	A	A	A	A	A	A	A
40006	36.60	0.77	A	A	A	A	A	A	A	A	A
40008	36.58	1.02	A	A	A	A	A	A	A	A+C	A+C
40010	41.13	1.43	A	A	A+C	A+C	A+C	A+C	A+C	A+C	A+C
40012	35.35	1.55	A	A+C	A+C	A+C	A+C	A+C	A+C	A+C	A+C
40014	36.96	1.78	A+C	A+C	A+C	A+C	A+C	A+C	A+C	A+C	A+C
40016	40.54	2.19	A+C	A+C	A+C	A+C	A+C	A+C	A+C	A+C	A+C
40018	41.62	1.98	A+C	A+C	A+C	A+C	A+C	A+C	A+C	A+C	A+C
40020	39.23	2.63	A+C	A+C	A+C	A+C	A+C	A+C	A+C	A+C	A+C
40022	37.65	2.80	A+C	A+C	A+C	A+C	A+C	A+C	A+C	A+C	A+C
40024	38.00	2.99	A+C	A+C	A+C	A+C	A+C	A+C	A+C	A+C	A+C
40027	36.55	3.04	A+C	A+C	A+C	A+C	A+C	A+C	A+C	A+C	A+C
40030	36.71	3.21	A+C	A+C	A+C	A+C	A+C	A+C	A+C	A+C	A+C

Note: A=austenite, γ iron ternary solid solution
C=carbide, C ternary solid solution

Table 9. Microscopic structure of quenched alloys containing almost the same amount of manganese and different amounts of carbon.

Specimen number	Mn %	C %	Quenching temperature °C and microscopic structure						
			1200	1150	1100	1050	1000	975	950
45000	45.58	0.51	A	A	A	A	A	A	A
45005	45.20	1.02	M	A	A	A	A	A	A
45009	45.26	1.27		M	A	A	A	A	A
45012	45.55	1.67		M	A	A	A+γ	A+γ	A+γ+C
45015	46.09	2.00			M	A+C	A+C	A+γ+C	A+γ+C
45021	45.94	2.77				A+C	A+C	A+C	A+C
45024	45.90	2.93				A+C	A+C	A+C	A+C
45027	45.90	3.04				A+C	A+C	A+C	A+C
45030	45.97	3.21				A+C	A+C	A+C	A+C

Specimen number	Mn %	C %	Quenching temperature °C and microscopic structure						
			850	800	775	750	725	700	550
45000	45.58	0.51	A	A				A	A
45005	45.20	1.02	A	A	A+α	A+α	A+α	A+α	
45009	45.26	1.27	A+γ	A+γ	A+γ	A+γ		A+α+C	A+α+C
45012	45.55	1.67	A+γ+C	A+γ+C					
45015	46.09	2.00	A+γ+C						
45021	45.94	2.77	A+γ+C						
45024	45.90	2.93	A+γ+C						
45027	45.90	3.04	A+γ+C						
45030	45.97	3.21	A+γ+C						

Note: M=partially melted
A=austenite, γ iron ternary solid solution
C=carbide, C ternary solid solution
γ=γ manganese ternary solid solution
α=α manganese ternany solid solution

Table 10. Microscopic structure of quenched alloys containing almost the same amount of carbon and different amounts of manganese.

Specimen number	Mn %	C %	Quenching temperature °C and microscopic structure		
			1100	1000	900
40075	44.99	0.85	A	A	A
45075	57.35	1.32	A+γ	A+γ	A+γ
47575	45.33	0.83	A	A	A
50075	47.27	0.86	A	A	A
52575	49.26	0.86	A	A	A
55075	51.46	0.85	A	A	A
57575	52.63	0.85	A	A	A+γ
60075	42.78	0.90	A	A	A
62575	60.47	0.98	A+γ	A+γ	A+γ
65075	62.45	1.00	A+γ	A+γ	A+γ
67575	65.78	1.01	A+γ	A+γ	A+γ+β
70075	68.42	0.99	A+γ	A+γ	A+γ+β
72575	70.51	0.93	γ	γ	A+γ+β
75075	74.02	0.98	γ	γ	γ+β
77575	69.35	1.02	γ	A+γ	A+γ+β
80075	78.48	0.91	γ	γ	γ+β
82575	75.42	1.13	γ	γ	γ+β
85075	76.40	0.72	γ	γ	γ+β
87575	96.94	1.20	γ	γ	γ
90075	80.82	0.88	γ	γ	γ+β
92575	79.98	1.25	γ	γ	γ+β
95075	84.62	1.10	γ	γ	γ+β

Note: A=austenite, γ iron ternary solid solution
γ=γ manganese ternary solid solution
β=β manganese ternary solid solution

Table 11. Microscopic structure of quenched alloys containing almost the same amount of carbon and different amounts of manganese.

Specimen number	Mn %	C %	Quenching temperature °C and microscopic structure						
			1050	1000	950	900	850	800	700
350175	32.45	1.78	A+C	A+C	A+C	A+C	A+C	A+C	A+C
375175	36.10	1.85	A+C	A+C	A+C	A+C	A+C	A+C	A+C
400175	40.17	1.87	A+C	A+C	A+C	A+C	A+C	A+C	A+C+α
425175	41.91	1.86	A+C	A+C	A+C	A+C	A+C+γ	A+C+γ	A+C+α
450175	42.81	1.96	A+C	A+C	A+C	A+C+γ	A+C+γ	A+C+γ	A+C+α
475175	44.37	1.88	A+C	A+C	A+C+γ	A+C+γ	A+C+γ	A+C+γ	A+C+α
500175	47.01	1.78	A+C+γ	A+C+γ	A+C+γ	A+C+γ	A+C+γ	A+C+γ	A+C+α
525175	51.55	1.98	A+C+γ	A+C+γ	A+C+γ	A+C+γ	A+C+γ	A+C+γ	A+C+α
550175	55.19	1.95	A+γ	A+γ	A+C+γ	A+C+γ	A+C+γ	A+C+γ	A+C+α
575175	56.35	2.07	A+γ	A+γ	A+γ	A+C+γ	A+C+γ	A+C+γ	A+C+α
600175	58.65	1.88	A+γ	A+γ	A+γ	A+γ	A+γ	A+γ	A+C+α
625175	60.55	1.77	A+γ	A+γ	A+γ	A+γ	A+γ	A+γ	A+C+α
650175	63.40	2.03	A+γ	A+γ	A+γ	A+γ	A+γ	A+γ	A+C+α
675175	64.15	2.04	A+γ	A+γ	A+γ	A+γ	A+γ	A+γ	A+C+α
700175	65.92	2.03	A+γ	A+γ	A+γ	A+γ	A+γ	A+γ	A+C+α

Note: A=austenite, γ iron ternary solid solution
γ=γ manganese ternary solid solution
α=α manganese ternary solid solution
C=carbide, C ternary solid solution

then sectional diagrams in neighbourhood of solubility surface could be drawn. Figs. 12, 13 and 14 are the sectional diagrams at iron-manganese side containing various amounts of manganese. The solubility of C ternary solid solution in γ iron ternary solid solution at binary eutectic temperature of γ iron and C ternary solid solution increases gradually with the content of manganese, but at lower temperatures it decreases at first and then increases. As will be seen from Fig. 14, the solubility line of C ternary solid solution in γ iron ternary solid solution slightly appears only at higher temperatures, and the solubility lines of γ manganese and α manganese ternary solid solution in γ iron ternary solid solution appear at lower temperatures in this order. Moreover, three-phase regions of γ iron, γ manganese and C ternary solid solution and of γ iron, α manganese and C ternary solid solution were confirmed in alloys containing higher percentage of carbon.

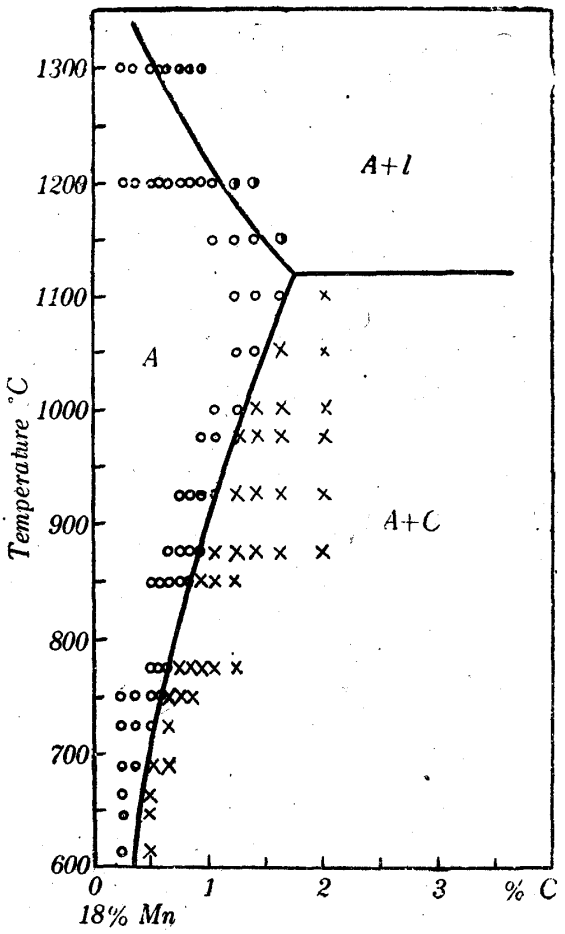

Fig. 12. Sectional diagram of iron-manganese-carbon ternary alloy at iron-manganese side with 18 per cent of manganese determined microscopically.
Small white circle: uniform γ iron ternary solid solution
Semi white circle: two-phase region of γ iron ternary solid solution and liquid.
Cross mark; two-phase region of γ iron ternary solid solution and C ternary solid solution.

(D) Solubility surface of manganese in γ iron ternary solid solution

To investigate the change of solubility of γ manganese ternary solid solution in γ iron ternary solid solution, alloys, each containing 1.0 and

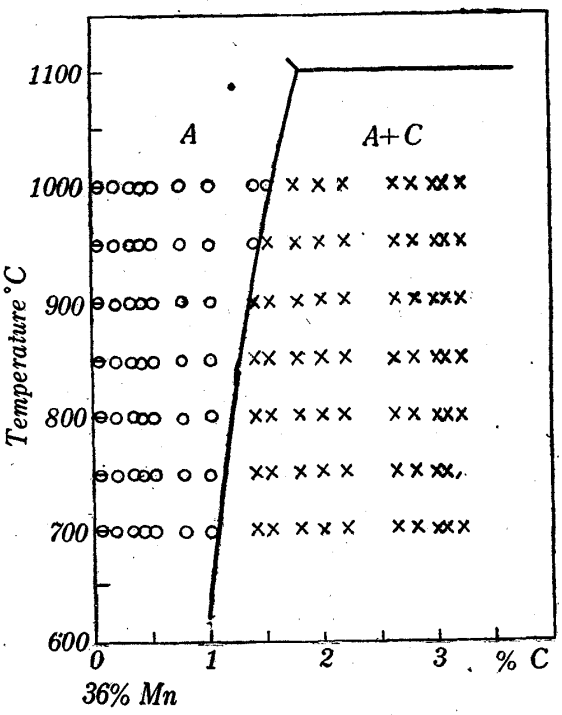

Fig. 13. Sectional diagram of iron-manganese-carbon ternary alloy at iron-manganese side with 36 per cent of manganese determined microscopically.
White small circle, uniform γ iron ternary solid solution; cross mark, two phase region of γ iron ternary solid solution and C ternary solid solution.

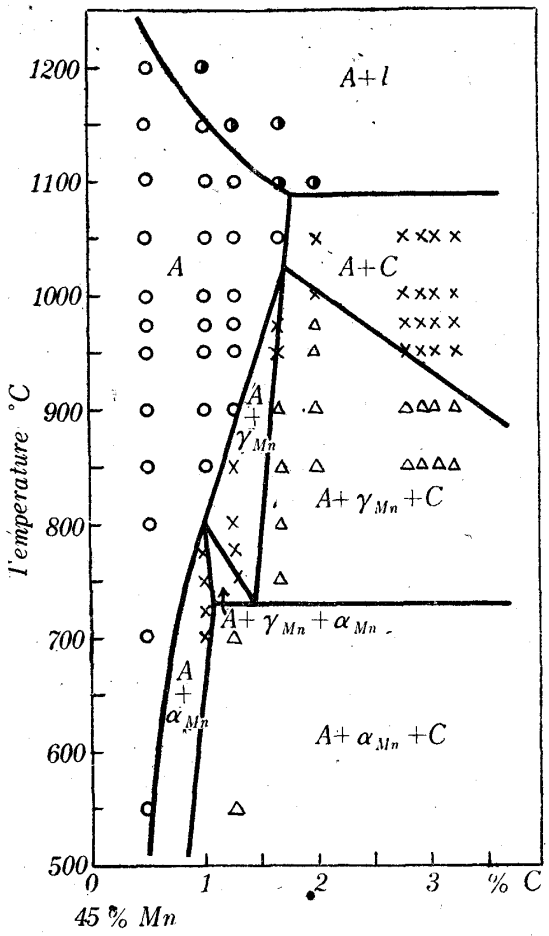

Fig. 14 Sectional diagram of iron-manganese-carbon ternary alloy at iron-manganese side with 45 per cent of manganese determined microscopically.

$A+l$: two phase region of liquid and γ iron ternary solid solution

A: uniform phase of γ iron ternary solid solution

$A+\gamma_{Mn}$: two phase region of γ iron and γ manganese ternary solid solution

$A+C$: two phase region of γ iron and C ternary solid solution

$A+\gamma_{Mn}+C$: three phase region of γ iron, γ manganese and C ternary solid solution

$A+\gamma_{Mn}+\alpha_{Mn}$: three phase region of γ iron, γ manganese and α manganese ternary solid solution

$A+\alpha_{Mn}$: two phase region of γ iron and α manganese ternary solid solution

$A+\alpha_{Mn}+C$: three phases region of γ iron, α manganese and C ternary solid solution.

1.8 per cent of carbon and different amounts of manganese, were quenched in brine ice water and were subjected to the same observation as the above. The results are shown in Tables 10 and 11. As will be seen from Table 10, the uniform phase region of γ iron ternary solid solution or of γ manganese ternary solid solution and their two-phase region were clearly seen at high temperatures, whereas two-phase region of γ and β manganese ternary solid solutions and three-phase region of γ iron, γ and β manganese ternary solid solutions appear at lower temperatures. In alloys containing about 1.9 per cent of carbon, at which the compositions were in the outside of the existing region of γ iron ternary solid solution, the uniform phase of γ iron ternary solid solution did not appear, whereas two-phase structures of γ iron and C ternary solid solution and of γ iron and γ manganese ternary solid solution or three-phase structures of γ iron, γ manganese and C ternary solid solution and of γ iron, α manganese and C ternary solid solution appeared.

Fig. 15 is the sectional diagram at the ternary alloy of 1 per cent of carbon, in which the mutual solubility of γ iron and γ manganese ternary solid solution is clearly shown, and from which three-phase regions of γ iron, γ manganese and β manganese ternary solid solution and two-phase region of γ and β manganese ternary solid solutions can be obtained. Fig. 16 shows the sectional diagram at the composition of 1.9 per cent of carbon, in which the binary eutectic structure of γ iron and C ternary solid solution, the ternary eutectic structure of γ iron, γ manganese and C ternary solid solution and the binary

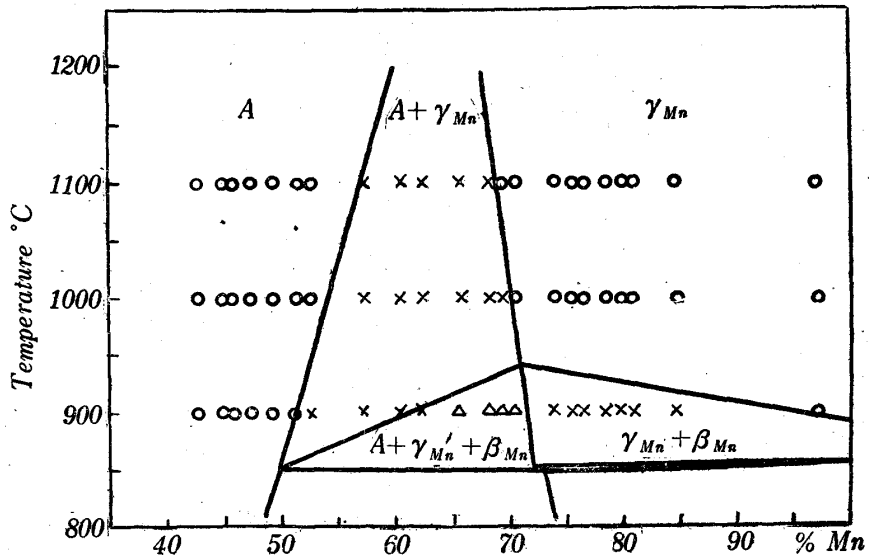

Fig. 15. Sectional diagram of iron-manganese-carbon ternary alloy at 1 per cent of carbon determined microscopically where the solubility of γ manganese ternary solid solution in γ iron ternary solid solution is clearly shown and vice versa.
White small circle : uniform phase.
Cross mark : two phase region.
Deltoid mark : three-phase region.

eutectic structure of γ manganese and γ iron ternary solid solution are seen at the left, middle and right parts, respectively. At lower temperatures the three-phase region of γ iron, α manganese and C ternary solid solution can be seen.

(E) γ iron ternary solid solution

Fig. 17 are the ternary diagram showing the existing region of γ iron ternary solid solution, in which fine lines on respective surfaces are isothermal lines. The meanings of the notations are as follows area $e'e_3e_4e_x\gamma e'$ = Acm surface ; area $e_3\mathrm{Fe}P_{11}e_4e_3 = Ar_3$ surface ; area $\gamma e_x a'P_3'\gamma$ = solubility surface of manganese in γ iron ternary solid solution, area $e_4P_{11}a'e_xe_4 = \gamma$-$h$ transformation surface ; $e'\gamma$ = solubility line of C in γ iron ternary solid solution at binary eutectic temperature of iron-

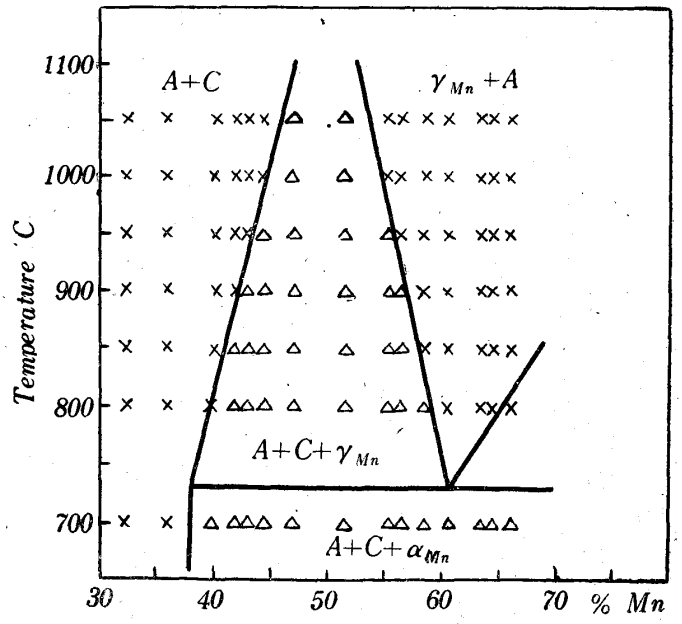

Fig. 16. Sectional diagram of iron-manganese-carbon ternary alloy at 1.9 per cent of carbon and different amounts of manganese determined microscopically.
White small circle : uniform phase.
Cross mark : two phase region.
Deltoid mark : three-phase region.

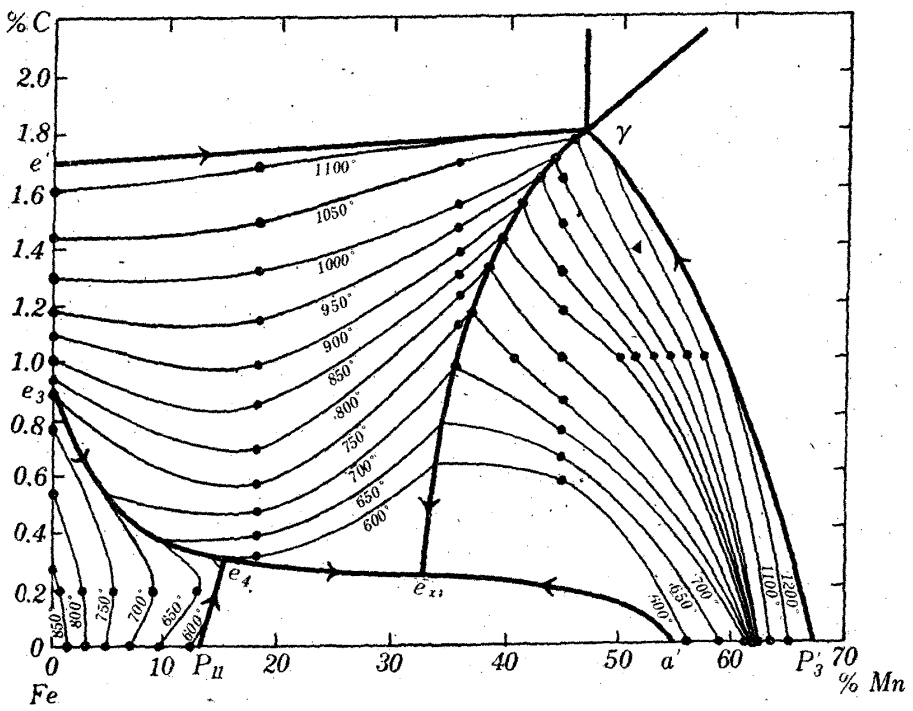

Fig. 17. Ternary diagram showing the existing region of γ iron ternary solid solution. Thin lines show the isothermal lines on respective surfaces.
Area $e'e_3e_4e_x\gamma e'$ is Acm surface. Area $e_3\mathrm{Fe}P_{11}e_4e_3$ is Ar_3 surface.
Area $\gamma e_x a' P_3'\gamma$ is solubility surface of manganese to γ iron ternary solid solution.
Area $e_4P_{11}a'e_xe_4$ is γ-h transformation surface.

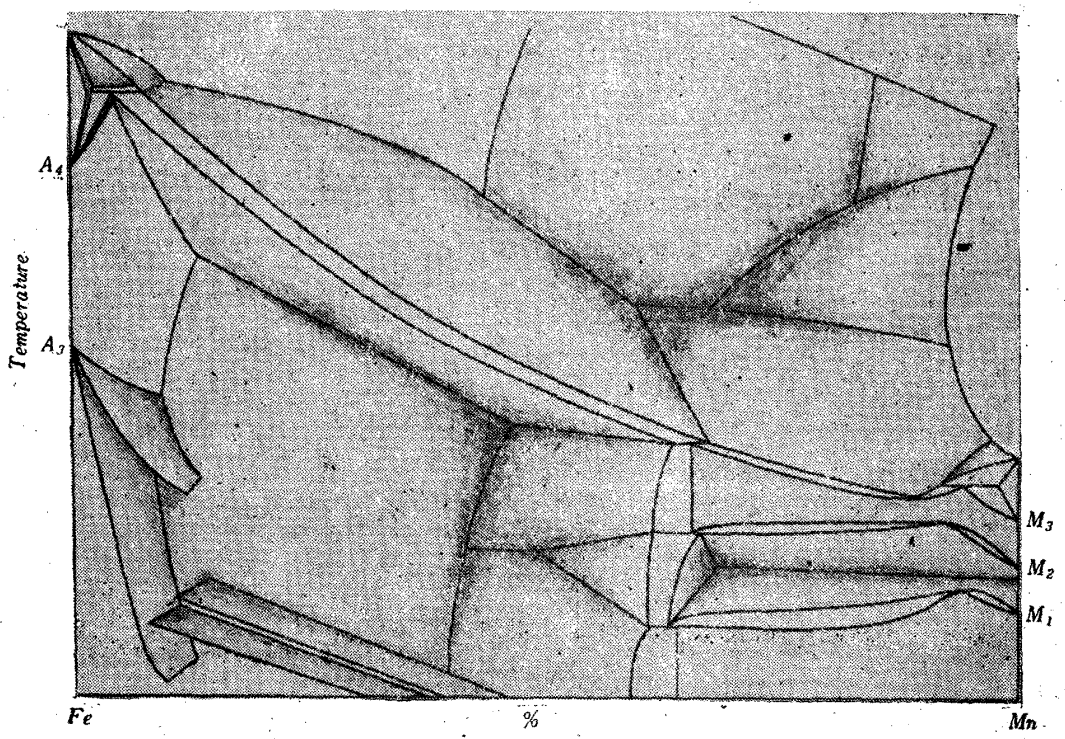

Fig. 18. Solid model of iron-manganese-carbon ternary diagram viewed from iron-manganese side. Regions of seven kinds of primary surfaces and of γ iron ternary solid solution are clearly shown.

carbon side; $P_3'\gamma$ = solubility line of γ manganese in γ iron ternary solid solution at peritectic and eutectic temperature of iron-manganese side; e_3e_4 = eutectoid line; $P_{11}e_4$ = peritectoid line; e_3 = eutectoid point of iron and carbon system; P_{11} = peritectoid point of iron and manganese system.

Fig. 18 is the cubic model of the ternary diagram viewed from the side of iron-manganese system, which is convenient to acquaint with the structure near to γ iron ternary solid solution.

(F) Structural diagrams

Figs. 19~23 are the structural diagrams of iron-manganese and carbon ternary alloys quenched at 1050°, 1000°, 900°, 800° and 700°C, respectively.

As will be seen from Fig. 19 there are seventeen kinds of regions in structural diagram of the specimens quenched at 1050°C. In the case of the quenching at 1000°C, behaviors are almost the same as above except that three-phase regions of γ iron, γ manganese and C ternary solid solution, and of βC, αC and C ternary solid solutions slightly extend toward iron side, and that regions of βC ternary solid solution and of βC and C ternary solid solutions become gradually narrow. In the structural diagram for the quenching at 900°C, the region of γ manganese ternary solid solution is greatly narrow and the two-phase region of γ manganese and β manganese ternary solid solution becomes to appear, and the two-phase re-

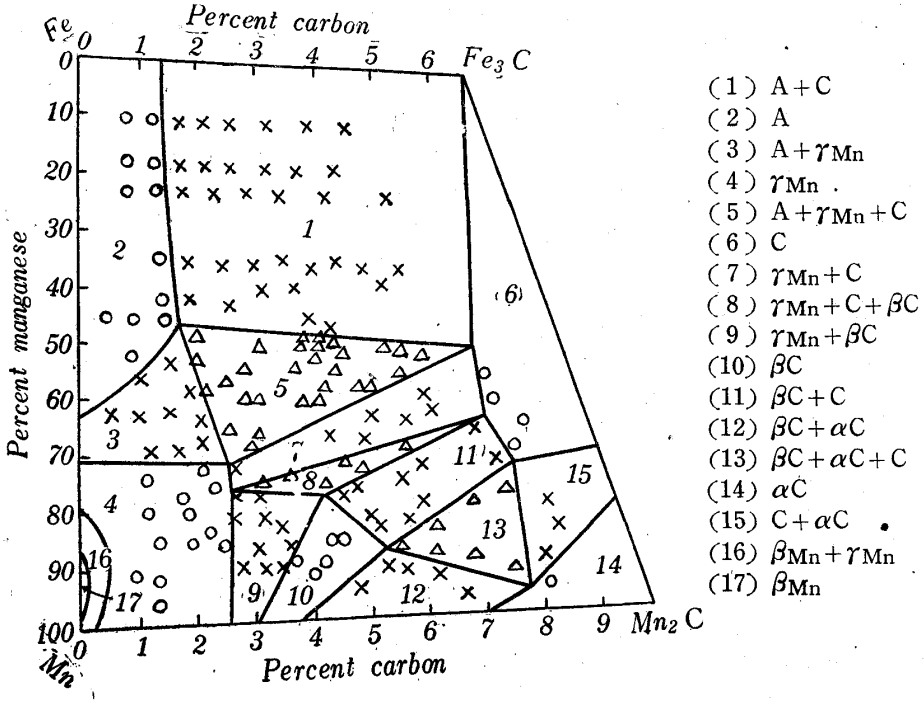

Fig. 19. Structural diagram of iron-manganese and carbon ternary alloy quenched from 1050°C in brine ice water.
White small circle shows uniform phase, cross mark two phase region and deltoid mark three phase region.
Numeral mark in each regions has the meaning as shown an appendix, respectively.

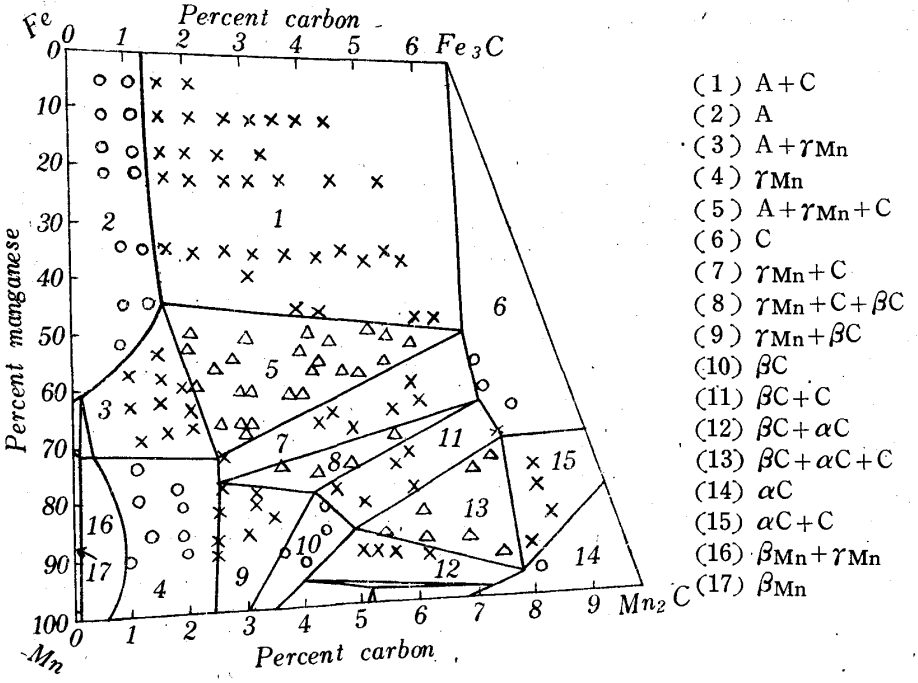

Fig. 20. Structual diagram of iron-manganese and carbon ternary alloy quenched from 1000℃ in brine ice water.
White small circle shows uniform phase, cross mark two phase regions and deltoid mark three phase region.
Numeral mark in each regions has the meaning as shown an appendix, respectively.

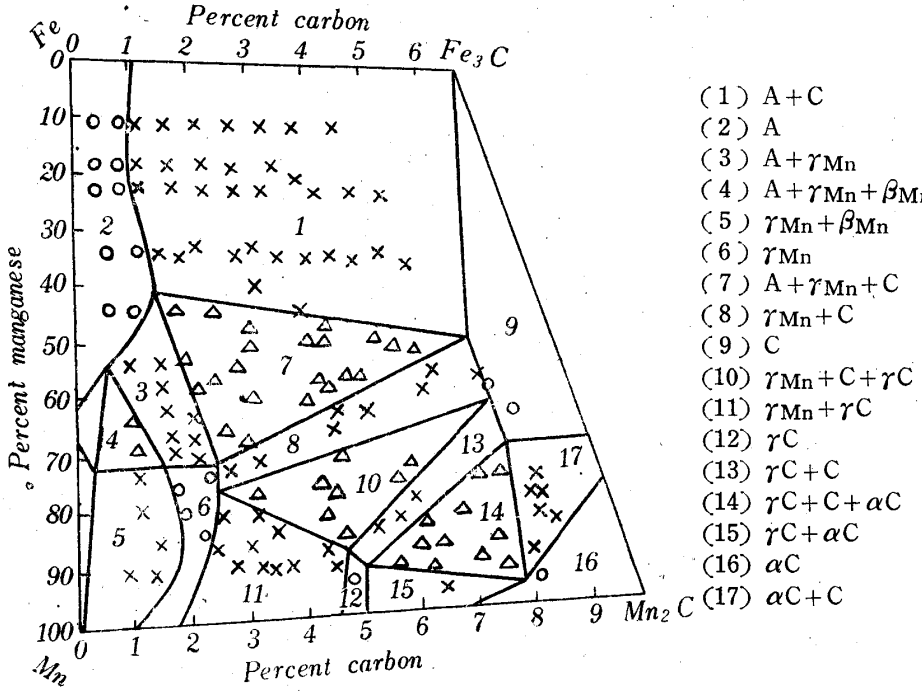

Fig. 21. Structural diagram of iron-manganese and carbon ternary alloy quenched from 900℃ in brine ice water.
White small circle shows uniform phase, cross mark two phase regions and deltoid mark three phase regions.
Numeral mark in each regions has the meaning as shown an appendix, respectively.

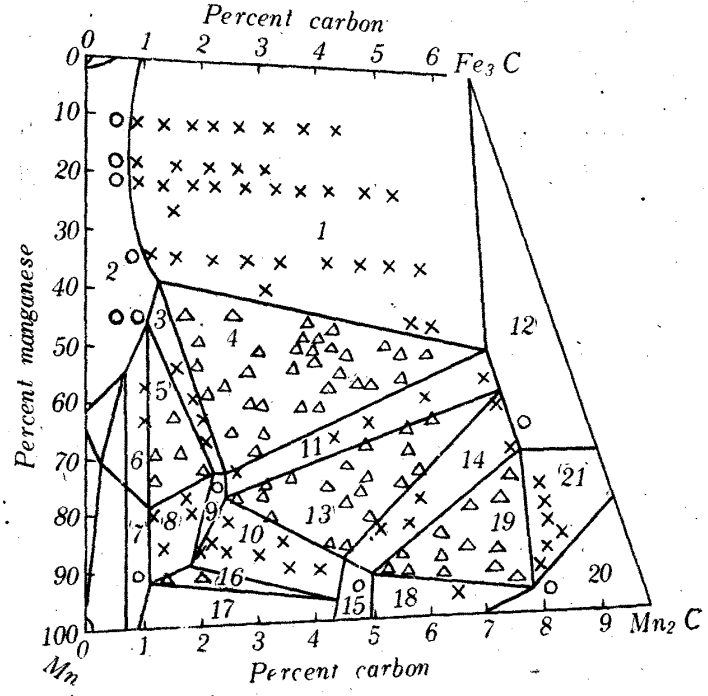

Fig. 22. Structural diagram of iron-manganese and carbon ternary alloy quenched from 800°C in brine ice water.
White small circle shows uniform phase, cross mark two phase regions and deltoid mark three phase regions.
Numeral mark in each regions has the meaning as shown an appendix, respectively.

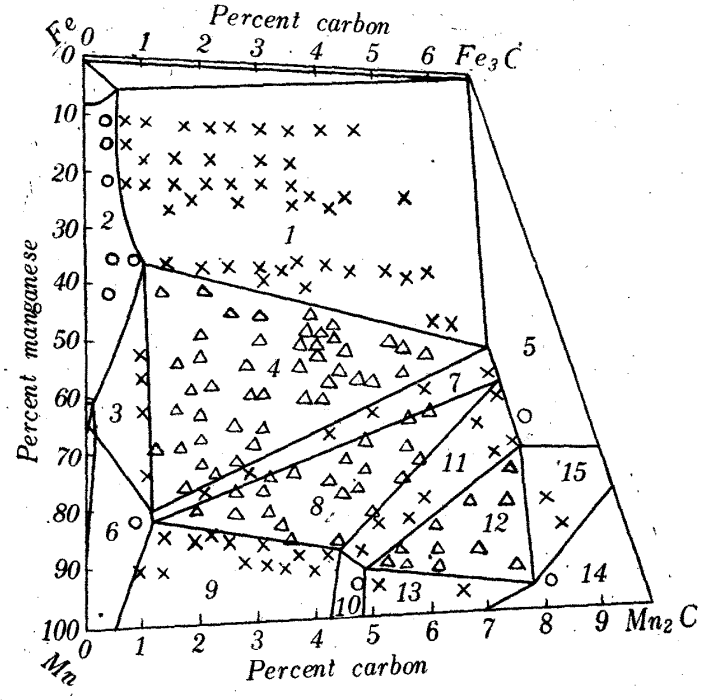

Fig. 23. Structural diagram of iron-manganese and carbon ternary alloy quenched from 700°C in brine ice water.
White small circle shows unifom phase, cross mark two phase regions and deltoid mark three phase regions.
Numeral mark in each regions has the meaning as shown an appendix, respectively.

gion of γ iron and γ manganese ternary solid solution becomes narrow and the three-phase region of γ iron, γ and β manganese ternary solid solutions newly appears. At this temperature βC ternary solid solution vanishes while γC ternary solid solution newly appears. Therefore, the differences in the mutual relationships among these phases will be recognized by comparing the regions of high carbon and high manganese in Figs. 21 and 20. Further fall of quenching temperature makes the structural diagram more complicated as shown in Fig. 22. The region of γ iron and γ manganese ternary solid solution becomes narrower and narrower and three-phase region of γ iron, γ manganese and α manganese ternary solid solution appears instead of γ iron, γ manganese and β manganese.The region of γ manganese ternary solid solution can yet clearly be recognized and the regions of α manganese ternary solid solution, and of α manganese and γ manganese ternary solid solution newly appear instead of two-phase region of γ and β manganese ternary solid solutions. The region of γ manganese and γC ternary solid solution becomes narrow and α manganese, γ manganese and γC ternary solid solution newly appear, and the region of γC ternary solid solution slightly extends. As the γ manganese ternary solid solution vanishes completely at 700°C, the structural diagram at this temperature becomes comparatively simple as shown in Fig. 23 and are not greatly different from that at room temperature.

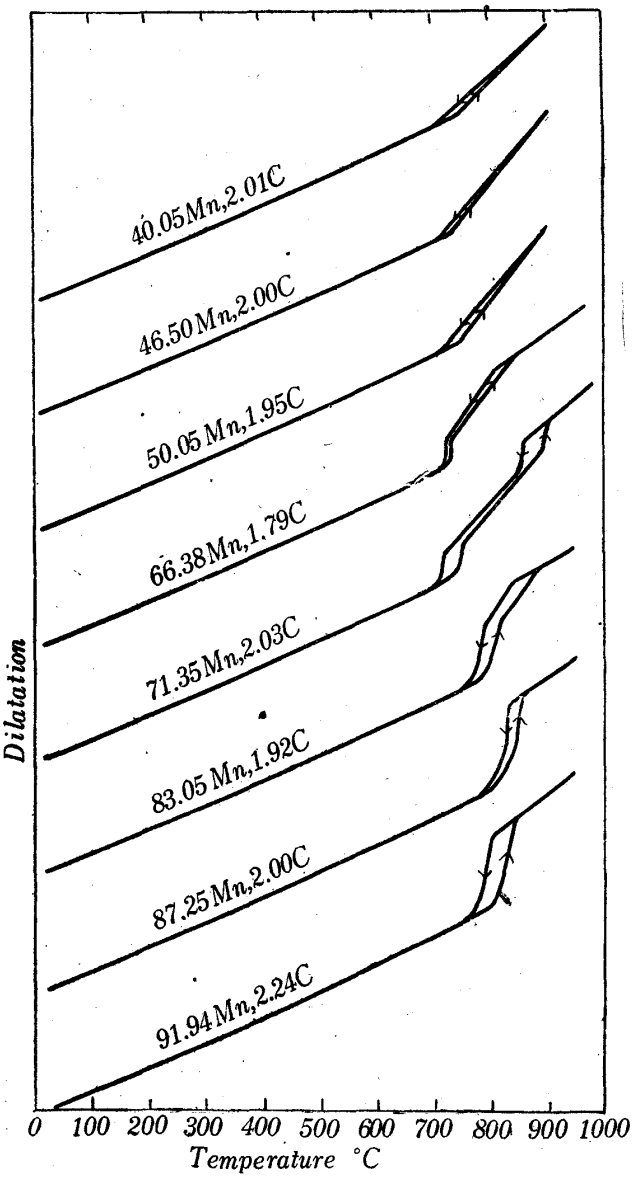

Fig. 24. Thermal dilatation curves of ternary alloy having constant carbon about 2 per cent. The compositions of alloys are annexed to respective curves.

(G) Dilatometric study of eutectoid reaction

To see the change of the eutectoid reaction at 820°C in manganese-carbon binary system owing to the addition of iron, dilatometric measurements were carried out with specimens containing about 2 per cent of carbon and different amounts of iron. The

results are shown in Fig. 24, in which the changes owing to the binary and ternary eutectoid reactions are clearly seen.

Fig. 25 is a part of sectional diagram of ternary alloy at 2 per cent of carbon constructed from the results of the dilatometric and microscopic examinations, in which cross marks are the transition points obtained by dilatation. As seen in the figure, the eutectoid temperature falls gradually as the content of iron increases and in alloys containing less than 70 per cent of manganese, the temperature is almost constant at about 730°C. This is caused by the ternary eutectoid reaction, as may be recognized from the complete diagram which will be mentioned later on. Besides the above, the change by which β manganese ternary solid solution or γC ternary solid solution crystallizes from γ manganese ternary solid solution, and the change of the co-existing region of γ iron ternary solid solution and γ manganese ternary solid solution into that of γ iron, γ manganese and α manganese ternary solid solution are seen.

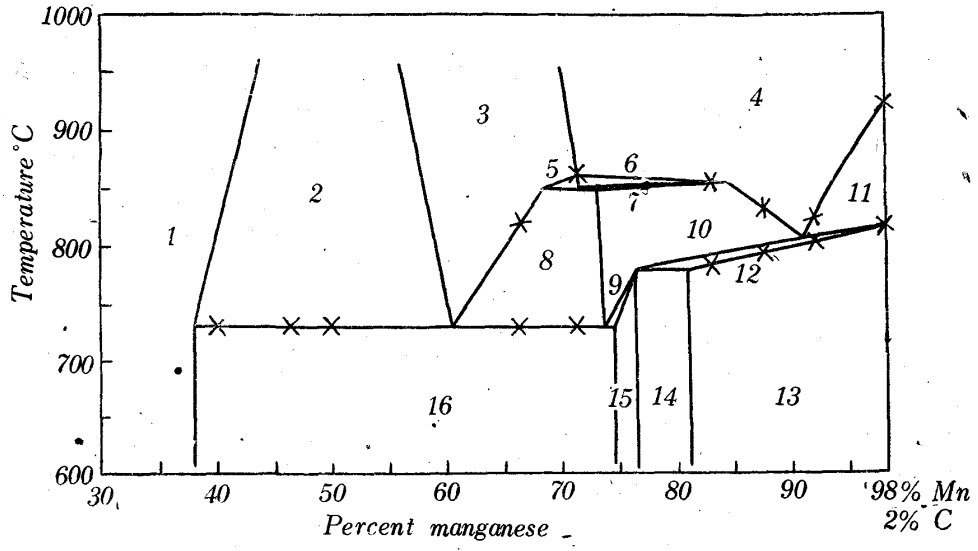

Fig. 25. A part of the 2 per cent carbon sectional diagram of iron-manganese and carbon ternary alloy in which the cross mark shows the results of dilatation measurement. A numeral mark added in the figure shows the following meaning.

1 γ iron ternary solid solution and C ternary solid soluton
2 γ iron, γ manganese and C ternary solid solution
3 γ iron and γ manganese ternary solid solution
4 γ manganese ternary solid solution
5 γ iron, γ manganese and β manganese ternary solid solution
6 γ and β manganese ternary solid solution
7 γ, β and α manganese ternary solid solution
8 γ iron, γ manganese and α manganese ternary solid solution
9 γ manganese, α manganese and C ternary solid solution
10 γ and β manganese ternary solid solution
11 γ manganese and γC ternary solid solution
12 γ and α manganese and γC ternary solid solution
13 α manganese and γC ternary solid solution
14 α manganese, γC and C ternary solid solution
15 α manganese and C ternary solid solution
16 γ iron, α manganese and C ternary solid solution

(H) Dilatometric study of alloys containing 0.21~6.15 per cent of carbon and different amounts of manganese

Some representative curves are shown in Fig. 26. In curve (1) the expansion at 750~850°C shows the behaviors of the transition from the co-existing region of α manganese, γC and C ternary solid solution to that of γ manganese ternary solid solution. Changes of α manganese ternary solid solution to β manganese ternary solid solution, and of the peritectoid reaction, γ manganese ternary solid solution + β manganese ternary solid solution $\rightleftarrows$ α manganese ternary solid solution, were clearly shown in curve (2). In curve (3) the progress of transition from the co-existing region of γ iron, α manganese and C ternary solid solution to uniform γ manganese ternary solid solution by way of that of γ manganese, α manganese and γ iron ternary solid solution is shown and the co-existing region of β manganese and γ manganese ternary solid solution are also seen. The change of the co-existing region of α manganese, γC and C ternary solid solution to that of uniform γ manganese ternary solid solution by way of the co-existing regions of γ manganese and γC ternary solid solution, and of γ manganese and βC ternary solid solution are shown in

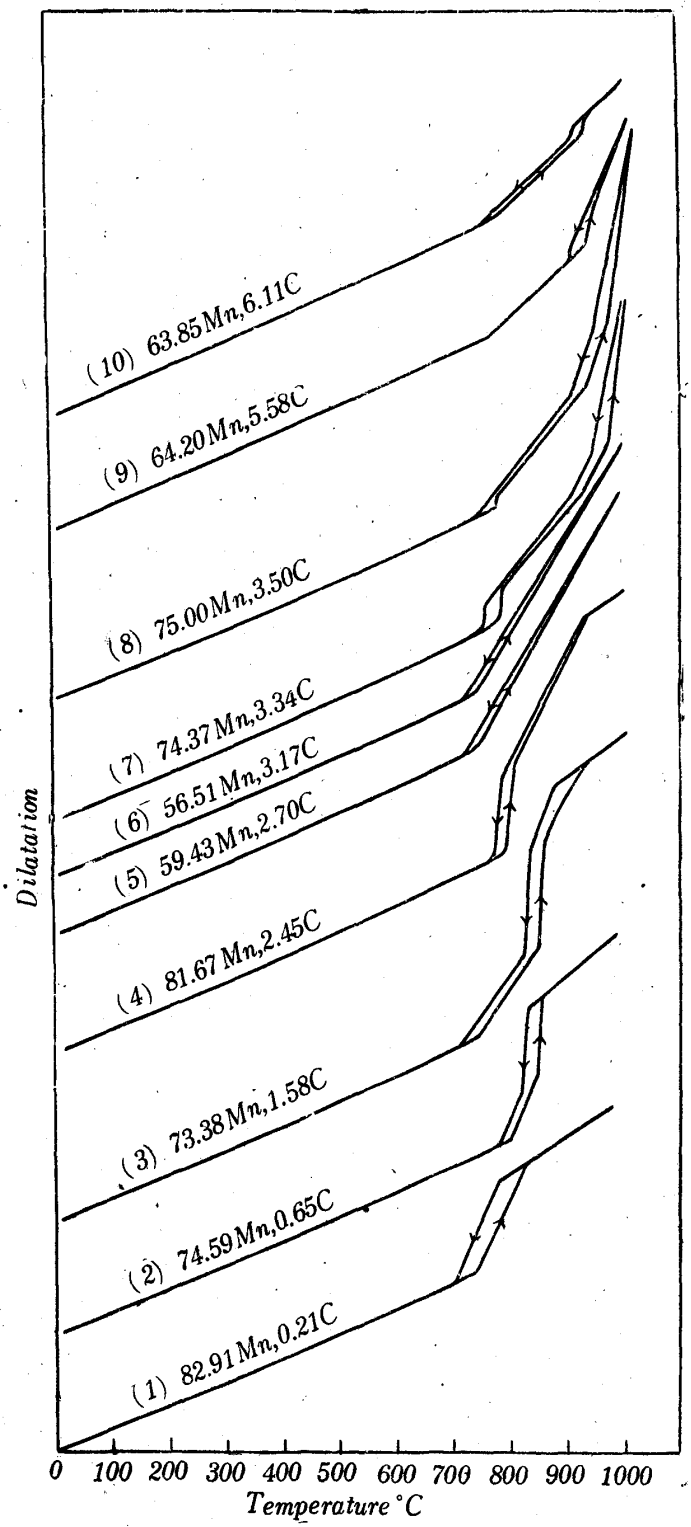

Fig. 26. Thermal dilatation curves of ternary alloys having different amount of carbon and manganese. The composition of alloys are added to the each curves.

curve (4). Curves (5) and (6) shows the behaviors of alloys containing different amounts of manganese and carbon, but both show the ternary eutectoid and change of the structure consisting of γ iron, α manganese and C ternary solid solution to that of γ iron, γ manganese and C ternary solid solution. Curves (7) and (8) show the results of alloys containing about 75 per cent of manganese and slightly different amount of carbon. Difference in the amount of peritecto-eutectoid reaction owing to slight difference in carbon content is clearly seen. In curve (9) the change of structure consisting of α manganese, γC and C ternary solid solutions to that of γ manganese, βC and C ternary solid solutions by way of γ manganese, γC and C ternary solid solutions is clearly shown by the eutectoid reaction of the latter. Curve (10) shows almost the same tendency as curve (9), but the alloy contains more carbon than the former, and accordingly the inclination of the curve at the region of γ manganese, βC and C ternary solid solutions is relatively slow compared with the former owing to the small amount of γ manganese ternary solid solution at the temperature above the eutectoid reaction.

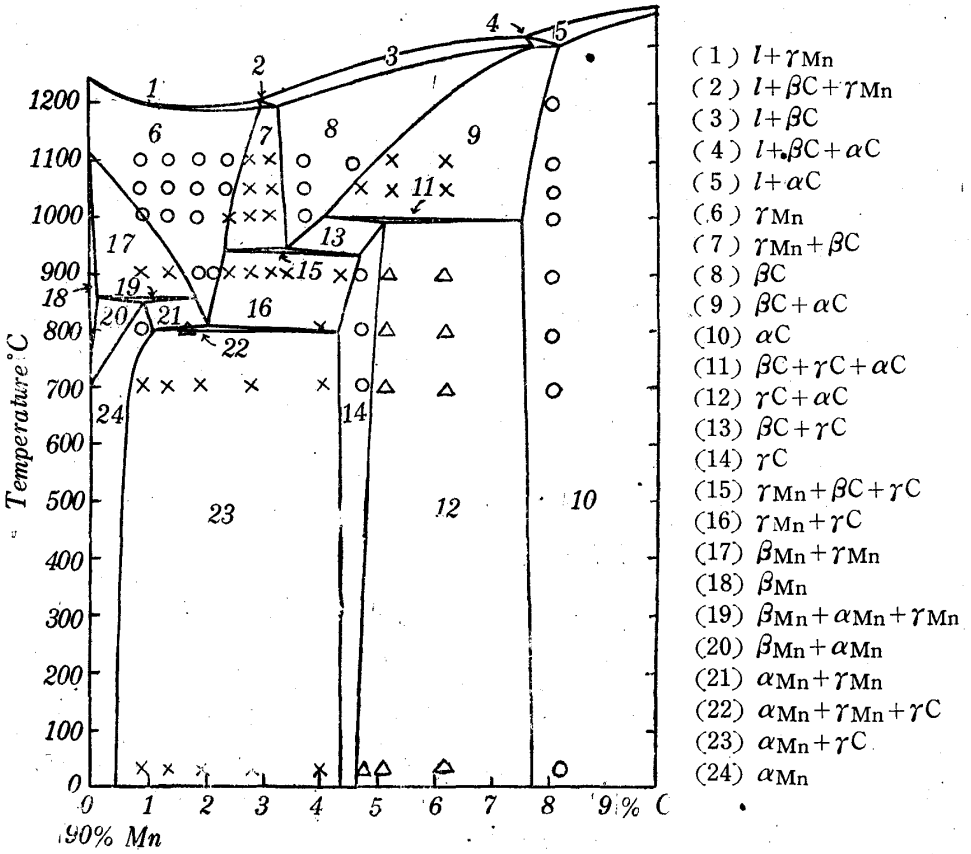

Fig. 27. 90 per cent manganese sectional diagram of iron-manganese and carbon ternary alloy.
Numeral mark in each regions has the meaning as shown an appendix, respectively.
White small circle shows uniform phase, cross mark two phase region, and deltoid three phase region, all of which show the results of microscopic investigation.

(I) Sectional diagrams

Figs. 27~35 show the sectional diagrams of alloys containing 90~50 per cent of manganese and different amounts of carbon. In these figures, white small circles signify uniform solid solutions, and cross marks the structures of two solid phases and deltoid marks the structures of three solid phases determined by microscopic investigations, and the numeral mark shows the kind of phase existing in each region.

The general tendency of Fig. 27 are not much different from the equilibrium diagram of manganese and carbon binary system except a small difference in temperature or in composition of reactions. In Fig. 28, peritecto-eutectic reaction at

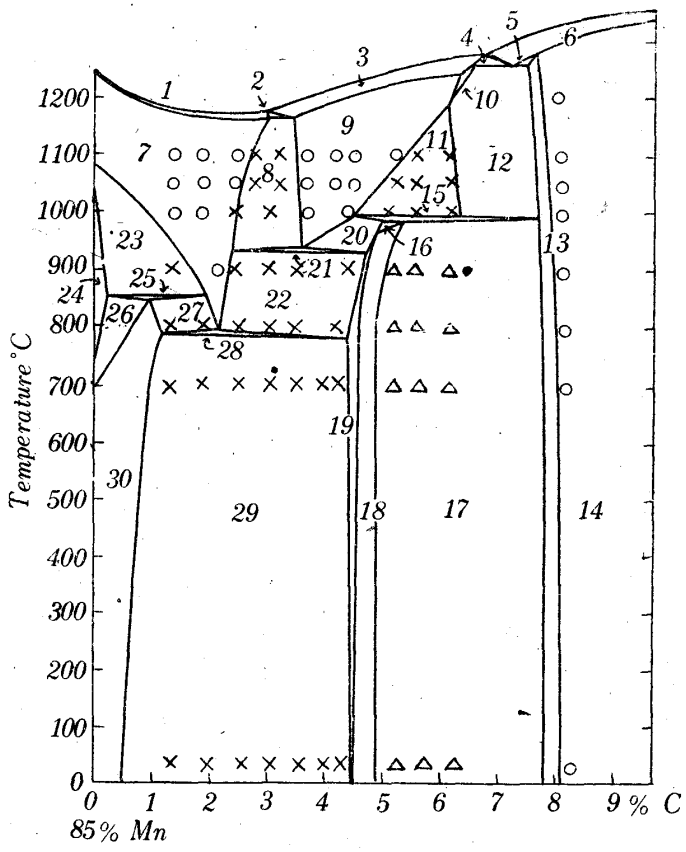

(1) $l+\gamma_{Mn}$
(2) $l+\gamma_{Mn}+\beta C$
(3) $l+\beta C$
(4) $l+\beta C+C$
(5) $l+\alpha C+C$
(6) $l+\alpha C$
(7) γ_{Mn}
(8) $\gamma_{Mn}+\beta C$
(9) βC
(10) $\beta C+C$
(11) $\beta C+\alpha C$
(12) $\beta C+\alpha C+C$
(13) $\alpha C+C$
(14) αC
(15) $\beta C+\gamma C+\alpha C$
(16) $\beta C+\gamma C+C$
(17) $\gamma C+\alpha C+C$
(18) $\gamma C+C$
(19) γC
(20) $\beta C+\gamma C$
(21) $\beta C+\gamma C+\gamma_{Mn}$
(22) $\gamma_{Mn}+\gamma C$
(23) $\beta_{Mn}+\gamma_{Mn}$
(24) β_{Mn}
(25) $\beta_{Mn}+\gamma_{Mn}+\alpha_{Mn}$
(26) $\beta_{Mn}+\alpha_{Mn}$
(27) $\alpha_{Mn}+\gamma_{Mn}$
(28) $\alpha_{Mn}+\gamma_{Mn}+\gamma C$
(29) $\alpha_{Mn}+\gamma C$
(30) α_{Mn}

Fig. 28. 85 per cent manganese sectional diagram of iron-manganese and carbon ternary alloy. Numeral mark in each regions has the meaning as shown an appendix, respectively. White small circle shows uniform phase, cross mark two phase region, and deltoid three phase region, all of which show the results of microscopic investigation.

1260°C is seen at the alloys of high carbon, and in solid state peritecto-eutectoid reaction comes to appear. The region of γC ternary solid solution scarcely remained, being replaced by two-phase region of γC and C ternary solid solutions. In Fig. 29, the region of αC ternary solid solution becomes narrow, whereas the coexisting region of αC and C ternary solid solution becomes broad. Ternary eutectoid reaction at 925°C and peritecto-eutectoid reaction at 780°C newly appears and at the temperatures lewer than that of latter, the structures consist of α man-

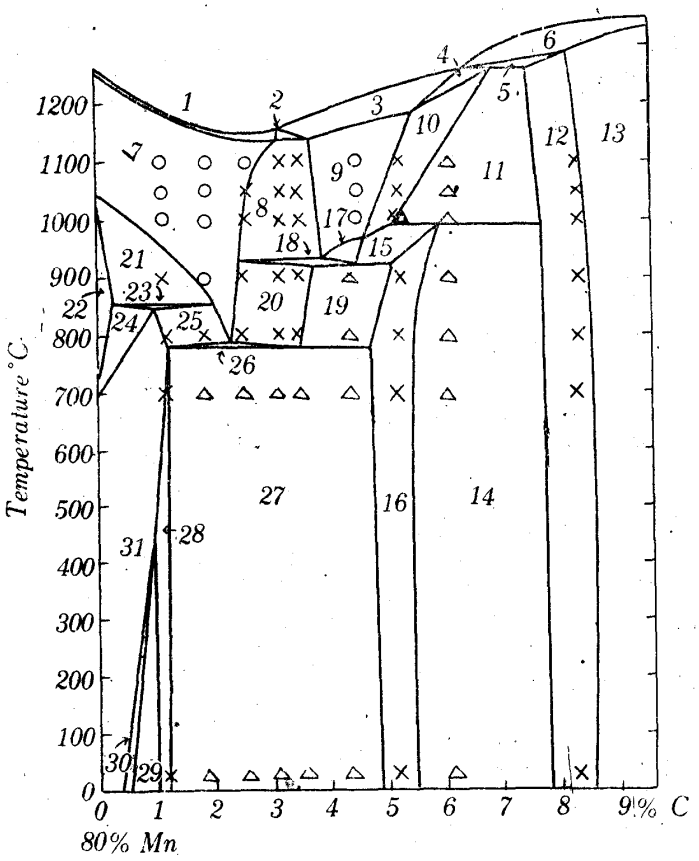

(1) $l+\gamma_{Mn}$
(2) $l+\gamma_{Mn}+\beta C$
(3) $l+\beta C$
(4) $l+\beta C+C$
(5) $l+\alpha C+C$
(6) $l+\alpha C$
(7) γ_{Mn}
(8) $\gamma_{Mn}+\beta C$
(9) βC
(10) $\beta C+C$
(11) $\beta C+\alpha C+C$
(12) $\alpha C+C$
(13) αC
(14) $\gamma C+\alpha C+C$
(15) $\beta C+\gamma C+C$
(16) $\gamma C+C$
(17) $\beta C+\gamma C$
(18) $\gamma_{Mn}+\beta C+\gamma C$
(19) $\gamma_{Mn}+\gamma C+C$
(20) $\gamma_{Mn}+\gamma C$
(21) $\beta_{Mn}+\gamma_{Mn}$
(22) β_{Mn}
(23) $\alpha_{Mn}+\beta_{Mn}+\gamma_{Mn}$
(24) $\beta_{Mn}+\alpha_{Mn}$
(25) $\alpha_{Mn}+\gamma_{Mn}$
(26) $\alpha_{Mn}+\gamma_{Mn}+\gamma C$
(27) $\alpha_{Mn}+\gamma C+C$
(28) $\alpha_{Mn}+C$
(29) $\alpha_{Mn}+A+C$
(30) $\alpha_{Mn}+A$
(31) α_{Mn}

Fig. 29. 80 per cent manganese sectional diagram of iron-manganese and carbon ternary alloy. Numeral mark in each regions has the meaning as shown an appendix, respectively. White small circle shows uniform phase, cross mark two phase region, and the deltoid three phase region, all of which show the results of microscopic investigation.

ganese, γC and C ternary solid solutions. A slight difference in the region of α manganese ternary solid solution is due to the change of mutual solubility of respective phases. In Fig. 30, the region of αC ternary solid solution becomes narrow at high carbon parts, and at low carbon parts, a peritecto-eutectoid reaction appears at 850°C and a ternary eutectoid reaction is slightly seen at 730°C. In Fig. 31, the uniform solid solution of αC vanishes completely at high carbon part, whereas the two-phase region of αC and C solid solution remains. The uniform region of βC solid solution vanishes completely but the solid solution remains only in two- and threephase coexisting regions. The region of γ manganese ternary solid solution becomes very narrow, remaining scarcely at high temperatures, and the coexisting region of γ iron and γ manganese ternary solid solution is developed. The coexisting region of α manganese, γ iron and C ternary solid solution is extended, and the region of α manganese is very small.

In Fig. 32, the uniform region of C ternary solid solution appears at high carbon and high temperature part and a trace of peritecto-eutectoid reaction is recognized at 990°C. The region of γ manganese solid solution vanishes completely, and that of γ iron ternary solid solution newly appears at low carbon and high temperature part. Ternary eutectic reaction fairly appears, and the region of γ manga-

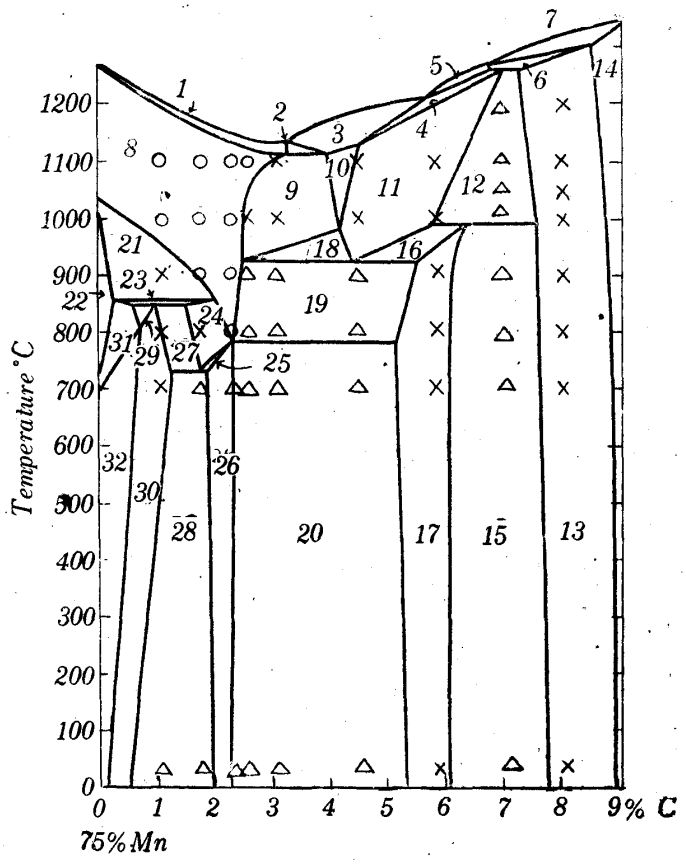

(1) $l+\gamma_{Mn}$
(2) $l+\gamma_{Mn}+\beta C$
(3) $l+\beta C$
(4) $l+\beta C+C$
(5) $l+C$
(6) $l+\alpha C+C$
(7) $l+\alpha C$
(8) γ_{Mn}
(9) $\gamma_{Mn}+\beta C$
(10) βC
(11) $\beta C+C$
(12) $\beta C+\alpha C+C$
(13) $\alpha C+C$
(14) αC
(15) $\gamma C+\alpha C+C$
(16) $\beta C+\gamma C+C$
(17) $\gamma C+C$
(18) $\gamma_{Mn}+\beta C+C$
(19) $\gamma_{Mn}+\gamma C+C$
(20) $\alpha_{Mn}+C+\gamma C$
(21) $\beta_{Mn}+\gamma_{Mn}$
(22) β_{Mn}
(23) $\beta_{Mn}+\gamma_{Mn}+\alpha_{Mn}$
(24) $\alpha_{Mn}+\gamma_{Mn}$
(25) $\alpha_{Mn}+C+\gamma_{Mn}$
(26) $\alpha_{Mn}+C$
(27) $\gamma_{Mn}+\alpha_{Mn}+A$
(28) $A+\alpha_{Mn}+C$
(29) $A+\alpha_{Mn}+\beta_{Mn}$
(30) $\alpha_{Mn}+A$
(31) $\beta_{Mn}+\alpha_{Mn}$
(32) α_{Mn}

Fig. 30. 75 per cent manganese sectional diagram of iron-manganese and carbon ternary alloy. Numeral mark in each regions has the meaning as shown an appendix, respectively. White small circle shows uniform phase, cross mark two phase region, and the deltoid three phase region, all of which show the results of microscopic investigation.

(1) $l+A$
(2) $l+A+\gamma_{Mn}$
(3) $l+\gamma_{Mn}$
(4) $l+\gamma_{Mn}+C$
(5) $l+\gamma_{Mn}+\beta C$
(6) $l+\beta C$
(7) $l+\beta C+C$
(8) $l+C$
(9) $l+\alpha C+C$
(10) $l+\alpha C$
(11) $A+\gamma_{Mn}$
(12) γ_{Mn}
(13) $\gamma_{Mn}+C$
(14) $\gamma_{Mn}+C+\beta C$
(15) $\beta C+C$
(16) C
(17) $\alpha C+C$
(18) $C+\beta C+\alpha C$
(19) $\gamma C+C+\alpha C$
(20) $\beta C+\gamma C+C$
(21) $\gamma C+C$
(22) $\gamma_{Mn}+\gamma C+C$
(23) $\alpha_{Mn}+\gamma C+C$
(24) $\gamma_{Mn}+\alpha_{Mn}+C$
(25) $\alpha_{Mn}+C$
(26) $\gamma_{Mn}+A+C$
(27) $\gamma_{Mn}+A+\beta_{Mn}$
(28) $A+\beta_{Mn}$
(29) β_{Mn}
(30) $A+\beta_{Mn}+\alpha_{Mn}$
(31) $\alpha_{Mn}+A+\gamma_{Mn}$
(32) $\alpha_{Mn}+A+C$
(33) $\alpha_{Mn}+A$
(34) $\alpha_{Mn}+\beta_{Mn}$
(35) α_{Mn}

Fig. 31. 70 per cent manganese sectional diagram of iron-manganese and carbon ternary alloy. Numeral mark in each regions has the meaning as shown an appendix, respectively. White small circle shows uniform phase, cross mark two phase region, and the deltoid three phase region, all of which show the results of microscopic investigation.

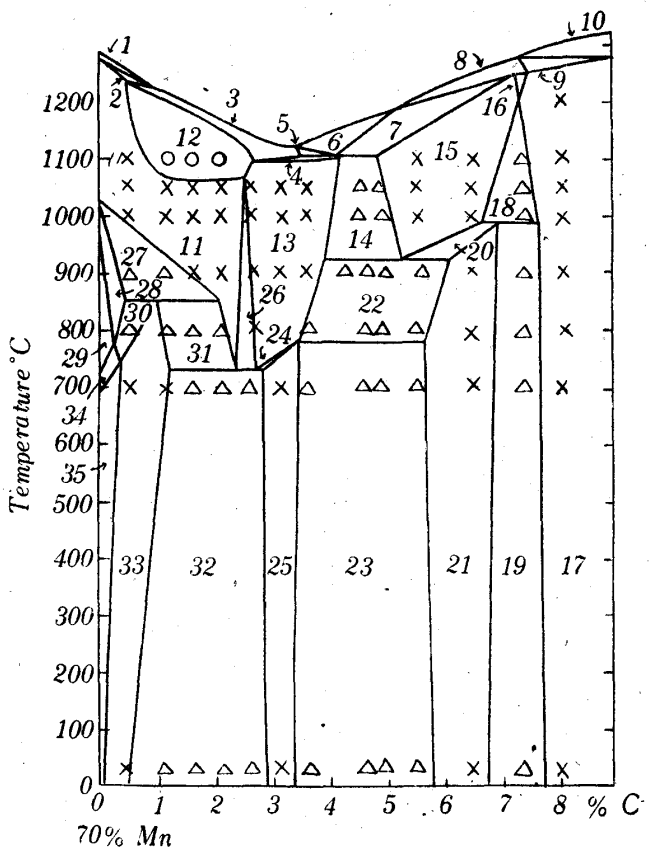

(1) l+A
(2) l+A+γ_{Mn}
(3) l+γ_{Mn}
(4) l+γ_{Mn}+C
(5) l+γ_{Mn}+βC
(6) l+βC
(7) l+βC+C
(8) l+C
(9) l+αC+C
(10) l+αC
(11) A
(12) A+γ_{Mn}
(13) γ_{Mn}+A+C
(14) γ_{Mn}+C
(15) γ_{Mn}+βC+C
(16) βC+C
(17) C
(18) αC+C
(19) βC+C+αC
(20) C+αC+γC
(21) βC+αC+C
(22) γC+C
(23) γ_{Mn}+γC+C
(24) α_{Mn}+γC+C
(25) γ_{Mn}+α_{Mn}+C
(26) α_{Mn}+C
(27) A+α_{Mn}+C
(28) A+γ_{Mn}+β_{Mn}
(29) β_{Mn}
(30) A+α_{Mn}+γ_{Mn}
(31) A+β_{Mn}+α_{Mn}
(32) A+α_{Mn}

Fig. 32. 65 per cent manganese sectional diagram of iron-manganese and carbon ternary alloy. Numeral mark in each regions has the meaning as shown an appendix, respectively. White small circle shows uniform phase region, cross mark two phase region, and deltoid three phase region, all of which show the results of microscopic investigation.

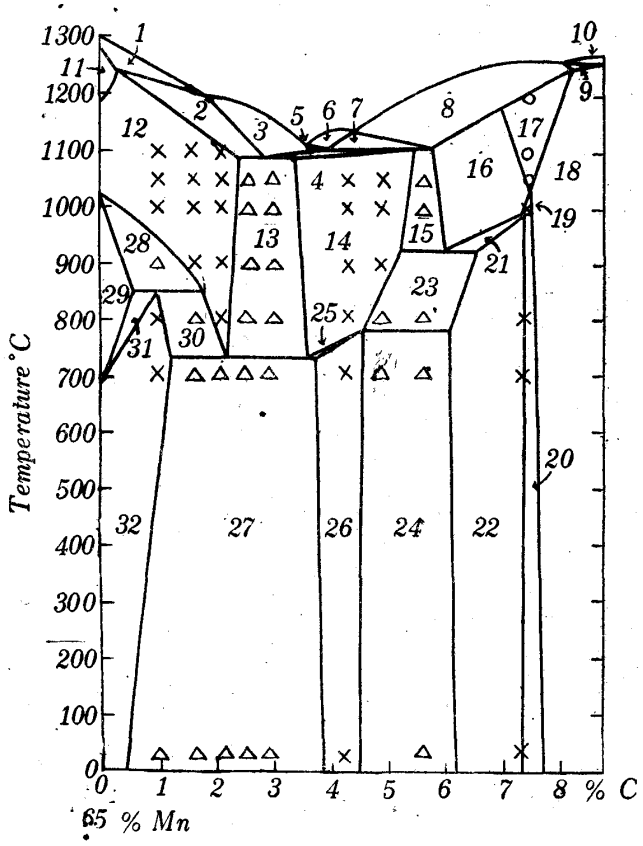

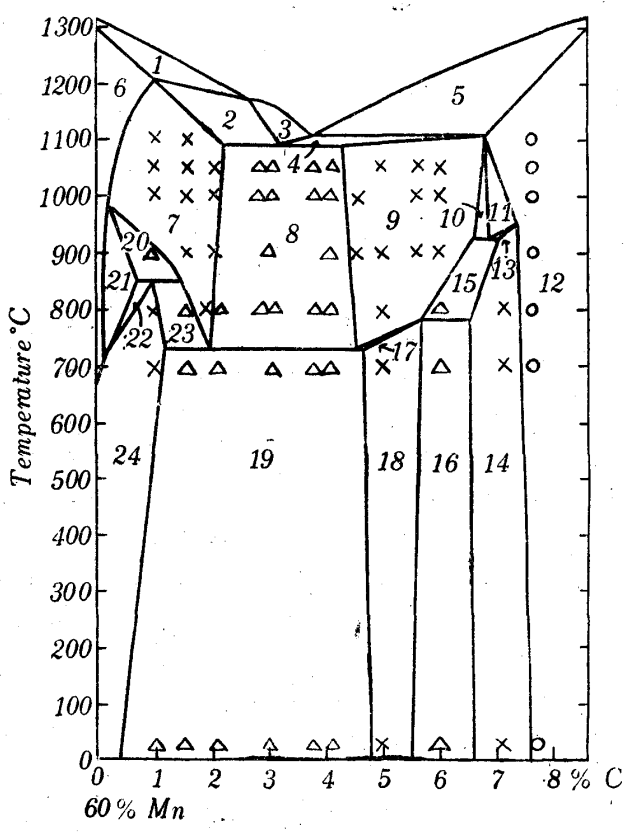

(1) l+A
(2) l+A+γ_{Mn}
(3) l+γ_{Mn}
(4) l+γ_{Mn}+C
(5) l+C
(6) A
(7) A+γ_{Mn}
(8) A+γ_{Mn}+C
(9) γ_{Mn}+C
(10) γ_{Mn}+C+βC
(11) βC+C
(12) C
(13) βC+γC+C
(14) γC+C
(15) γ_{Mn}+C+γC
(16) α_{Mn}+γC+C
(17) γ_{Mn}+α_{Mn}+C
(18) α_{Mn}+C
(19) A+α_{Mn}+C
(20) A+γ_{Mn}+β_{Mn}
(21) A+β_{Mn}
(22) A+β_{Mn}+α_{Mn}
(23) A+γ_{Mn}+α_{Mn}
(24) A+α_{Mn}

Fig. 33. 60 per cent manganese sectional diagram of iron-manganese and carbon ternary alloy. Numeral mark in each regions has the meaning as shown an appendix, respectively. White small circle shows uniform phase region, cross mark two phase region, and deltoid three phase region, all of which show the results of microscopic investigation.

nese, γ iron and C ternary solid solution is developed after this reaction. Ternary eutectoid reaction becomes more and more conspicuous, and the region of α manganese ternary solid solution at low carbon vanished completely. In Fig. 33 the region of αC and C ternary solid solutions vanishes and the region of C ternary solid solution becomes clear and the reactions of ternary eutectic and of ternary eutectoid are still remarkable. The region of γ iron ternary solid solution is developed, confirming the existence even in the neighbourhood of 700°C. In Fig. 34, the change of the peritecto-eutectic reaction at 1105°C vanishes completely and the

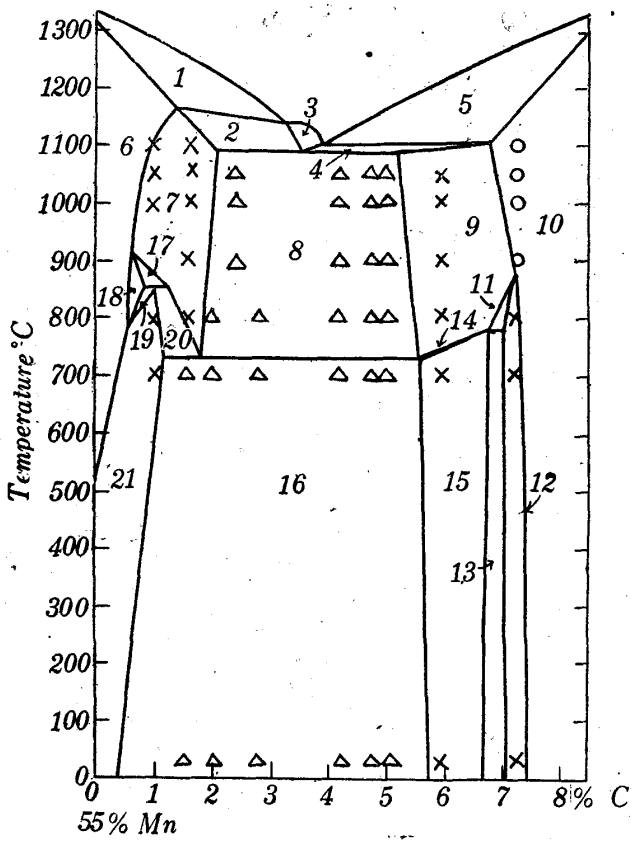

(1) l+A
(2) l+A+γ_{Mn}
(3) l+γ_{Mn}
(4) l+γ_{Mn}+C
(5) l+C
(6) A
(7) A+γ_{Mn}
(8) A+γ_{Mn}+C
(9) γ_{Mn}+C
(10) C
(11) γ_{Mn}+γC+C
(12) C+γC
(13) α_{Mn}+C+γC
(14) γ_{Mn}+α_{Mn}+C
(15) α_{Mn}+C
(16) A+α_{Mn}+C
(17) A+γ_{Mn}+β_{Mn}
(18) A+β_{Mn}
(19) A+β_{Mn}+α_{Mn}
(20) A+γ_{Mn}+α_{Mn}
(21) A+α_{Mn}

Fig. 34. 55 per cent manganese sectional diagram of iron-manganese and carbon ternary alloy. Numeral mark in each regions has the meaning as shown an appendix, respectively. White small circle shows uniform phase region, cross mark two phase region, and deltoid three phase region, all of which show the results of microscopic investigation.

peritecto-eutectoid reaction at 780°C is very small. The region of γ iron ternary solid solution is more developed and the peritecto-eutectoid reaction at 850°C is very small. In Fig. 35, peritecto-eutectoid reaction at 780°C vanishes completely, and the peritecto-eutectoid reaction at 850°C also vanishes at lower carbon parts, because the alloying composition becomes beyond that of the region of this reaction. Ternary eutectic and ternary eutectoid reactions are both conspicuous. In general, kinds of crystallizing phases diminish and the sectional diagram becomes very simple as the amount of manganese falls. The primary surface of γ manganese ternary solid solution scarcely appears in this section. In the sectional diagrams at alloys containing still lower percentage of manganese, primary surfaces are composed of γ iron and C ternary solid solution and the surface of γ manganese solid solution vanishes, and the region of γ iron ternary solid solution extends to room temperature, and then the sectional diagrams are simplified.

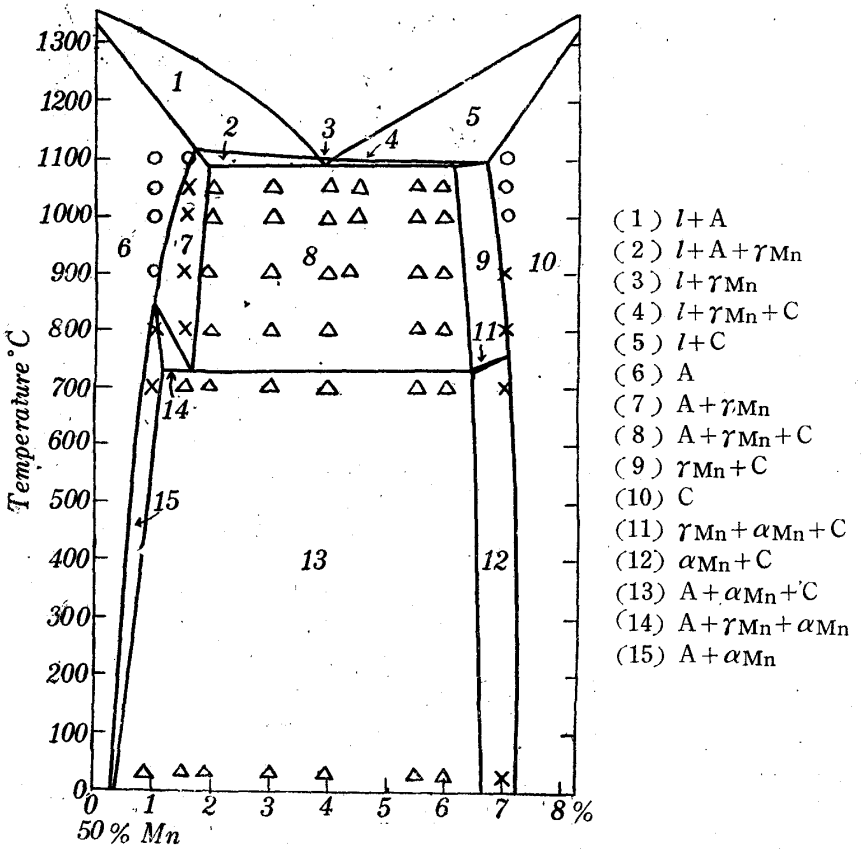

Fig. 35. 50 per cent manganese sectional diagram of iron-manganese and carbon ternary alloy. Numeral mark in each regions has the meaning as shown an appendix, respectively. White small circle shows uniform phase region, cross mark two phase region, and deltoid three phase region, all of which show the results of microscopic investigation.

Figs. 36~46 show the sectional diagrams of alloys containing 1.0~6.0 per cent of carbon and different amounts of manganese. In Fig. 36, as the alloys contain more carbon than solubility limit in γ iron ternary solid solution, the region of γ iron and C ternary solid solution clearly appears below about 900°C, and the regions of phases concerning the peritecto-eutectoid reaction at 150°C become remarkable at low temperatures. In alloys containing about 50~70 per cent of manganese, the coexisting region of γ iron and γ manganese ternary solid solution appears owing to the peritectic reaction of iron-manganese binary system at high temperatures. The region of γ manganese and β manganese ternary solid solution also appears. As the temperature falls, the eutecto-peritectoid reaction at 850°C grows clear. A part of region of α manganese ternary solid solution also appears. At lower temperatures, the coexisting region of γ iron, α manganese and C ternary solid solution, and that of α manganese and γC ternary solid solution, and other regions become to appear owing to the changes of mutual solubilities. In Fig. 37, the region of γ iron ternary solid solution scarcely remains at high temperatures, and the region of γ manganese ternary solid solution, and the coexisting region of γ manganese and γ iron ternary solid solution and that of γ iron, α manganese and

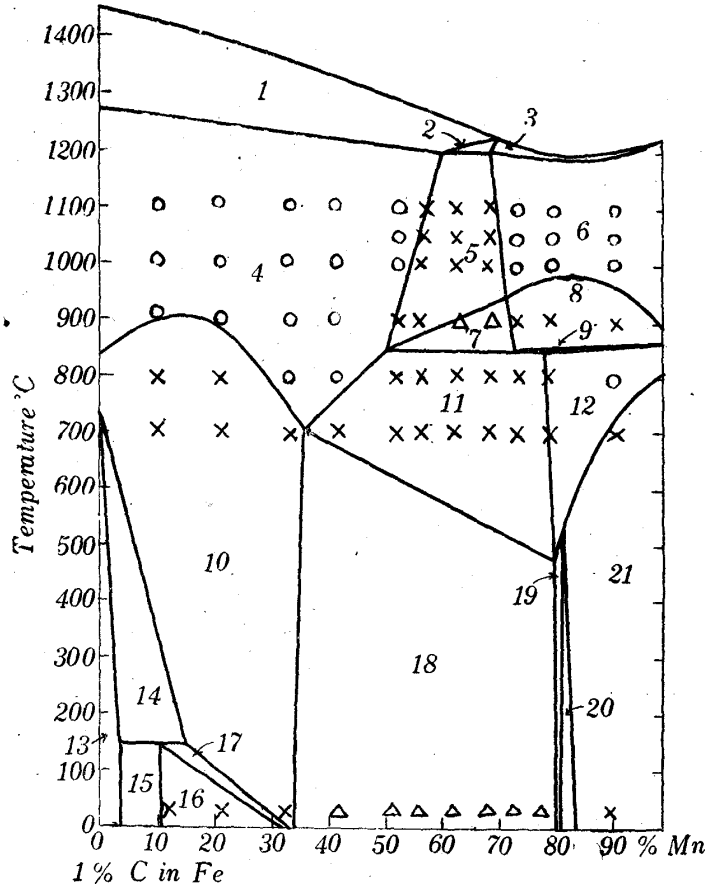

(1) l+A
(2) l+A+γ_{Mn}
(3) l+γ_{Mn}
(4) A
(5) A+γ_{Mn}
(6) γ_{Mn}
(7) A+γ_{Mn}+β_{Mn}
(8) γ_{Mn}+β_{Mn}
(9) γ_{Mn}+β_{Mn}+α_{Mn}
(10) A+C
(11) A+α_{Mn}
(12) α_{Mn}
(13) F+C
(14) A+F+C
(15) F+h+C
(16) h+C
(17) A+h+C
(18) A+α_{Mn}+C
(19) α_{Mn}+C
(20) α_{Mn}+γC+C
(21) α_{Mn}+γC

Fig. 36. 1.0 per cent carbon sectional diagram of iron-manganese and carbon ternary alloy. Numeral mark in each regions has the meaning as shown in an appendix, respectively. White small circle shows uniform phase region, cross mark two phase region, and deltoid three phase region, all of which show the results of microscopic investigation.

(1) l+A
(2) l+A+γ_{Mn}
(3) l+γ_{Mn}
(4) A
(5) A+γ_{Mn}
(6) γ_{Mn}
(7) A+γ_{Mn}+β_{Mn}
(8) γ_{Mn}+β_{Mn}
(9) γ_{Mn}+β_{Mn}+α_{Mn}
(10) A+C
(11) A+γ_{Mn}+C
(12) A+γ_{Mn}+α_{Mn}
(13) γ_{Mn}+β_{Mn}
(14) γ_{Mn}+γC
(15) γ_{Mn}+α_{Mn}+γC
(16) γ_{Mn}+α_{Mn}+C
(17) F+C
(18) A+F+C
(19) F+C+h
(20) h+C
(21) A+h+C
(22) A+α_{Mn}+C
(23) α_{Mn}+C
(24) α_{Mn}+C+γC
(25) α_{Mn}+γC

Fig. 37. 1.5 per cent carbon sectional diagram of iron-manganese and carbon ternary alloy. Numeral mark in each regions has the meaning as shown in an appendix, respectively. White small circle shows uniform phase region, cross mark two phase region, and deltoid three phase region, all of which show the results of microscopic investigation.

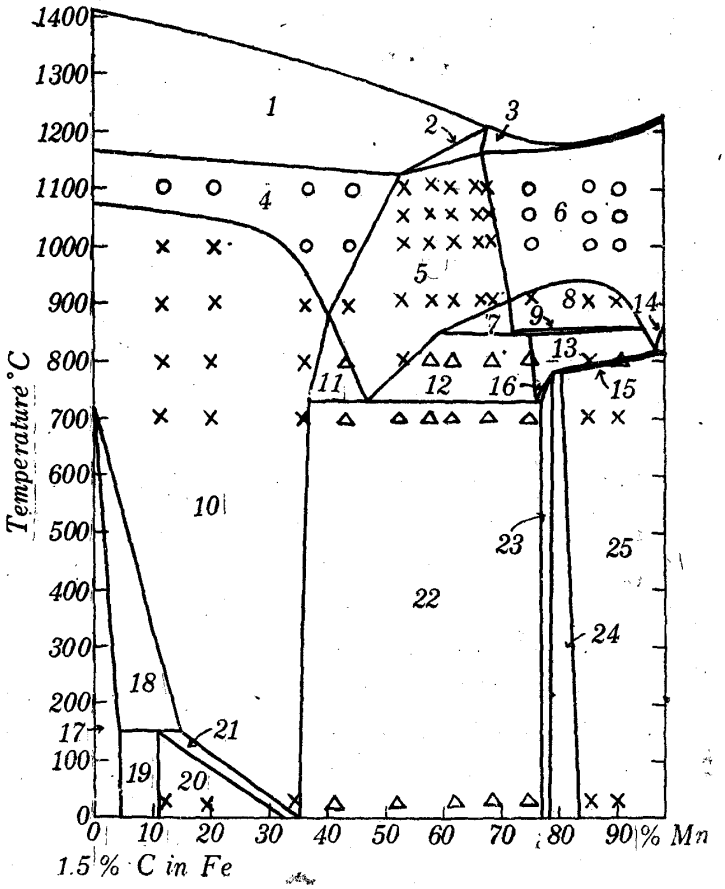

C ternary solid solution are extended. The coexisting region of γ iron, γ manganese and α manganese ternary solid solution is clearly recognized. Changes at 720° and 780°C are also recognized besides the change due to the transformation at 850°C. In Fig. 38, the region of γ iron ternary solid solution wholly disappears,

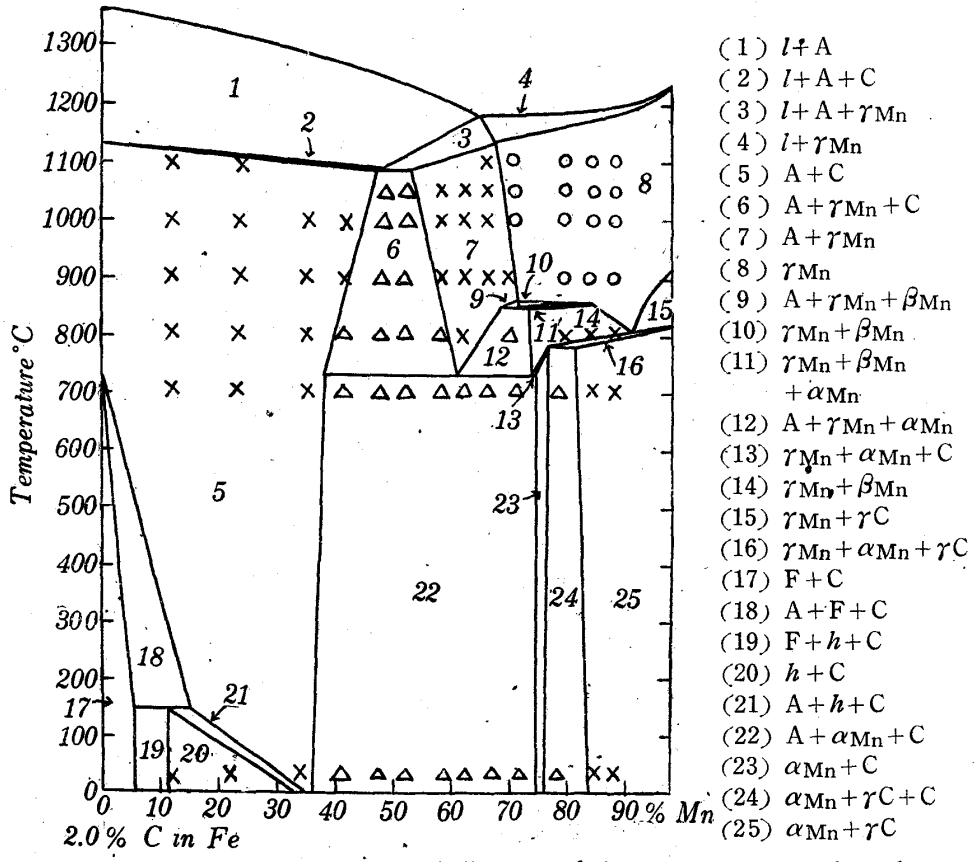

Fig. 38. 2.0 per cent carbon sectional diagram of iron-manganese and carbon ternary alloy. Numeral mark in each regions has the meaning as shown in an appendix, respectively. White small circle shows uniform phase region, cross mark two phase region, and deltoid three phase region, all of which show the results of microscopic investigation.

forming the coexisting region of γ iron and C ternary solid solution. The coexisting region of γ iron, γ manganese and C ternary solid solution clearly appears in addition to that of γ iron and γ manganese ternary solid solution, and the coexisting regions of α manganese and γC, and of α manganese, γC and C ternary solid solution are clearly seen. In Fig. 39, trace of the coexisting region of γ iron and γ manganese ternary solid solution is scarcely recognized. The region of γ manganese ternary solid solution exists only at high temperatures. Changes of phases due to the transformation at 925°C is newly recognized, more conspicuous with increasing carbon content as shown in the sectional diagram at alloy containing more carbon. The change due to the transformation at 850°C vanishes.

In Fig. 40, the compositions of alloys containing high percentage of manganese, correspond to those in the coexisting region of γ manganese and βC binary solid solution in manganese-carbon bir ary system and the region of γ manganese ternary solid solutions is changed to the coexisting region of γ manganese and βC

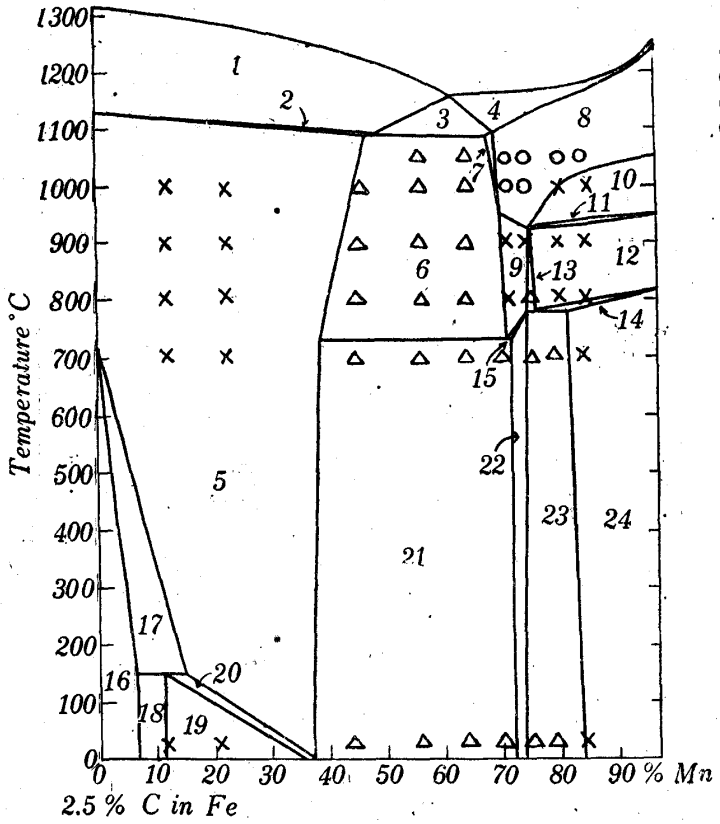

(1) l+A
(2) l+A+C
(3) l+A+γ_{Mn}
(4) l+γ_{Mn}
(5) A+C
(6) A+γ_{Mn}+C
(7) A+γ_{Mn}
(8) γ_{Mn}
(9) γ_{Mn}+C
(10) γ_{Mn}+βC
(11) γ_{Mn}+βC+γC
(12) γ_{Mn}+γC
(13) γ_{Mn}+γC+C
(14) α_{Mn}+γ_{Mn}+γC
(15) γ_{Mn}+α_{Mn}+C
(16) F+C
(17) A+F+C
(18) F+C+h
(19) h+C
(20) A+h+C
(21) A+α_{Mn}+C
(22) α_{Mn}+C
(23) α_{Mn}+γC+C
(24) α_{Mn}+γC

Fig. 39. 2.5 per cent carbon sectional diagram of iron-manganese and carbon ternary alloy.
Numeral mark in each regions has the meaning as shown in an appendix, respectively.
White small circle shows uniform phase region, cross mark two phase region, and deltoid three phase region, all of which show the results of microscopic investigation.

(1) l+A
(2) l+A+C
(3) l+A+γ_{Mn}
(4) l+γ_{Mn}
(5) l+γ_{Mn}+C
(6) l+βC
(7) l+βC+γ_{Mn}
(8) A+C
(9) A+C+γ_{Mn}
(10) γ_{Mn}+C
(11) γ_{Mn}
(12) γ_{Mn}+βC
(13) γ_{Mn}+βC+C
(14) γ_{Mn}+βC+γC
(15) γ_{Mn}+γC+C
(16) γ_{Mn}+γC
(17) α_{Mn}+γ_{Mn}+γC
(18) α_{Mn}+γ_{Mn}+C
(19) F+C
(20) A+F+C
(21) F+C+h
(22) h+C
(23) A+h+C
(24) A+α_{Mn}+C
(25) α_{Mn}+C
(26) α_{Mn}+C+γC
(27) α_{Mn}+γC

Fig. 40. 3.0 per cent carbon sectional diagram of iron-manganese and carbon ternary alloy.
Numeral mark in each regions has the meaning as shown in an appendix, respectively.
White small circle shows uniform phase region, cross mark two phase region, and deltoid three phase region, all of which show the results of microscopic investigation.

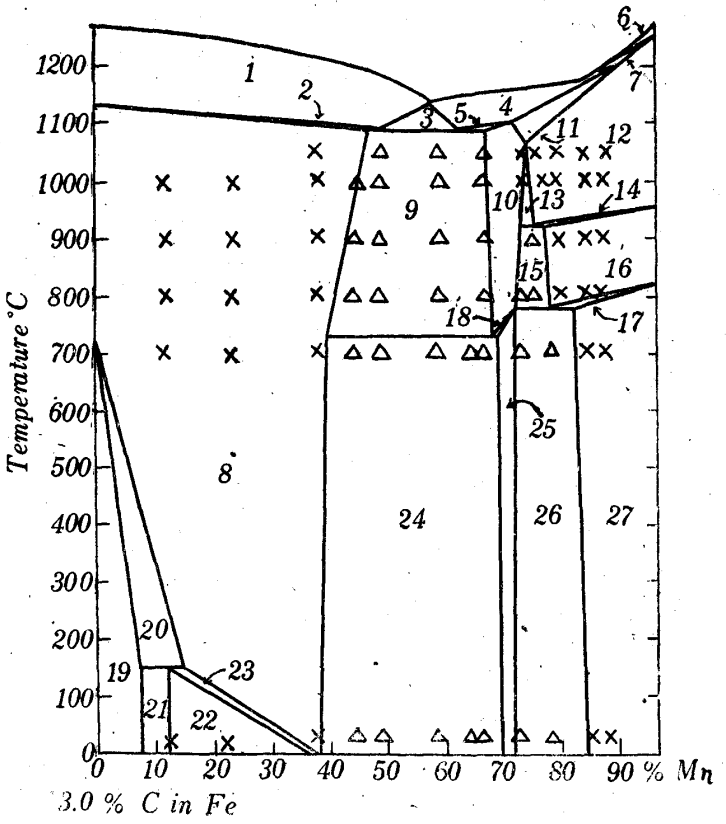

(1) l+A
(2) l+A+C
(3) l+A+γ_{Mn}
(4) l+γ_{Mn}
(5) l+γ_{Mn}+C
(6) l+βC
(7) l+βC+γ_{Mn}
(8) A+C
(9) A+γ_{Mn}+C
(10) γ_{Mn}+C
(11) γ_{Mn}+C+βC
(12) γ_{Mn}+βC
(13) βC
(14) βC+αC
(15) βC+αC+γC
(16) βC+γC
(17) γ_{Mn}+βC+γC
(18) γ_{Mn}+C+γC
(19) γ_{Mn}+γC
(20) α_{Mn}+γ_{Mn}+γC
(21) α_{Mn}+γ_{Mn}+C
(22) F+C
(23) A+F+C
(24) F+C+h
(25) h+C
(26) A+h+C
(27) A+α_{Mn}+C
(28) α_{Mn}+C
(29) α_{Mn}+γC+C
(30) α_{Mn}+γC

Fig. 41. 3.5 per cent carbon sectional diagram of iron-manganese and carbon tenary alloy. Numeral mark in each regions has the meaning as shown in an appendix, respectively. White small circle shows uniform phase region, cross mark two phase region, and deltoid three phase region, all of which show the results of microscopic investigation.

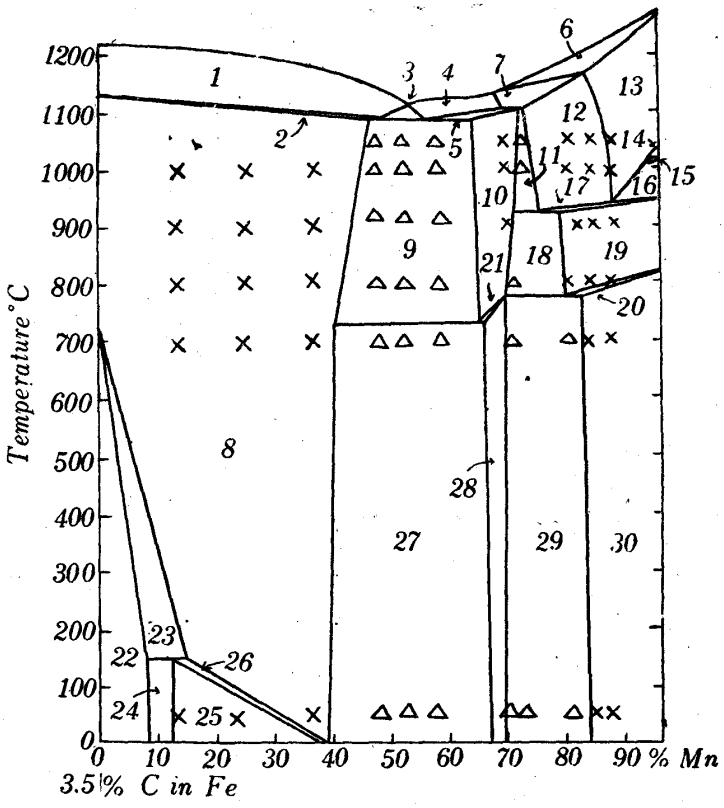

(1) l+A
(2) l+A+C
(3) l+C
(4) l+γ_{Mn}+C
(5) l+C+βC
(6) l+βC
(7) l+βC+γ_{Mn}
(8) A+C
(9) A+C+γ_{Mn}
(10) γ_{Mn}+C
(11) γ_{Mn}+βC+C
(12) βC+γ_{Mn}
(13) βC
(14) βC+αC
(15) βC+αC+γC
(16) βC+γC
(17) γ_{Mn}+βC+γC
(18) γ_{Mn}+C+γC
(19) γ_{Mn}+γC
(20) α_{Mn}+γ_{Mn}+γC
(21) α_{Mn}+γ_{Mn}+C
(22) F+C
(23) A+F+C
(24) F+C+h
(25) h+C
(26) A+h+C
(27) A+α_{Mn}+C
(28) α_{Mn}+C
(29) α_{Mn}+γC+C
(30) α_{Mn}+γC

Fig. 42. 4.0 per cent carbon sectional diagram of iron-manganese and carbon ternary alloy. Numeral mark in each regions has the meaning as shown in an appendix, respectively. White small circle shows uniform phase region, cross mark two phase region, and deltoid three phase region, all of which show the results of microscopic investigation.

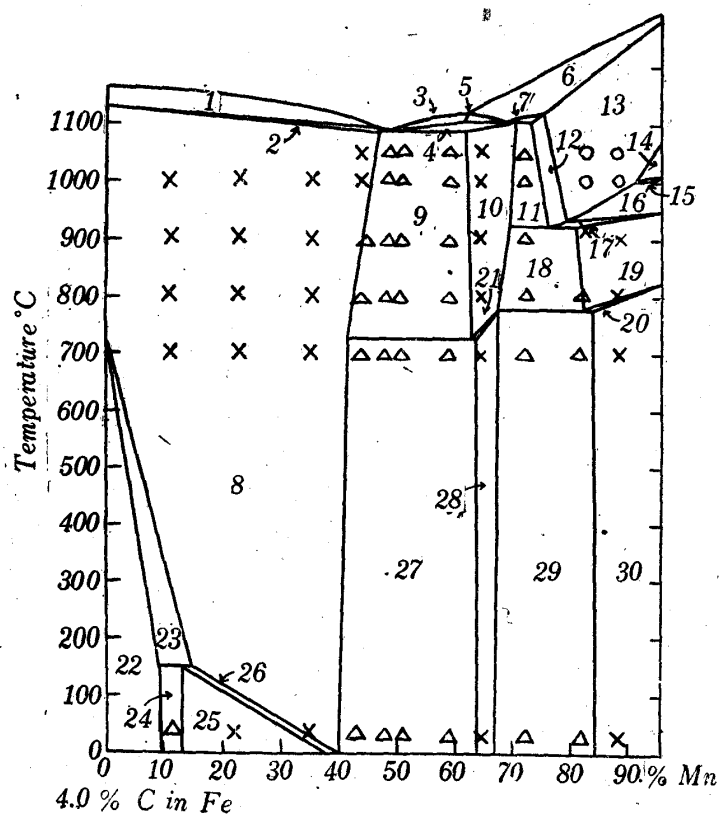

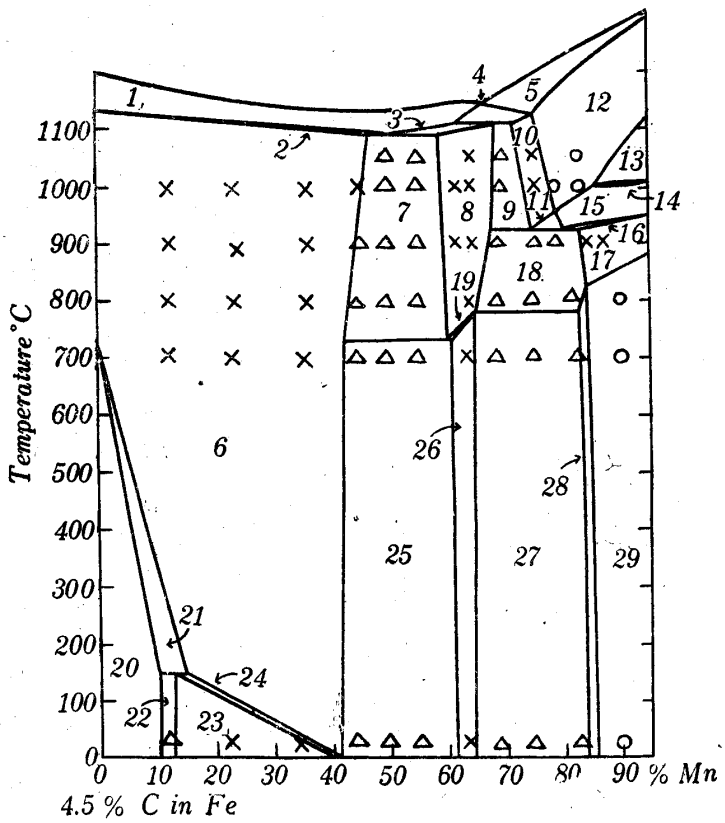

(1) l+C
(2) l+C+A
(3) l+C+γ_{Mn}
(4) l+C+βC
(5) l+βC
(6) A+C
(7) A+C+γ_{Mn}
(8) γ_{Mn}+C
(9) γ_{Mn}+C+βC
(10) βC+C
(11) βC+γC+C
(12) βC
(13) βC+αC
(14) βC+αC+γC
(15) βC+γC
(16) γ_{Mn}+βC+γC
(17) γ_{Mn}+γC
(18) γ_{Mn}+γC+C
(19) α_{Mn}+γ_{Mn} +γC
(20) F+C
(21) A+F+C
(22) F+C+h
(23) h+C
(24) A+h+C
(25) A+α_{Mn}+C
(26) α_{Mn}+C
(27) α_{Mn}+γC+C
(28) γC+C
(29) γC

Fig. 43. 4.5 per cent carbon sectional diagram of iron-manganese and carbon ternary alloy. Numeral mark in each regions has the meaning as shown in an appendix, respectively. White small circle shows uniform phase region, cross mark two phase region, and deltoid three phase region, all of which show the results of microscopic investigation.

(1) l+C
(2) l+C+A
(3) l+γ_{Mn}+C
(4) l+C+βC
(5) l+βC
(6) A+C
(7) A+γ_{Mn}+C
(8) γ_{Mn}+C
(9) γ_{Mn}+βC+C
(10) C+βC
(11) βC
(12) βC+αC+C
(13) βC+αC
(14) βC+αC+γC
(15) βC+γC
(16) γC
(17) βC+γC+C
(18) γ_{Mn}+γC+C
(19) γ_{Mn}+α_{Mn} +C
(20) F+C
(21) A+F+C
(22) F+C+h
(23) h+C
(24) A+h+C
(25) A+C+α_{Mn}
(26) α_{Mn}+C
(27) α_{Mn}+C+γC
(28) C+γC
(29) γC+αC+C
(30) γC+αC

Fig. 44. 5.0 per cent carbon sectional diagram of iron-manganese and carbon ternary alloy. Numeral mark in each regions has the meaning as shown in an appendix, respectively. White small circle shows uniform phase region, cross mark two phase region, and deltoid three phase region, all of which show the results of microscopic investigation.

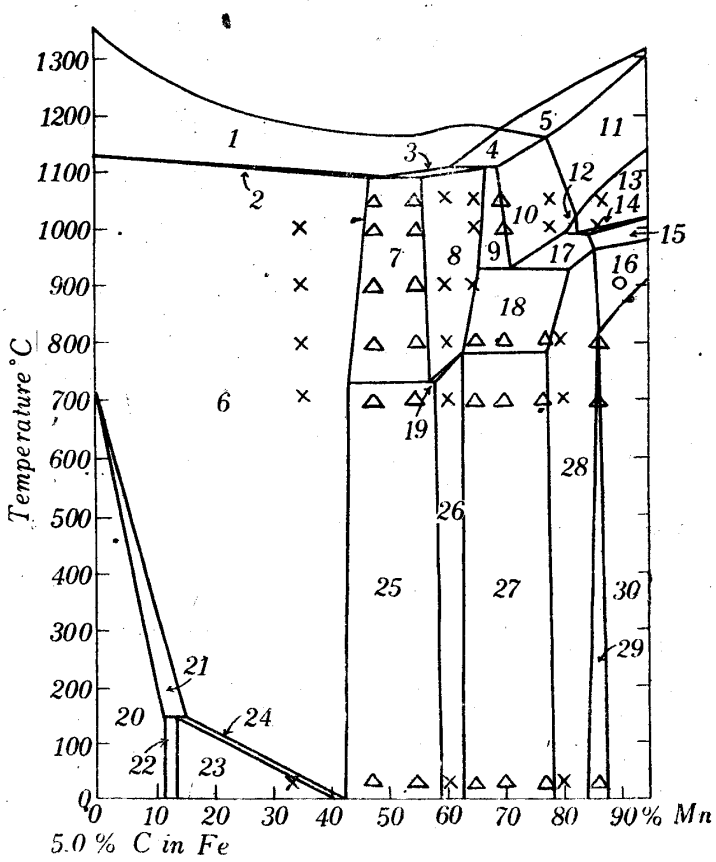

ternary solid solution, leaving a very small amount of γ manganese ternary solid solution at high temperatures. Changes of eutectoid reactions at 950° and 820°C in manganese and carbon binary system due to the addition of iron is clearly seen. In Fig. 41, the uniform region of βC ternary solid solution newly appears at high manganese parts. A part of peritectoid reaction in manganese and carbon binary system at 1010°C scarcely appears. The region of βC ternary solid solution is more noticeable in Fig. 42. The coexisting region of γ manganese and βC ternary solid solution is small, and others are almost unchanged. In Fig. 43, the coexisting region of γ manganese and γC solid solution is small and that of α manganese and γC ternary solid solution vanishes and the region of γC ternary solid solution newly appears. This region of γC ternary solid solution scarcely remains at comparatively high temperatures in Fig. 44. In this figure, the coexisting regions of αC and γC ternary solid solutions, and of γC, αC and C ternary solid solutions appear and ranges of the coexisting regions of γ iron, α manganese and C ternary solid solution, and of α manganese, γC and C ternary solid solutions become narrow. These ranges grow narrower and narrower with increasing carbon

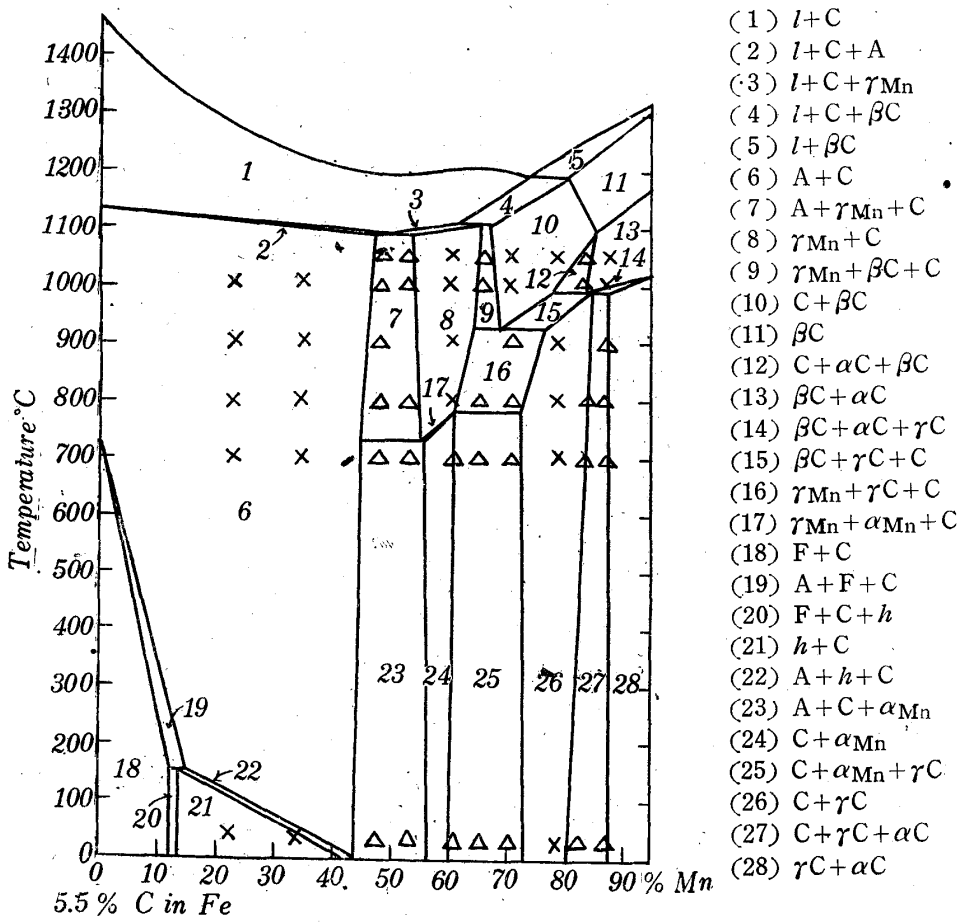

Fig. 45. 5.5 per cent carbon sectional diagram of iron-manganese and carbon ternary alloy. Numeral mark in each regions has the meaning as shown in an appendix, respectively. White small circle shows uniform phase region, cross mark two phase region, and deltoid three phase region, all of which show the results of microscopic investigation.

content as shown in figures indicating the sectional diagrams at alloys containing higher percentage of carbon. The coexisting region of γC and C ternary solid solutions slowly broadens towards high percentage of iron. In Fig. 45, the uniform phase of γC ternary solid solution is not seen. In Fig. 46, the ranges of compositions in respective regions are not very different from figures just mentioned above. The change due to the peritecto-eutectoid reaction at 990°C is more clearly seen.

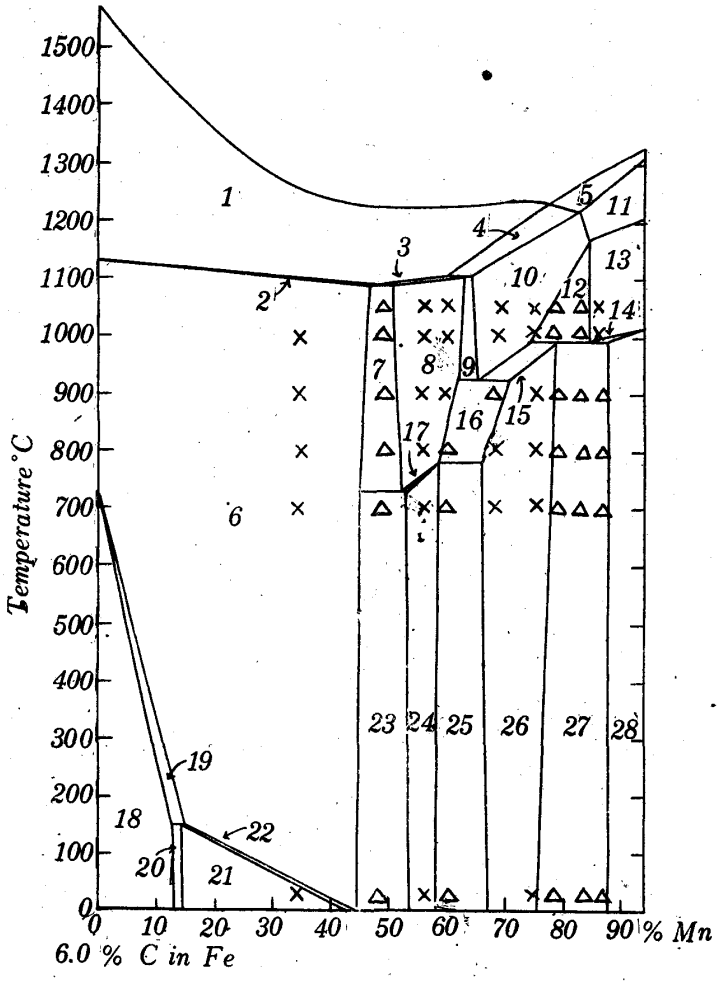

Fig. 46. 6.0 per cent carbon sectional diagram of iron-manganese and carbon ternary alloy. Numeral mark in each regions has the meaning as shown in an appendix, respectively. White small circle shows uniform phase region, cross mark two phase region, and deltoid three phase region, all of which show the results of microscopic investigation.

(J) Magnetic analysis of alloys containing about 85 per cent of manganese and different amounts of carbon.

Precise magnetic analyses were carried out with alloys containing about 85 per cent of manganese and different amounts of carbon. The results are shown in Fig. 47.

Next, some explanations about the curves in Fig. 47 will be given.

Curve (1) is referred to the alloy containing 82.91 per cent of manganese and 0.31 per cent of carbon. When this alloy is heated, its magnetization does not

change at first as seen in *ab*, but it increases rapidly at the point *b*, which shows the beginning of the transformation of α manganese ternary solid solution into β manganese ternary solid solution. The transformation develops up to the point *c*, at which the intensity of magnetization increases almost at constant temperature as shown in *cd*. This is due to the reaction, α manganese ternary solid solution $\rightarrow$ β manganese ternary solid solution + γ manganese ternary solid solution. After the completion of this reaction at the point *d*, the intensity of magnetization gradually increases up to the point *e*, at which the alloy is composed of uniform γ manganese ternary solid solution, β manganese ternary solid solution vanishing completely. The intensity of magnetization begins to increase rapidly at the point *f*, at which the solidus lines meet together. The segment *fg* means the solidification range. The magnetization undergoes little change after the alloy is melted.

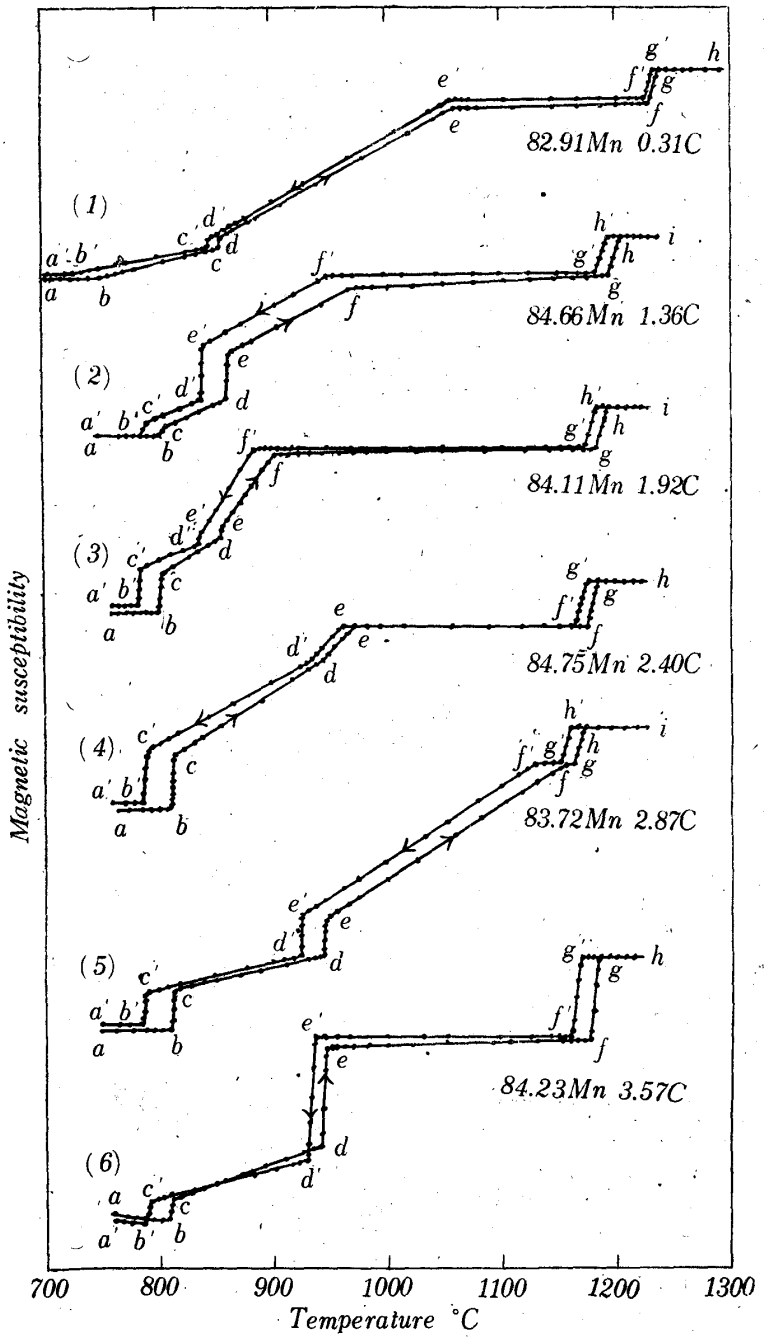

Fig. 47. Magnetic susceptibility curves at high temperatures of ternary alloys having compositions about 85 per cent of manganese and different amount of carbon.

On cooling the alloy, the points of phase change corresponding to those in the heating curve are denoted by letters with dash and a special explanation will, therefore, be unnecessary, except that a considerable difference in temperature exists between liquidus and solidus.

Curve (2) is the heating and cooling curves of the alloy containing 84.66 per cent of manganese and 1.36 per cent of carbon. The segments *ab* and *b'a'* show the magnetic susceptibilety of the alloy due to the change of temperature of the

coexisting region of α manganese ternary solid solution and γC ternary solid solution; *bc* and *c'b'* show the change brought about by the eutectoid reaction, γ manganese ternary solid solution $\rightleftarrows$ α manganese ternary solid solution + γC ternary solid solution. The change between *cd* and *d'c'* is caused by the change of amount of each phase in the two-phase coexisting region of α manganese ternary solid solution and γ manganese ternary solid solution, showing that the intensity of magnetization increases with the increase of γ manganese ternary solid solution. *de* and *e'd'* indicate the reaction, β manganese ternary solid solution + γ manganese ternary solid solution $\rightleftarrows$ α manganese ternary solid solution; *ef* and *f'e'* the change of the two phase coexisting region of β manganese ternary solid solution and γ manganese ternary solid solution; *fg* and *g'f'* the change caused by the temperature of γ manganese ternary solid solution; *gh* and *h'g'* the solidification range; *hi* and *i'h'* the magnetization in the melt.

Curve (3) is the result of the alloy containing 84.11 per cent of manganese and 1.92 per cent of carbon and its properties are almost the same as those of the alloy shown in the curve (2), the difference being only quantitative.

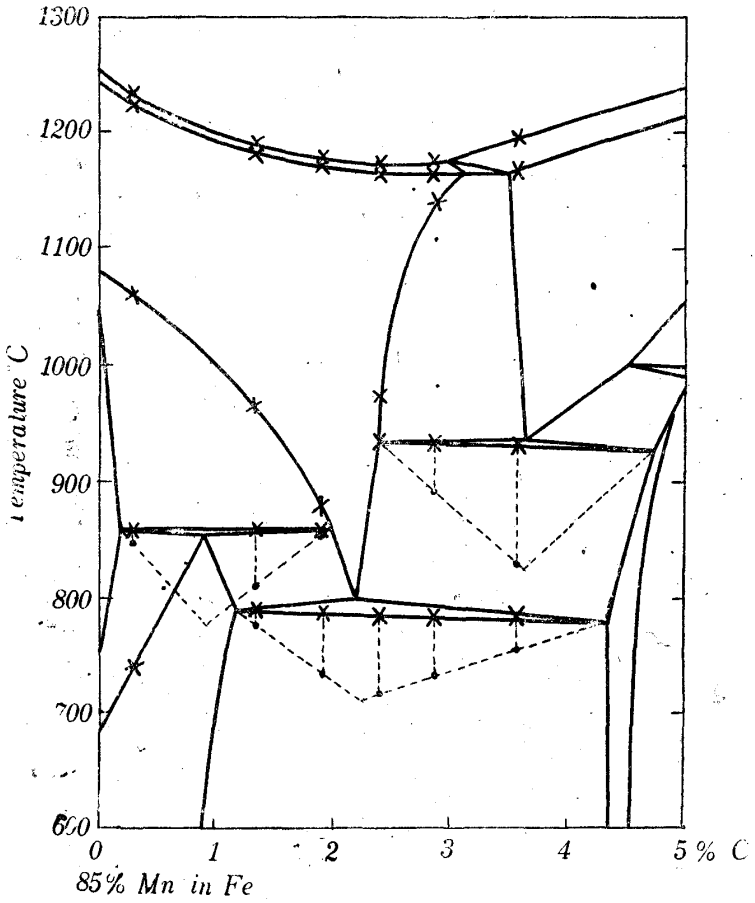

Fig. 48. 85 per cent manganese section of iron-manganese-carbon ternary diagram obtained by magnetic analysis. Cross mark shows the transformation point and change point in magnetic susceptibility curves, and triangular figure denoted by dotted line shows the amount of magnitude of transformation.

In curve (4) a new change is observable in *de* and *e'd'*. The points *d* and *d'* indicate the eutectoid reaction, βC ternary solid solution $\rightleftarrows$ γ manganese ternary solid solution + γC ternary solid solution, and both segments *de* and *e'd'* are the two-phase coexisting region of γ manganese ternary solid solution and βC ternary solid solution, and the points *e* and *e'* mean that all the alloys at the temperature above this point consist only of γ manganese ternary solid solution.

In curve (5), the reaction, βC ternary solid solution $\rightleftarrows$ γ mangenese ternary solid solution + γC ternary solid solution, increases its amount and

the temperature range in which γ manganese ternary solid solution and βC ternary solid solution coexist also increases, whereas the range in which γ manganese ternary solid solution exists only, decreases as shown in *fg* and *g'f'*.

In curve 6), the amounts of the change at about 800°C decreases and that at about 940°C is very remarkable. After the completion of this change, the magnetization undergoes little change, which is attributed to the reaction, βC ternary solid solution $\rightleftarrows$ γ manganese ternary solid solution + γC ternary solid solution.

Fig. 48 shows a part of the sectional diagram of the alloy containing 85 per cent of manganese, in which cross marks are the transformation points on curves obtained magnetometrically and triangular figures drawn by dotted lines indicate the amount of the change in the intensity of magnetization at respective transformation temperatures. Liquidus and solidus can accurately be determined by magnetic method. Also the behaviours in the eutectoid reactions at 950°C and 820°C and in the peritectoid reaction at 857°C and the changes in solubilities of β manganese ternary solid solution and of βC ternary solid solution in γ manganese ternary solid solution with the addition of iron in manganese-carbon binary system, are all fairly seen.

(K) Determination of temperatures of non-variant and other reactions by means of magnetic method.

Precise magnetic analyses were specially carried out with the alloys containing about 70 per cent of manganese and different amounts of carbon, because their sectional diagrams, which enabled us to determine accurately the temperatures of various phase changes, seemed to be most complicated. The results are shown in Fig. 49, and Fig. 50 are the sectional diagram at the alloy containing 70 per cent of manganese. In the figure, cross marks signify the temperature at which magnetic intensity changed and a triangular figures drawn by dotted lines indicate the magnitude of the intensity of magnetic transformation at respective temperatures. Some explanations about the curves in Fig. 49 will be given below.

In curve (1),

ab: γ iron ternary solid solution + α manganese ternary solid solution.

b : at this point, the reaction, γ iron ternary solid solution + α manganese ternary solid solution $\rightleftarrows$ β manganese ternary solid solution, begins to take place, in which the compositions of the alloy is represented by the equation, γ iron ternary solid solution + α manganese ternary solid solution $\rightleftarrows$ γ iron ternary solid solution + β manganese ternary solid solution + α manganese ternary solid solution.

bc: γ iron ternary solid solution + β manganese ternary solid solution + α manganese ternary solid solution.

c : at this point, the reaction of transformation, γ iron ternary solid solution + α manganese ternary solid solution $\rightleftarrows$ β manganese ternary solid solution + γ manganese ternary solid solution takes place, the structure being represented by the equation, γ iron ternary solid solution + β manganese ternary solid solution + α manganese ternary solid solution $\rightleftarrows$ γ

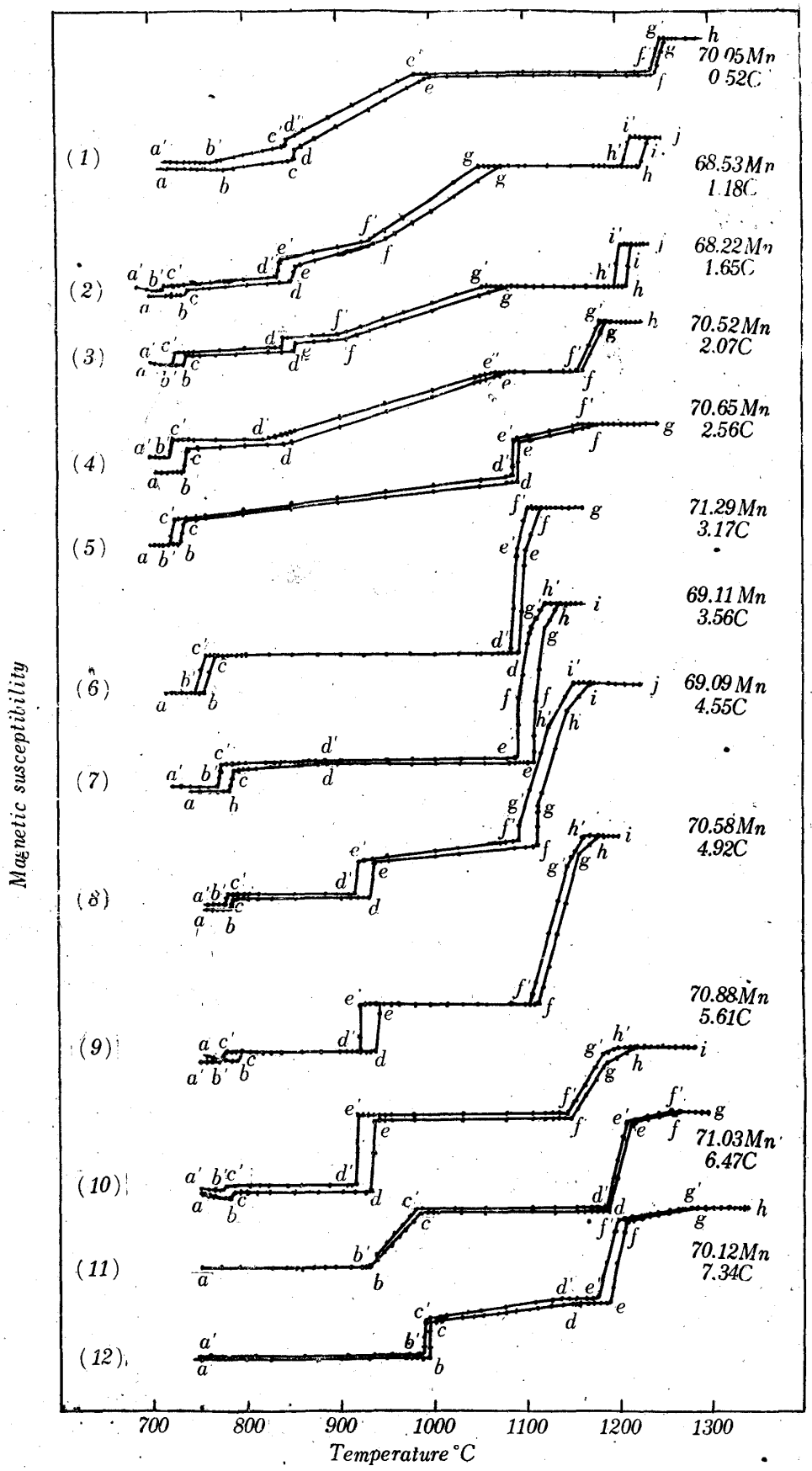

Fig. 49. Magnetic susceptibility curves at high temperatures of ternary alloys containing about 70 per cent of manganese and different amount of carbon.

manganese ternary solid solution + β manganese ternary solid solution + γ iron ternary solid solution.

cd: non-variant reaction at 850°C.

de: γ manganese ternary solid solution + β manganese ternary solid solution + γ iron ternary solid solution.

e : at this point, three phases coexisting stucture of γ manganese ternary solid solution, β manganese ternary solid solution and γ iron ternary solid solution change into that of γ iron ternary solid solution and γ manganese ternary solid solution.

ef : γ iron ternary solid solution + γ manganese ternary solid solution.

fg : solidification range.

gh: the magnetization in melt.

In curve (2),

ab: α manganese ternary solid solution + γ iron ternary solid solution + C ternary solid solution.

bc : the change at about 730°C is due to the ternary eutectoid reaction, γ manganese ternary solid solution $\rightleftarrows$ α manganese ternary solid solution + γ iron ternary solid solution + C ternary solid solution.

cd: the change in the three phase coexisting region, α manganese ternary solid solution + γ iron ternary solid solution + γ manganese ternary solid solution.

de: non-variant reaction, γ iron ternary solid solution + α manganese ternary solid solution $\rightleftarrows$ β manganese ternary solid solution + γ manganese ternary solid solution, at 850°C.

ef : the change in the region of three phases, γ manganese ternary solid solution + γ iron ternary solid solution + β manganese ternary solid solution.

fg : the change of two phases, γ iron ternary solid solution + γ manganese ternary solid solution.

gh: uniform γ manganese ternary solid solution phase alone.

h : :solidification range.

i : melting point.

ij : the magnetization in melt.

The behaviors of the changes in curve (3) are almost the same as in the curve (2), except that the amount of change at 730°C increases, whereas it decreases at 850°C and that the melting point falls. In curve (4), the amount of the change at 730°C increases gradually, while it decreases at 850°C, other respects being similar to the former two cases.

In curve (5) the change at 850°C cannot be seen.

ab: α manganese ternary solid solution + γ iron ternary solid solution + C ternary solid solutions.

bc : ternary eutectoid reaction begins at *b* and complete at *c*. The alloy of this composition changes into γ manganese ternary solid solution, γ iron ternary solid solution and C ternary solid solution after the completion of the reaction.

cd: the change of above mentioned range.

d : at this point melting begins by the reaction, γ manganese ternary solid solution + γ iron ternary solid solution + C ternary solid solution → melt.
de: ternary eutectic reaction.
ef : after the close of above ternary eutectic reaction, the alloy gradually melts.
fg : magnetization in the molten state, the change of which being small.

In curve (6)

ab : two-phase region of α manganese ternary solid solution and C ternary solid solution.
bc : γ manganese ternary solid solution + α manganese ternary solid solution + C ternary solid solution.
cd: γ manganese ternary solid solution + C ternary solid solution.
d : the alloy begins to melt.
de: melt + γ manganese ternary solid solution + C ternary solid solution.
ef : melt + γ manganese ternary solid solution.
f : melting point.
fg : the change in the magnetization after melting.

In curve (7),

ab: the three-phase region of α manganese ternary solid solution, γC ternary solid solution and C ternary solid solution.
bc : the non-variant reaction at 780°C.
cd: the three-phase region of γ manganese ternary solid solution, γC ternary solid solution and C ternary solid solution region, γC ternary solid solution phase disappearing at *d*.
de: γ manganese ternary solid solution + C ternary solid solution.
e : the alloy begins to melt.
ef : melt + γ manganese ternary solid solution + C ternary solid solution.
fg : melt + γ manganese ternary solid solution + βC ternary solid solution.
gh : melt + βC ternary solid solution.
h : the melting point.
hi : the change of the magnetization after melting.

In this alloy, the non-variant reaction at 780°C, which was not seen so far, becomes observable and the peritecto-eutectic reaction at 1105°C appears, too.

In curve (8),

ab: the three-phase region of α manganese ternary solid solution, γC ternary solid solution and C ternary solid solution.
bc : non-variant reaction at 780°C.
cd: the three-phase region of γ manganese ternary solid solution, γC ternary solid solution and C ternary solid solution.
de: the ternary eutectoid reaction, βC ternary solid solution $\rightleftarrows$ γ manganese ternary solid sloution + γC ternary solid solution + C ternary solid solution, at 925°C.
ef: the three-phase region of γ manganese ternary solid solution, C ternary solid solution and βC ternary solid solution.

f : the alloy begins to melt.
fg : non-variant reaction at 1105°C.
gh: melt + βC ternary solid solution + C ternary solid solution.
hi : melt + βC ternary solid solution.
i : melting point.
ij : the change of the magnetization after melting.

In curve (9),

ab: α manganese ternary solid solution + γC ternary solid solution + C ternary solid solution.
bc : non-variant reaction, the amount of the change at this temperature decreases with the increasing amount of carbon.
cd: γ manganese ternary solid solution + γC ternary solid solution + C ternary solid solution.
de: the ternary eutectoid reaction, the amount of it is greater than that in curve (8).
ef : γ manganese ternary solid solution + C ternary solid solution + βC ternary solid solution.
f : the alloy begins to melt.
fg: melt + βC ternary solid solution + C ternary solid solution.
gh: melt + βC ternary solid solution.
h : the alloy finishes meltings.
hi: the change of the magnetization after melting.

In curve (10),

ab: α manganese ternary solid solution + γC ternary solid solution + C ternary solid solution.
bc : the peritecto-eutectoid reaction. It will be seen that the amount of the change at this temperature gradually decreases with the increasing amount of carbon.
cd: γ manganese ternary solid solution + γC ternary solid solution + C ternary solid solution.
de: the ternary eutectoid reaction.
ef: βC ternary solid solution + C ternary solid solution.
fg : melt + βC ternary solid solution + C ternary solid solution; in the alloy of this composition the non-variant reaction at 1105°C as shown in the curve (8) vanishes.
gh: melt + C ternary solid solution.
h : the point at which the melting finishes.
hi: the magnetization after melting.

In curve (11),

ab: γC ternary solid solution + C ternary solid solution.
bc : βC ternary solid solution + γC ternary solid solution + C ternary solid solution.
cd: βC ternary solid solution + C ternary solid solution.
de: melt + βC ternary solid solution + C ternary solid solution, in this region, the melt bigins to appear.

ef : melt and C ternary solid solution where the βC ternary solid solution phase vanishes.
f : the point at which melting finishes.
fg: the magnetization after melting.

In curve (12),

ab: γC ternary solid solution + C ternary solid solution + αC ternary solid solution.
b : the non-variant reaction at 990°C.
bc: the amount of reaction mentioned above.
cd: C ternary solid solution+βC ternary solid solution + αC ternary solid solution.
de: αC ternary solid solution + C ternary solid solution.
e : the alloy begins to melt.
ef: melt + αC ternary solid solution + C ternary solid solution.
fg: the region of melt and αC ternary solid solution where the melt increases with vanishings of C ternary solid solution, and in this region αC ternary solid solution gradually decreases accompanying the increasing amount of melt with rise of temperature.
g : the temperature at which melting finishes.
gh: the magnetization after melting.

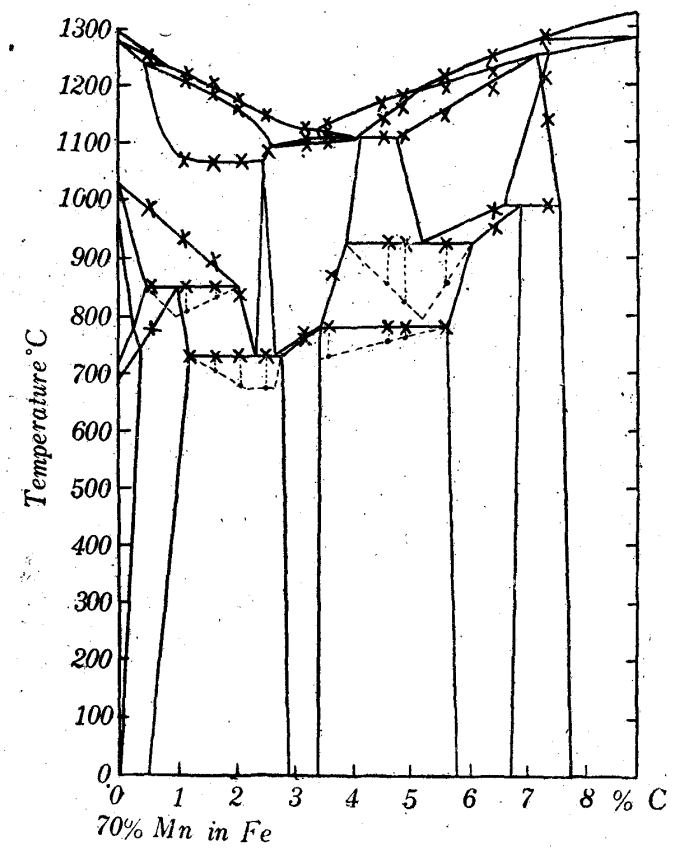

Fig. 50. 70 per cent manganese sectional diagram of iron-manganese-carbon ternary alloy obtained by magnetic analysis. Cross mark shows the transformation or change point in magnetic susceptibility curves, and triangular figures denoted by dotted line shows the amount of magnitude of transformation.

From the above results, the temperatures of non-variant reactions and those concerning several kinds of reactions can be determined. The cross marks on each curves in Fig. 50 are the transition point in the sectional diagram at 70 per cent of manganese obtained by means of magnetic analysis, and the mutual relations between respective phases are well explained.

(L) γ manganese ternary solid solution

From the results of magnetic analyses, thermal dilatations and the microscopic examinations of quenched specimens, the limiting region of γ manganese ternary solid solution can be obtained and it is also possible to ascertain the changes which the eutectoid point, peritectic point and maximum solubility may undergo when the binary system

is extended to the ternary system. Fig. 51 illustrates these results. In the figure, white small circles signify the solubility, eutectoid point and peritectoid points obtained from the above measurements, and the broad full lines are the solubility

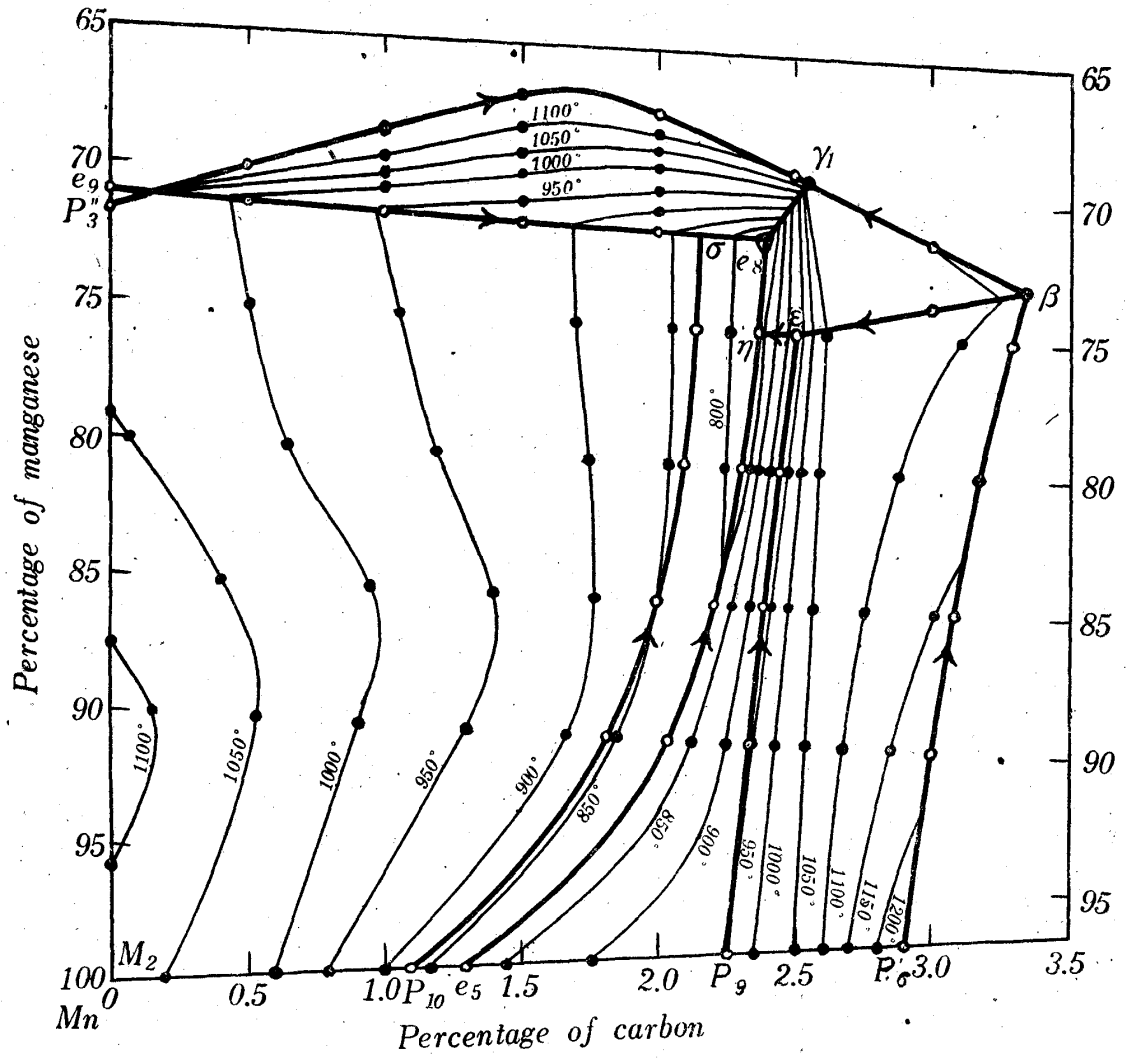

Fig. 51. γ manganese ternary solid solution region of iron-manganese-carbon ternary diagram. Solid lines show the solubility line, eutectoid line and peritecto-eutectoid line, and lean lines are isothermal line.

line, eutectoid line and peritectic line, from which the peritecto-eutectoid point and ternary eutectoid point can be found, and black circles signify isothermal points and lean lines are the isothermal lines. The meanings of respective lines, phases, and points are as follows:

$P_3''\gamma$ line — the maximum solubility line of γ iron ternary solid solution in γ manganese ternary solid solution in the case of coexisting with melt.

$\gamma_1\beta$ line — the maximum solubility line of C ternary solid solution in γ manganese ternary solid solution in the case of coexisting with melt.

$\beta P_6'$ line — the maximum solubility line of βC ternary solid solution in γ manganese ternary solid solution in the case of coexisting with melt.

$e_9\sigma$ line — eutectoid line, γ manganese ternary solid solution $\rightleftarrows$ γ iron ternary solid solution + β manganese ternary solid solution.

$P_{10}\sigma$ line — peritectoid line, γ manganese ternary solid solution + β manganese ternary solid solution $\rightleftarrows$ α manganese ternary solid solution.

σe_8 line — eutectoid line, γ manganese ternary solid solution $\rightleftarrows$ γ iron ternary solid solution + α manganese ternary solid solution.

$\gamma_1 e_8$ line — eutectoid line, γ manganese ternary solid solution $\rightleftarrows$ γ iron ternary solid solution + C ternary solid solution.

$\beta\varepsilon$ line — conjugate line of the reaction, βC ternary solid solution $\rightleftarrows$ C ternary solid solution + γ manganese ternary solid solution.

$P_9\varepsilon$ line — maximum solubility line of βC ternary solid solution in γ manganese ternary solid solution at eutectoid temperature.

$\varepsilon\eta$ line — eutectoid line, γ manganese ternary solid solution $\rightleftarrows$ γC ternary solid solution + αC ternary solid solution.

$e_5\eta$ line — eutectoid line, γ manganese ternary solid solution $\rightleftarrows$ α manganese ternary solid solution + γC ternary solid solution.

ηe_8 line — eutectoid line, γ manganese ternary solid solution $\rightleftarrows$ α manganese ternary solid solution + C ternary solid solution.

σ point — peritecto-eutectoid point, γ manganese ternary solid solution + β manganese ternary solid solution $\rightleftarrows$ γ iron ternary solid solution + α manganese ternary solid solution, at 850°C.

ε point — maximum solubility point of βC ternary solid solution in γ manganese ternary solid solution at ternary eutectoid temperature.

η point — eutectoid point, γ manganese ternary solid solution $\rightleftarrows$ α manganese ternary solid solution + γC ternary solid solution + C ternary solid solution, at 780°C.

e_8 point — eutectoid point, γ manganese ternary solid solution $\rightleftarrows$ α manganese ternary solid solution + C ternary solid solution + γ iron ternary solid solution, at 730°C.

$P_3''\gamma_1 e_8 \sigma e_9 P_3''$ surface — solubility surface of γ iron ternary solid solution in γ manganese ternary solid solution.

$e_9\sigma P_{10}M_2e_9$ surface — solubility surface of β manganese ternary solid solution in γ manganese ternary solid solution.

$P_{10}\sigma e_8\eta e_5 P_{10}$ surface — solubility surface of α manganese ternary solid solution in γ manganese ternary solid solution.

$e_5\eta\varepsilon P_9 e_5$ surface — solubility surface of γC ternary solid solution in γ manganese ternary solid solution.

$P_9\varepsilon\beta P_6'P_9$ surface — solubility surface of βC ternary solid solution in γ manganese ternary solid solution.

$\beta\varepsilon\eta e_8\gamma_1\beta$ surface — solubility surface of C ternary solid solution in γ manganese ternary solid solution.

(M) βC ternary solid solution

Fig. 52 shows the existing region of βC ternary solid solution, which was obtained on the basis of microscopic investigation, thermal dilatation, magnetic analysis, etc. The explanations of notations in the figure are as follows:

$P_6''\beta_1$ line — the maximum solubility line of γ manganese. ternary solid solution in βC ternary solid solution in the case of coexisting with melt.

$\beta_1\alpha$ line — the maximum solubility line of C ternary solid solution in βC ternary solid solution in the case of coexisting with melt.

$\alpha P_7'$ line — the maximum solubility line of αC ternary solid solution in βC ternary solid solution in the case of coexisting with melt.

$\alpha\delta$ line — conjugate line of βC ternary solid solution, αC ternary solid solution and C ternary solid solution.

$P_9\delta$ line — peritectoid line, βC ternary solid solution + αC ternary solid solution $\rightleftarrows$ γC ternary solid solution.

δe_7 line — eutectoid line, βC ternary solid solution $\rightleftarrows$ γC ternary solid solution + C ternary solid solution.

e_6e_7 line — eutectoid line, βC ternary solid solution $\rightleftarrows$ γ manganese ternary solid solution + γC ternary solid solution.

β_1e_7 line — eutectoid line, βC ternary solid solution $\rightleftarrows$ γ manganese ternary solid solution + C ternary solid solution.

δ point — peritecto-eutectoid point, βC ternary solid solution + αC ternary solid

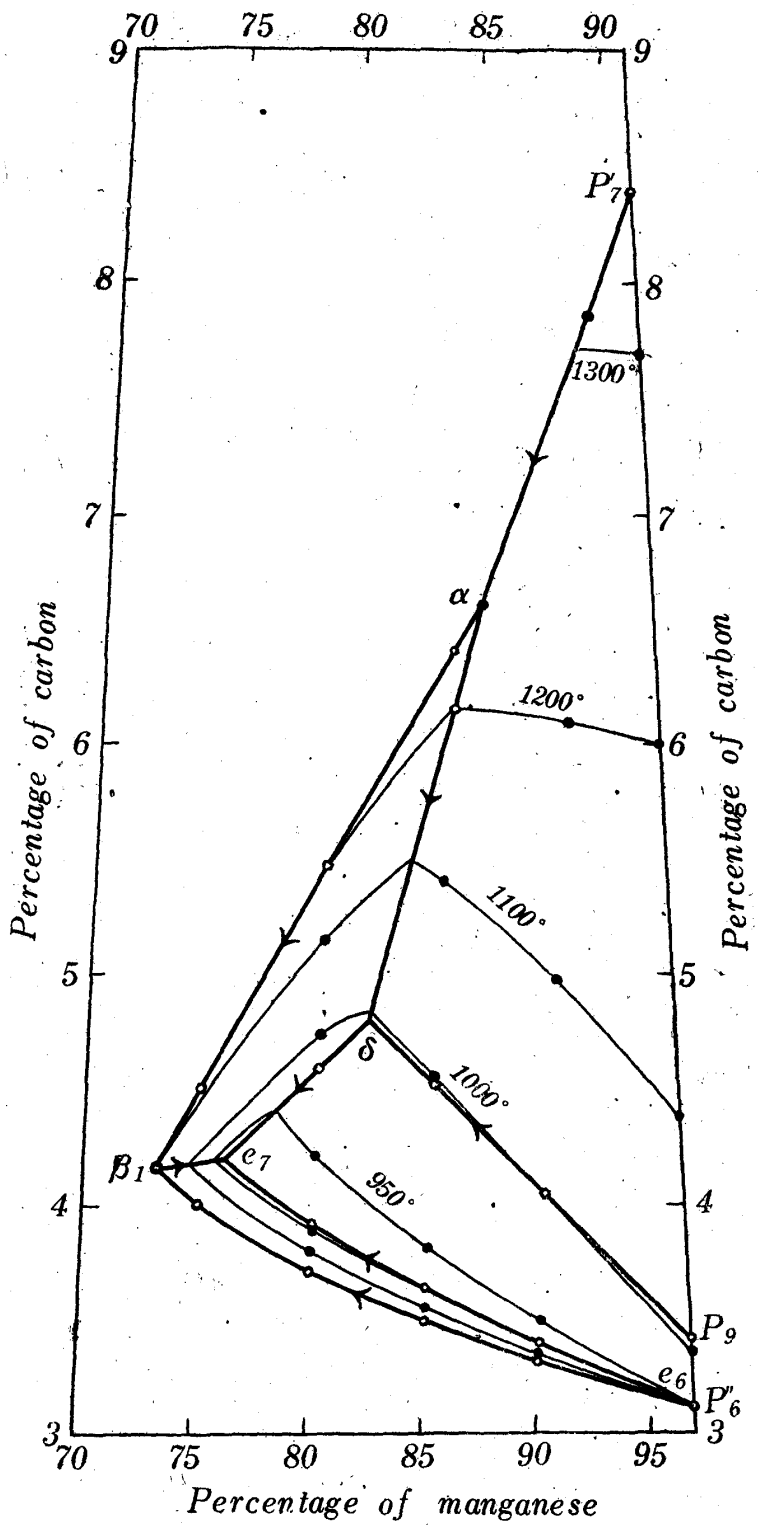

Fig. 52. βC ternary solid solution region of iron-manganese-carbon ternary diagram.
Solid lines show the solubility line, eutectoid line and peritecto-eutectoid line, and lean lines are isothermal line.

solution $\rightleftarrows$ γC ternary solid solution + C ternary solid solution.

e_7 point — ternary eutectoid point, βC ternary solid solution $\rightleftarrows$ γ manganese ternary solid solution + γC ternary solid solution + C ternary solid solution.

$P_6''\beta_1 e_7 e_6 P_6''$ surface — solubility surface of γ manganese ternary solid solution in βC ternary solid solution.

$\beta_1\alpha\delta e_7\beta_1$ surface — solubility surface of C ternary solid solution in βC ternary solid solution.

$\alpha P_7' P_9\delta\alpha$ surface — solubility surface of αC ternary solid solution in βC ternary solid solution.

$P_9\delta e_7 e_6 P_9$ surface — solubility surface of γC ternary solid solution in βC ternary solid solution.

In the above figure, white small circles signify the solubility, eutectoid point and peritectoid points obtained from the results already described, and broad full lines are the solubility line, eutectoid line and peritectoid line, from which the peritecto-eutectoid point and ternary eutectoid point can be found, and black circles signify isothermal points and lean lines are the isothermal lines. The behavior of βC ternary solid solution at high temperatures can clearly be recognized from the figure.

Fig. 53 shows the diagram in which the liquids surfaces and solidus surfaces are taken away, the meanings and signs of respective points being the same as those explained before. The conjugate lines and meshes are shown on the two-phase and three-phase equilibrium regions, respectively, and the direction of the reaction is indicated by arrow.

(N) Microscopic structures of heat treated specimens

Microscopic structures of specimens quenched in brine ice water are shown in Photos. 24~64. The compositions of the specimens, the quenching temperatures and the constituents are all written at the photographs, and accordingly, some special remarks alone will be mentioned below.

Photo. 24 shows the structure of uniform γ manganese ternary solid solution, quenched at 1000°C, which represents the structures in the regions (4) and (7) in Figs. 20 and 29, respectively. The compositions of alloys containing almost the same percentage of carbon as this but with decreasing manganese are in the two-phase region of γ iron and γ manganese ternary solid solution, that is, in the region (3) of Fig. 20 or in (7) of Fig. 33, and accordingly, the structure is composed of two phases, as shown in Photo. 25.

Typical structure of γ manganese ternary solid solution and C ternary solid solution in the regions of (7) and (9) in Figs. 20 and 33, respectively, is shown in Photo. 26. Although it was difficult to distinguish γ manganese ternary solid solution from C ternary solid solution by means of ordinary degree of etching, it was still possible in the case of intense etching, because the former was less resistant to etching than the latter.

Photo. 27 shows the structure of γ manganese ternary solid solution and βC ternary solid solution in the regions (9) and (8) in Figs. 20 and 29, respectively.

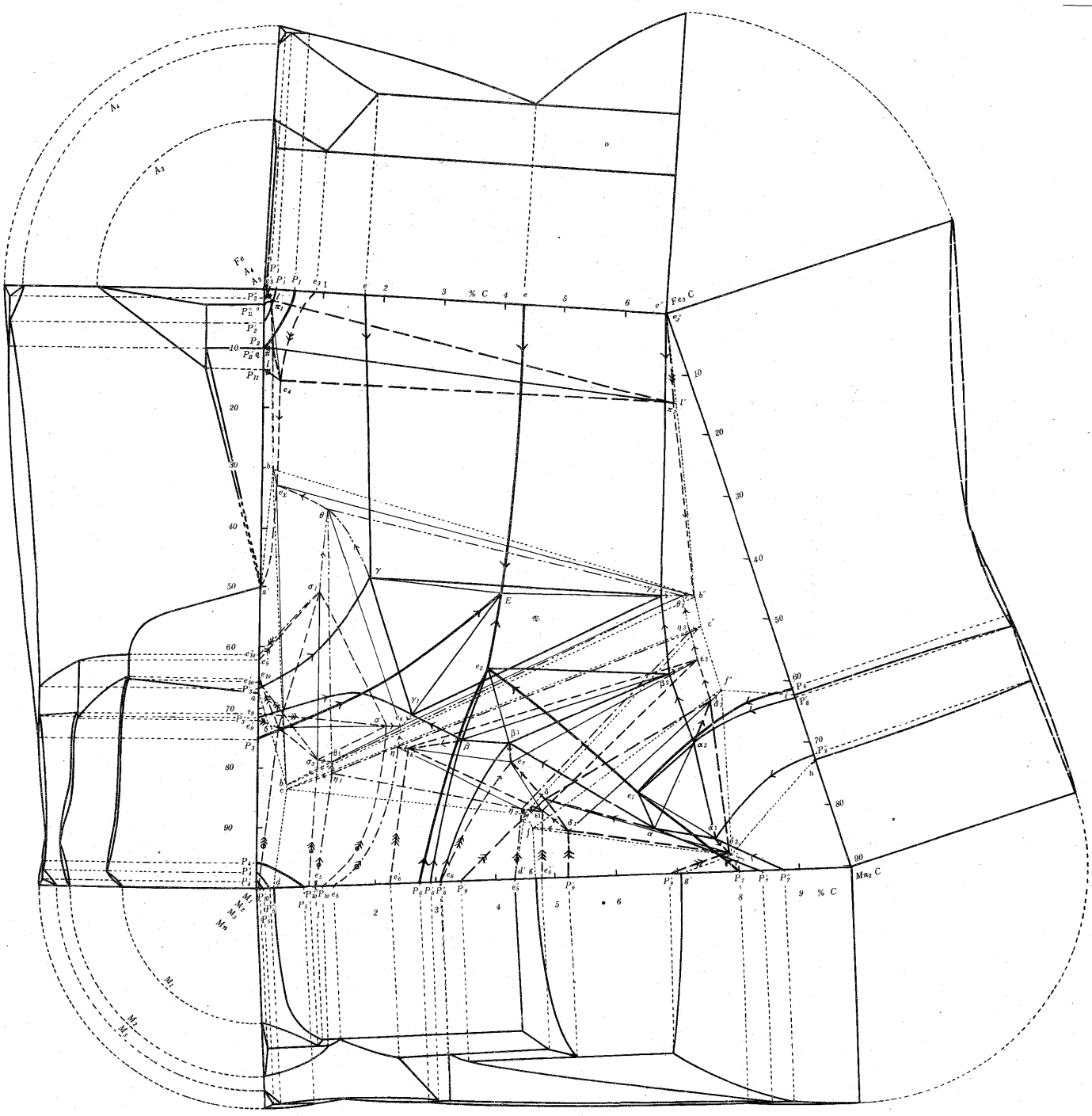

Fig. 54. Ternary equilibrium diagram of iron-manganese-carbon alloy.

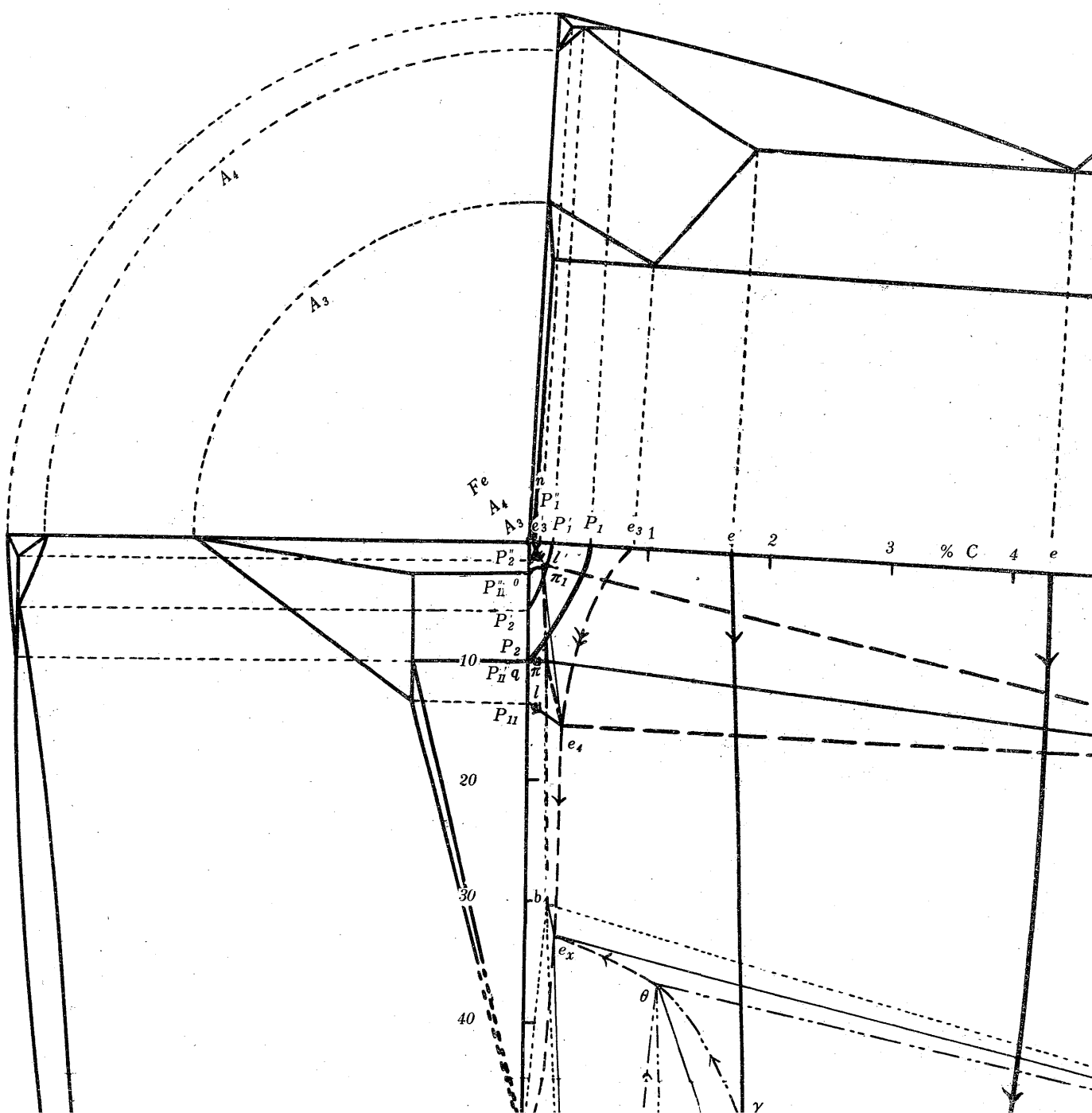
A4
A3
Fe
A4
A3
n
P'1
e'3
P'1
P1
e3
1
e
2
3
% C
4
e
P'2
l'
π1
P''II 0
P'2
P2
10
P'II
q
π
l
PII
e4
20
30
b
ex
40
θ
γ

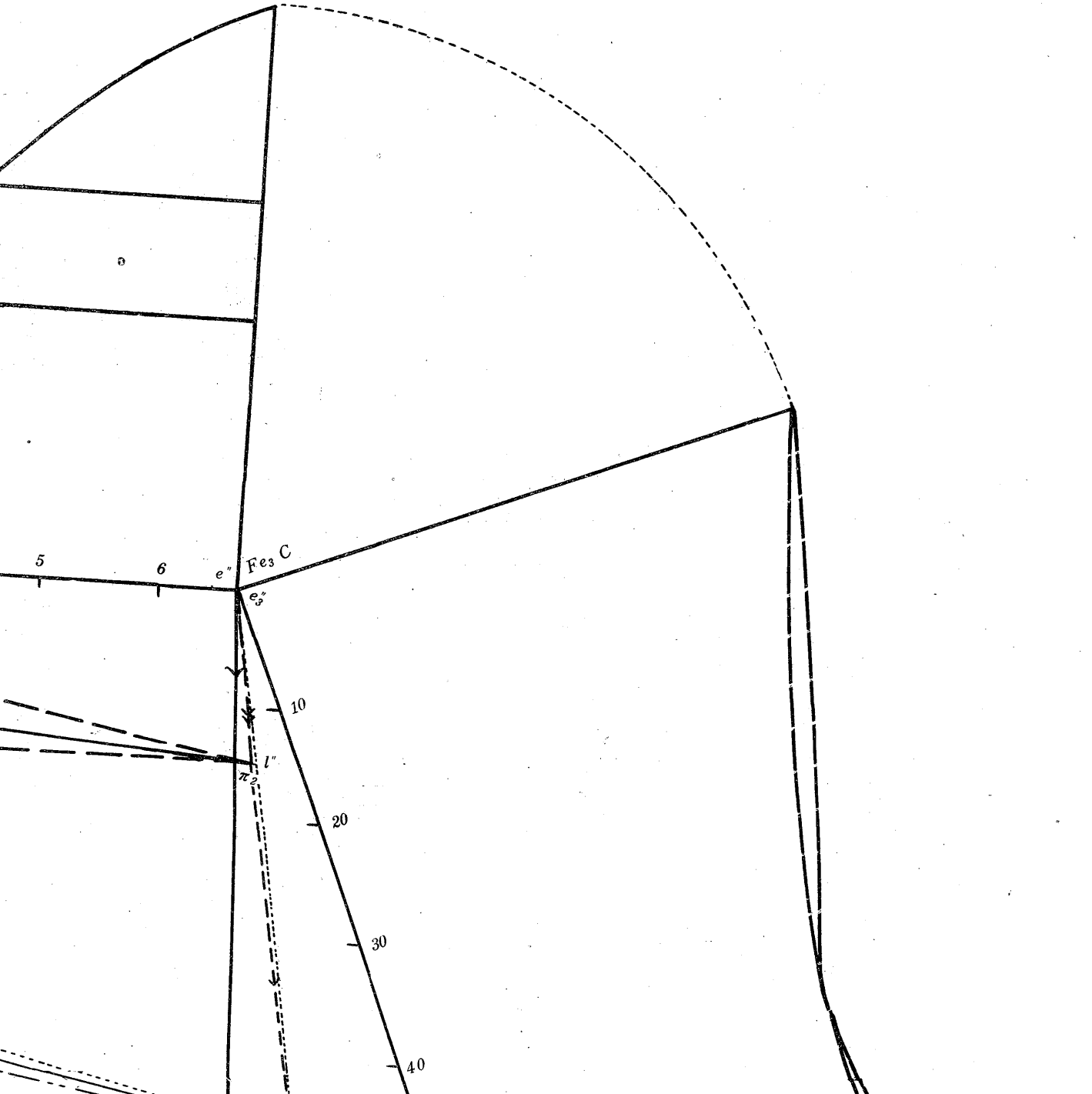
5
6
e''
Fe3 C
e3''
10
l''
π2
20
30
40

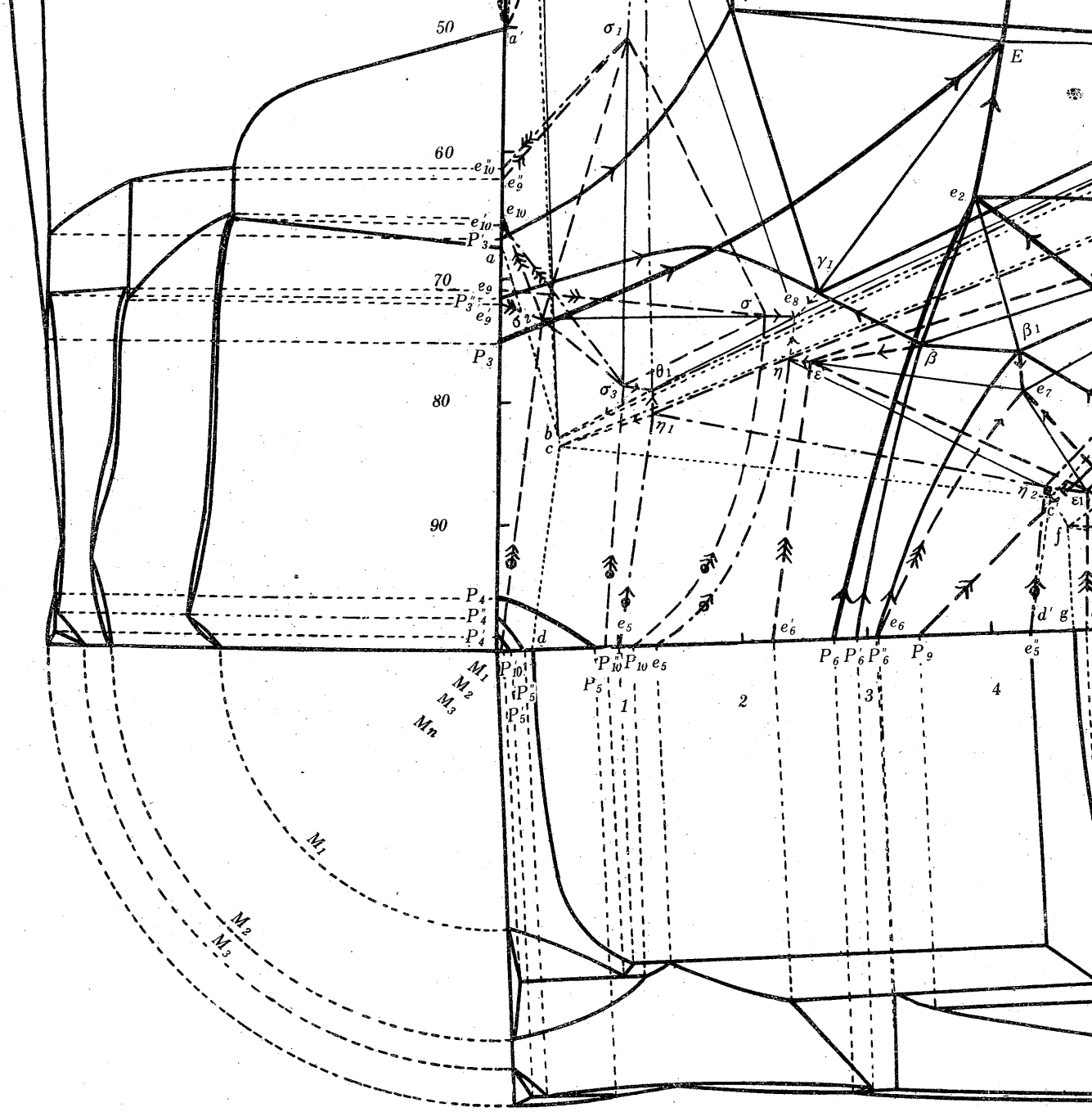

Fig. 54. Ternary equilibrium diagram of iron-ma

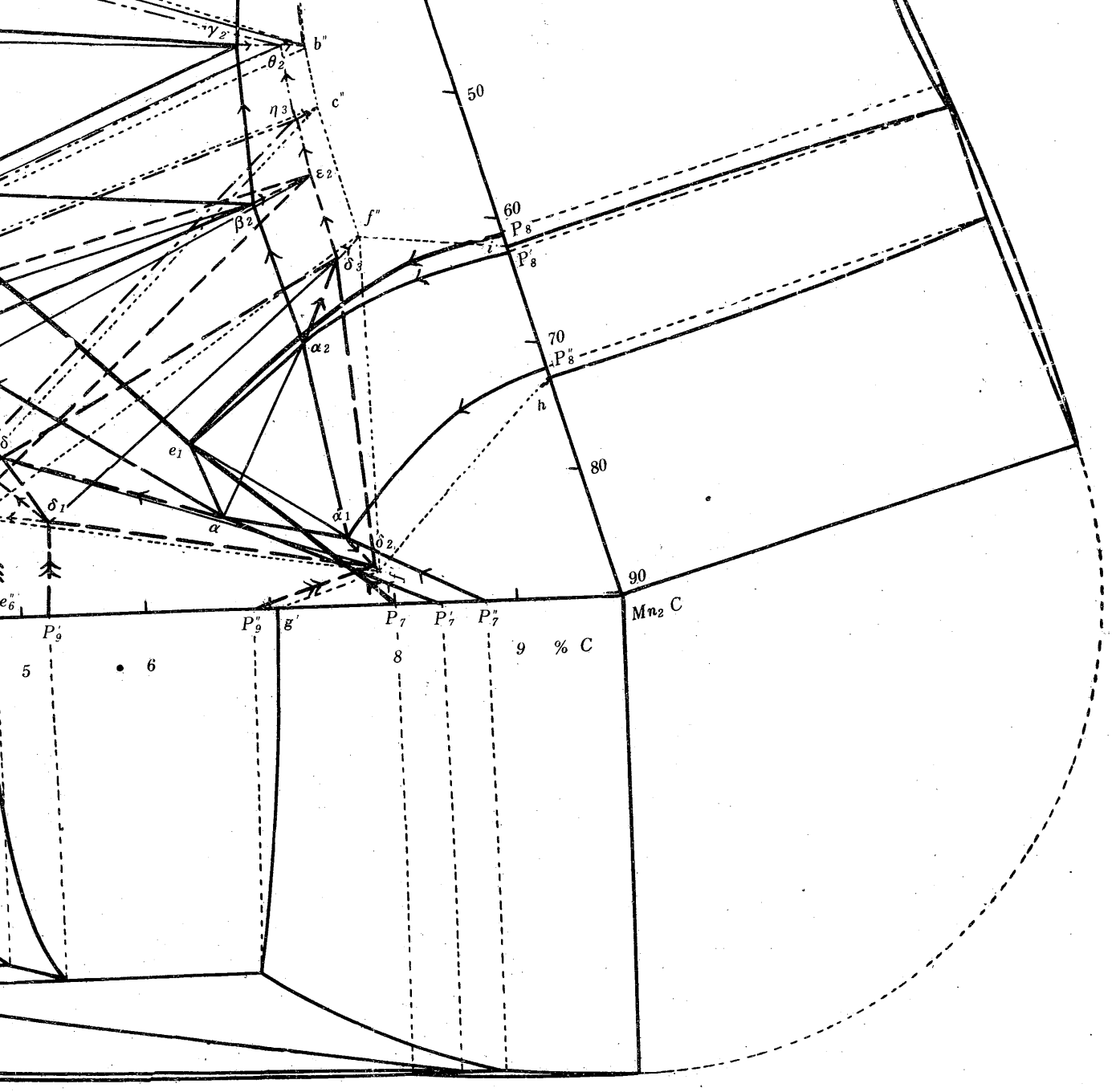

anganese-carbon alloy.

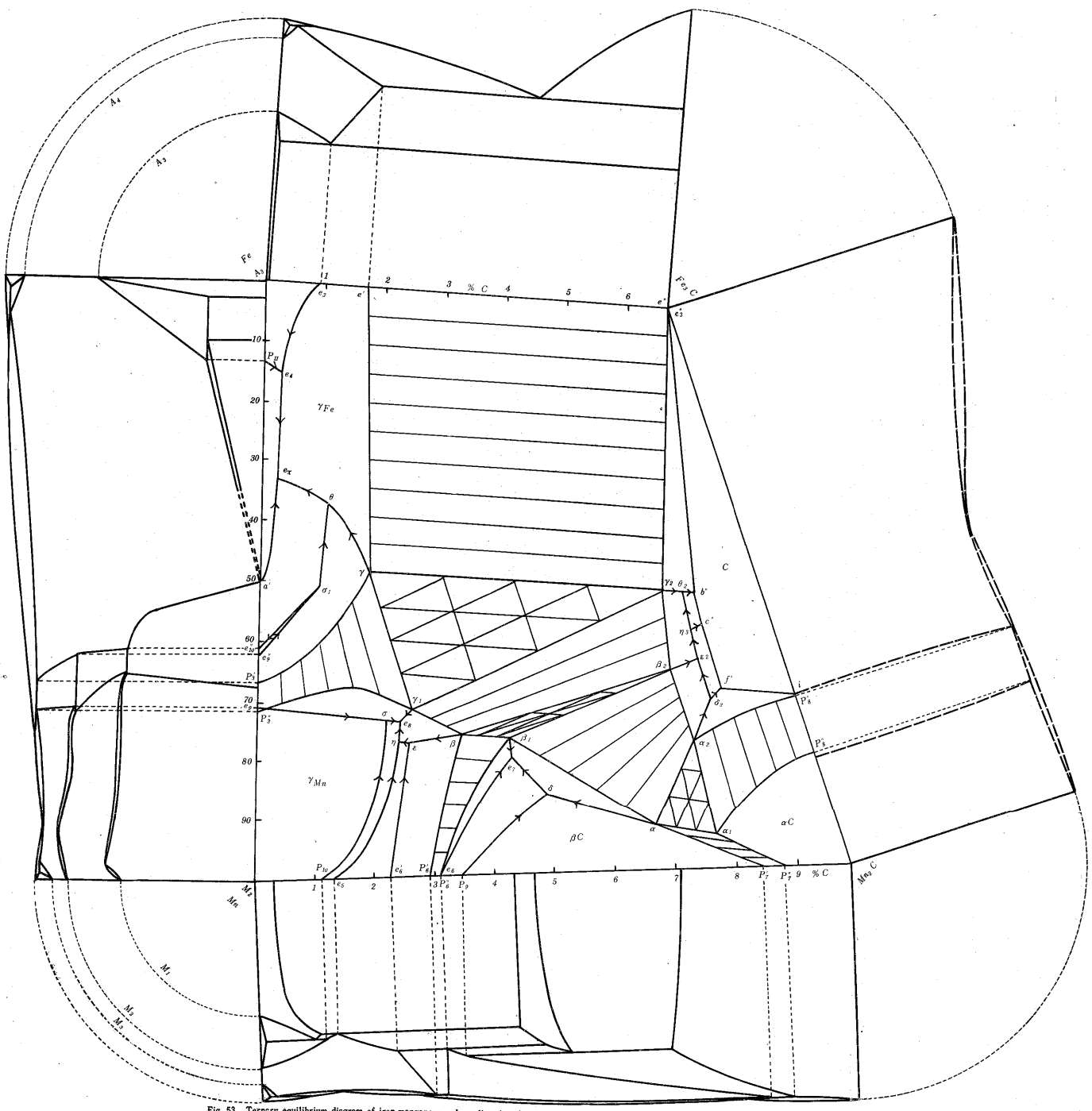

Fig. 53. Ternary equilibrium diagram of iron-manganese-carbon alloy, in which the liquidus and solidus surfaces is taken away and conjugate lines and meshes are drawn on the two-phase equilibrium and three-phase equilibrium respectively.

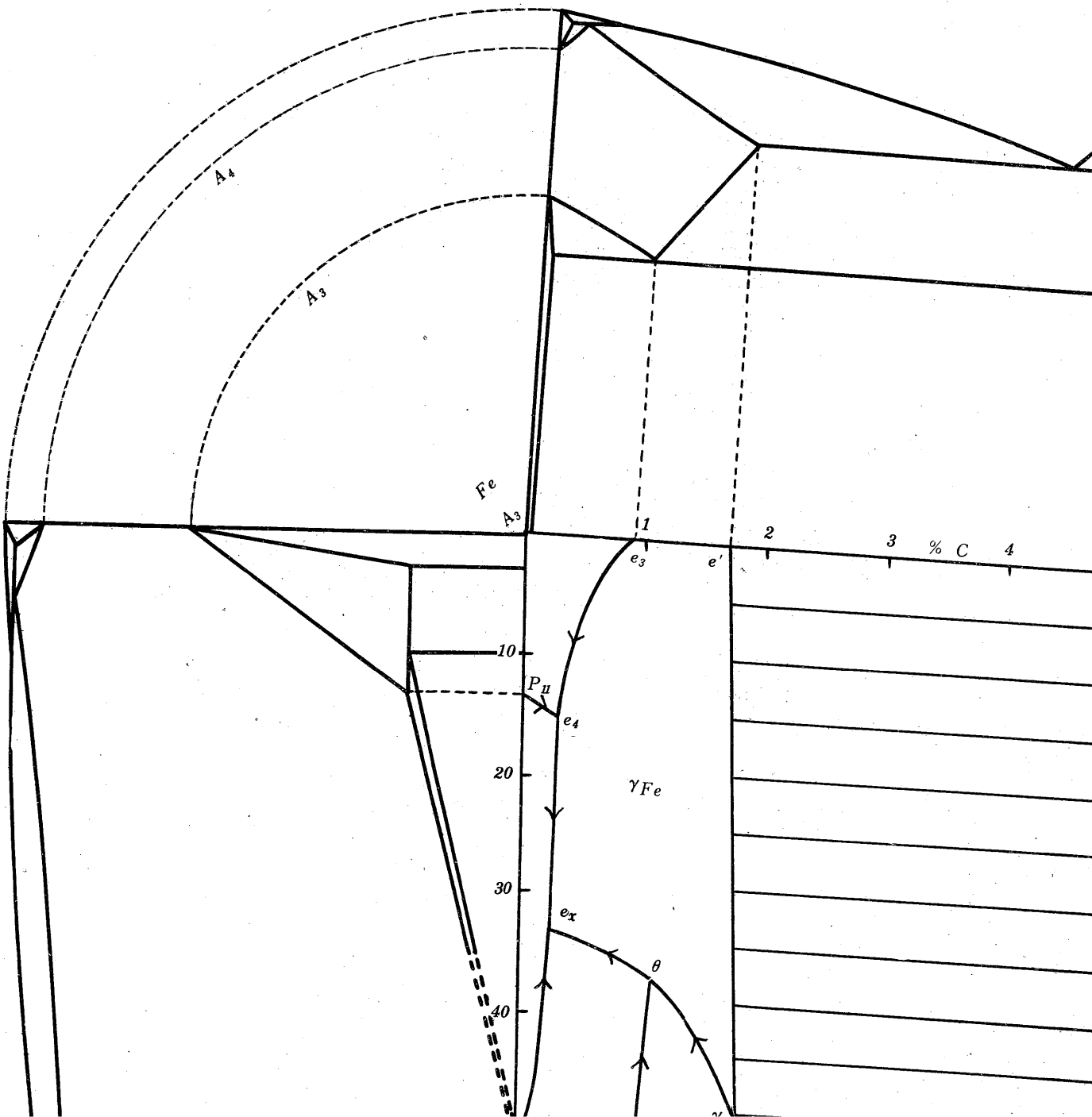
A4
A3
Fe
A3
1
2
3
% C
4
e3
e'
10
PII
e4
20
γFe
30
ex
θ
40

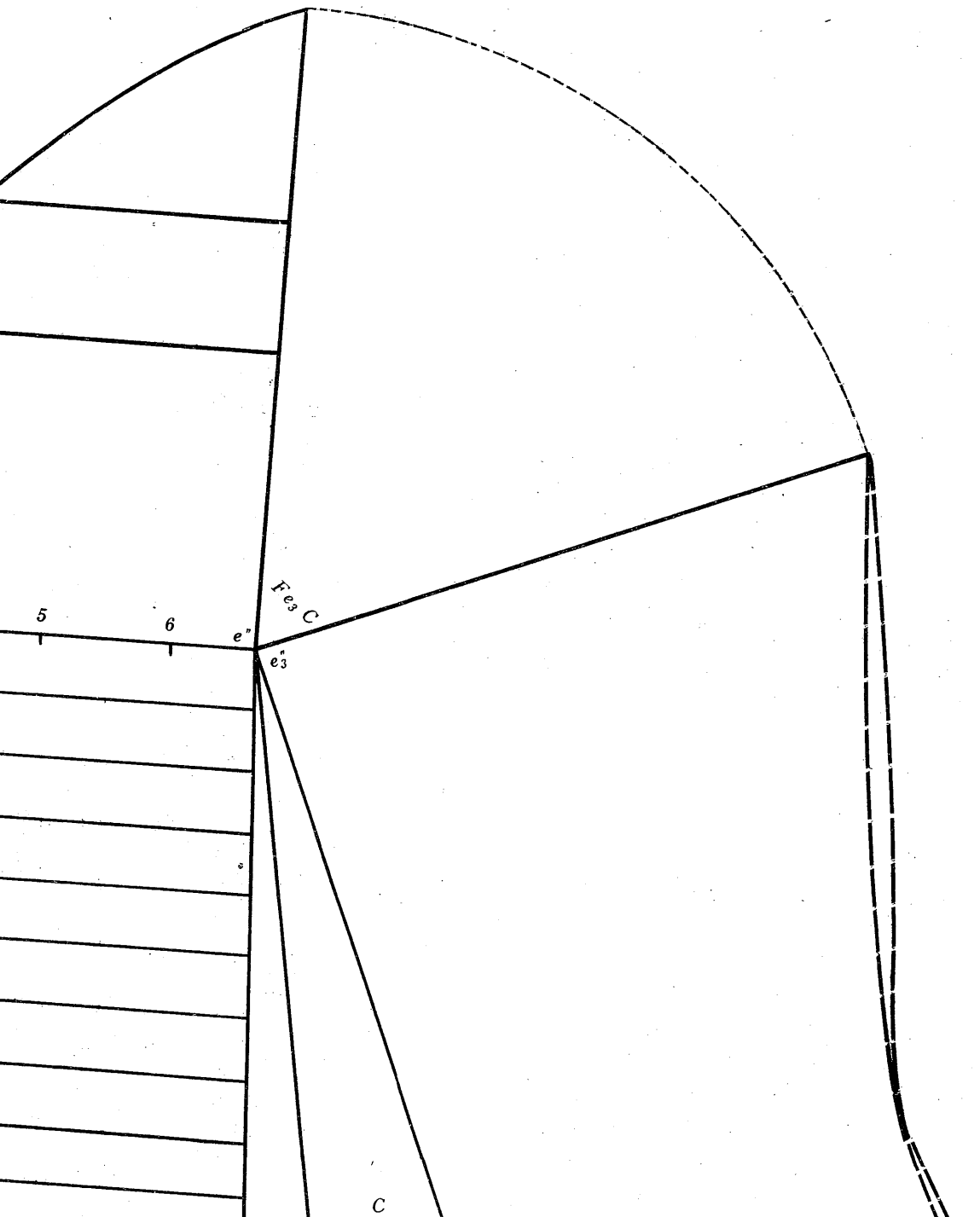
5
6
e''
Fe_3C
e''_3
C

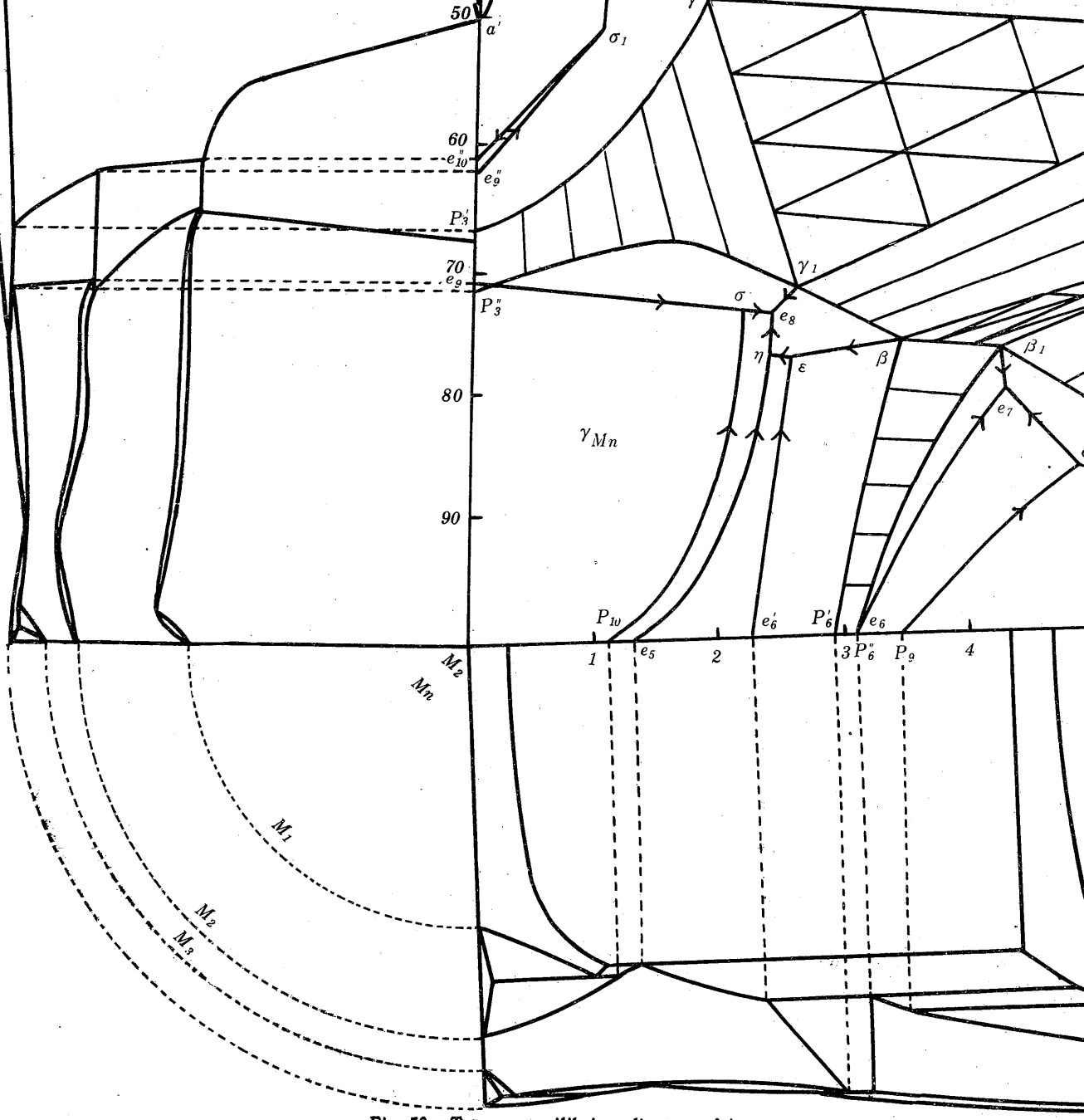

Fig. 53. Ternary equilibrium diagram of iron-manganese-carbon alloy, in which th
and meshes are drawn on the two-phase equilibrium and three-phase equilibrium r

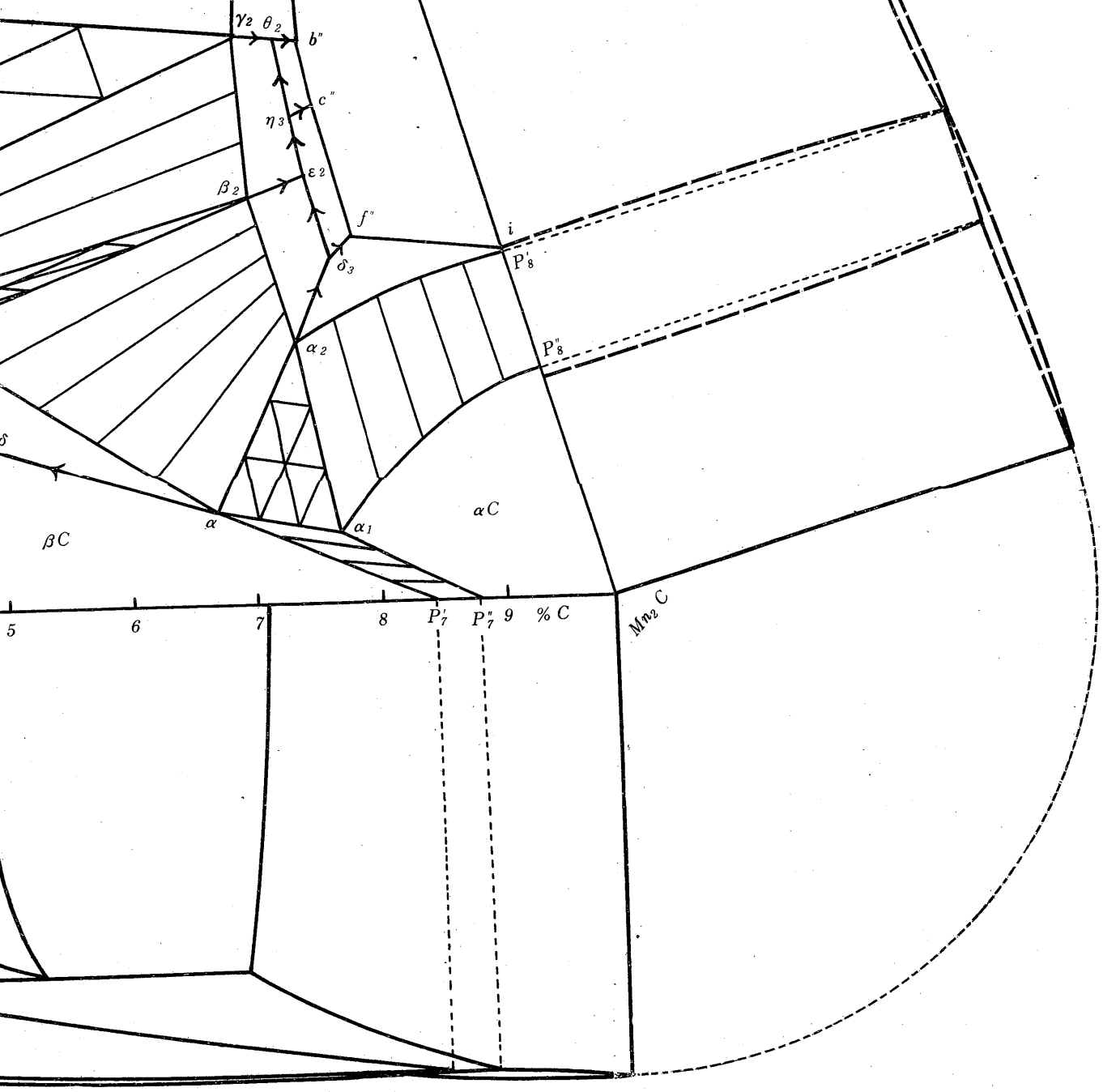

e liquidus and solidus surfaces is taken away and conjugate lines
espectively.

In Photos. 28 and 29, the most etched part is βC ternary solid solution and the white part C ternary solid solution and the midcoloured part αC ternary solid solution. The alloy consists of three phases and represents the structure in the regions (13) and (11) in Figs. 20 and 29, respectively.

Photos. 30 and 31 show the structure of single phase of γ manganese ternary solid solution quenched at high temperatures and represent the structure in the region (12) in Fig. 31. Photo. 32 shows the structure of two phases of γ manganese ternary solid solution and γ iron ternary solid solution, representing that in the regions of (11) and (5) in Figs. 31 and 36, respectively. Comparing Photos. 31 and 33 with each other, it will be seen that a small difference in quenching temperature caused the structure to change, that is, that the alloy quenched at 1050°C consists of two phases, whereas the same alloy quenched at 1100°C consists of the single phase of γ manganese ternary solid solution. The same will also be noticed in Photos. 32 and 35.

The composition of the alloy shown in Photo. 34 is the same as that in Photo. 31, but when the quenching temperature is 900°C, its structure consists of two phases of γ iron ternary solid solution and γ manganese solid solution, the amount of former being increased. This structure represents that in the regions (11) and (7) in Figs. 31 and 38, respectively.

The quenching structure of an alloy containing the same amount of manganese as the above and a small amount of carbon consists of three phases as shown in Photo. 35, though the quenching temperature is the same as above, and it represents the structure in the regions (27) and (7) in Figs. 31 and 36, repectively.

In Photo. 36, the ground mass is α manganese ternary solid solution, which is less etched than γC ternary solid solution. It represents the structures in the regions (23) and (21) in Figs. 27 and 36, respectively.

In Photo. 37, the constituent of white appearance is C ternary solid solution, and the primary crystal of γ manganese ternary solid solution is also seen. This is the structure in the regions (13) and (10) in Figs. 31 and 40, respectively.

Photo. 38 shows the structure of the alloy containing 70.65 per cent of manganese and 2.56 per cent of carbon, quenched at 900°C. It consists of three phases, that is, a large amount of ground mass of γ manganese ternary solid solution and small amounts of γ iron ternary solid solution and of C ternary solid solution, because the composition of the alloy is in the neighbourhood of the vertex of the triangular figure of ternary eutectic, which represents the composition of γ manganese ternary solid solution.

Photo. 39 is the structure immediately after the completion of the ternary eutectoid reaction, γ manganese ternary solid solution $\rightleftarrows$ α manganese ternary solid solution + γ iron ternary solid solution + C ternary solid solution, at 730°C.

The composition of the alloy represented by Photo. 40 is in the region (8) close by (7) in Fig. 23, and the structure consists almost of α manganese ternary solid solution and C ternary solid solution, γC ternary solid solution being scarcely observable.

In Photo. 41, white part is C ternary solid solution and black part βC ternary solid solution and midcoloured part γ manganese ternary solid solution.

Photo. 42 shows two-phase structure of βC ternary solid solution and C ternary solid solution, representing the structure in the regions of (11), (15) and (10) in Figs. 19, 31 and 46, respectively.

In Photo. 43, white part is C ternary solid solution and black part βC ternary solid solution and the amount of αC ternary solid solution is the least.

In Photo. 44, black part is βC ternary solid solution and white part C ternary solid solution and gray part αC ternary solid solution. This represents the structure in the regions (13) and (18) in Figs. 19 and 31, respectively.

The structure of the alloy containing about 70 per cent of manganese and 4.6 per cent of carbon, when quenched at 900°C, consists of three phases of γ manganese ternary solid solution, γC ternary solid solution and C ternary solid solution, as shown in Photo. 45, in which γC ternary solid solution is black and very small in amount, because the composition of the alloy is far apart from the vertex of the triangular figure of the region (10) in Fig. 21, which indicats the γC ternary solid solution.

The structure of an alloy quenched at 900°C, that is, at the temperature just after the completion of the ternary eutectoid reaction at 925°C, consists of three phases of γ manganese ternary solid solution, γC ternary solid solution and C ternary solid solution, as shown in Photo. 46, in which γC ternary solid solution is black coloured and C ternary solid solution is scarcely etched.

The alloy shown in Photo. 47 contains almost the same amount of manganese but different amount of carbon as compared with the above. In this case, the black coloured part of γC ternary solid solution is decreased and gray coloured part of α manganese ternary solid solution is increased instead of the disappearance of γ manganese ternary solid solution. This represents the structure in the regions (8), (23) and (27) in Figs. 23, 31 and 44, respectively.

In Photo. 48, gray part is α manganese ternary solid solution and black part γC ternary solid solution and white part C ternary solid solution, and the amount of α manganese ternary solid solution is small and that of black coloured γC ternary solid solution is increased. This represents the structure in the regions (8), (23) and (25) in Figs. 23, 31 and 45, respectively.

In Photo. 49, the structure of alloy consists of two phases of γC ternary solid solution and C ternary solid solution, showing large primary crystals of C ternary solid solution and binary eutectic. This represents the structure in the regions (11), (21) and (26) in Figs. 23, 31 and 46, respectively.

In Photo. 50, the black parts is γC ternary solid solution and white part is C ternary solid solution and αC ternary solid solution is scarcely observable, because the composition of the alloy is in the neighbourhood of the line which connects the vertices of the triangular figure in Fig. 23 which represent the composition of γC ternary solid solution and of C ternary solid solution, and is accordingly, far apart from the other vertex which represents the αC ternary solid solution.

The composition of the alloy shown in Photo. 51 is in the same triangular figure as that in Photo. 50, but in the former it lies in the neighbourhood of the line connecting the vertices of αC ternary solid solution and of C ternary solid solution, and moreover, it is near to the side rich in C ternary solid solution and is far apart from the vertex indicating the γC ternary solid solution. Hence, white coloured C ternary solid solution. middle coloured αC ternary solid solution and black coloured γC ternary solid solution are seen in Photo. 51, showing a very small amount of γC ternary solid solution. This represents the structure in the regions (12) and (15) in Figs. 23 and 30, respectively.

From Photos. 30~51, it was possible to gave a satisfactory explanation of the relations between phases in the sectional diagram at the alloy containing 70 per cent of manganese.

Photo. 52 is the structure of the alloy containing 74.84 per cent of manganese and 4.54 per cent of carbon and quenched at 900°C, that is, at the temperature just after the eutectoid reaction, βC ternary solid solution $\rightarrow$ γ manganese ternary solid solution + γC ternary solid solution + C ternary solid solution, ended. In the photograph, γC ternary solid solution looks black and γ manganese ternary solid solution gray and C ternary solid solution white. The structure of this alloy is a uniform βC ternary solid solution at high temperatures, but, when quenched at 1100°C, it becomes βC ternary solid solution containing a very small amount of C ternary solid solution as shown in Photo. 21, in which βC ternary solid solution appears martensitic.

Photo. 53 illustrates the structure of the alloy quenched at 900°C whose composition is corresponding to that near the eutectoid line e_6e_7 in Fig. 52, and accordingly, the structure, which is uniform βC ternary solid solution at high temperatures, decomposes at 900°C into two phases, γ manganese ternary solid solution of ground mass and black coloured γC ternary solid solution.

Photo. 54 is the eutectoid structure, βC binary solid solution $\rightarrow$ γ manganese binary solid solution + γC binary solid solution, in binary system of manganese and carbon. Structures of ternary alloys containing a small amount of iron showed almost the same structures as those of binary alloys.

Photo. 55 shows the structure of uniform γC ternary solid solution discovered first by the present writer, in which black lines are quenching cracks. This is the structure in the region (12) in Fig. 21.

Photo. 56 illustrates the structure of an alloy containing more carbon and less manganese than the above-mentioned and indicates the structure in the region (13) in Fig. 21, which consists of γC ternary solid solution and C ternary solid solution.

Photo. 57 shows the structure of uniform αC ternary solid solution discovered first by the present writer. The alloys containing high carbon and high manganese show the structure of single phase which is considered to be the ternary solid solution of manganese carbide Mn_3C in which manganese and iron are dissolved.

The alloy containing almost the same amount of carbon but less manganese than that in Photo. 57, consists of two phases, αC ternary solid solution and C ternary solid solution, as shown in Photo. 58, and represents the structure in the region (17) in Fig. 21.

In the case of further decreasing content of manganese, the structure of single phase is obtained as shown in Photo. 59, which represents the structure in the region (9) in Fig. 21.

From the above results, it will be ascertained that alloys containing less than 60 per cent of manganese and those containing more than about 90 per cent of manganese consist all of uniform phase, while alloys of intermediate composition between them consist of two phases. That is, iron carbide, cementite, and manganese carbide do not make the so-called uniform solid solution in all proportions, as previously considered.

Photo. 60 shows the pearlitic structure near the ternary eutectoid point, in which α manganese ternary solid solution looks gray and C ternary solid solution white, the amount of γ iron ternary solid solution being very small. As shown in Photo. 39, the amount of γ iron ternary solid solution becomes appreciable as the manganese content decreases. This ternary eutectoid point is very near the side $\theta_1\theta_2$ of the triangular figure in Fig. 54, whose vertices θ_1, θ_2 and θ represent α manganese ternary solid solution, C ternary solid solution and γ iron ternary solid solution, respectively and hence the amount of γ iron ternary solid solution is very small in the eutectoid structure. The ternary eutectoid structure can, therefore, discerned only when magnified one thousand or more times.

In Photo. 61 α manganese ternary solid solution forms the groundmass and C ternary solid solution looks white. This structure is a representative of the structures shown by the eutectic line ηe_8 in Fig. 51.

The structure shown in Photo. 62 consists of two phases, groundmass of α manganese ternary solid solution and black part of γC ternary solid solution, and is the eutectoid structure shown by the line $e_5\eta$ in Fig. 51.

Photo. 63 is the structure subjected to the reaction at the point η in Fig. 51, and hence it consists of three phases, that is, gray part of α manganese ternary solid solution, black part of γC ternary solid solution and white part of C ternary solid solution.

Photo. 64 shows the structure of alloy containing 75.07 per cent of manganese and 2.46 per cent of carbon and quenched at 700°C, in which the amount of γC ternary solid solution is very small. This represents the structure in the regions (8), (20) and (23) in Figs. 23, 30 and 39, respectively.

As mentioned above, these microscopic photographs can give us a satisfactory explanation of the sectional diagrams of the ternary alloy system. Furthermore, X-ray examinations were made with alloys of cast, quenched and annealed states, ranging the all compositions of ternary alloy system, and especially, with alloys containing 52.57~87.01 per cent of manganese and 6.97~8.07 per cent of carbon, which could also ascertained that both cementite and manganese carbide in the

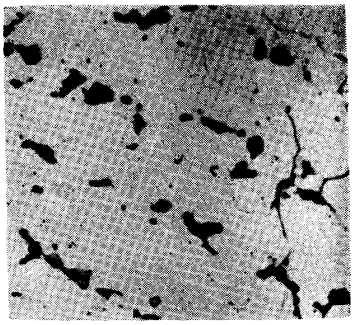

Photo. 25. ×100
61.58%Mn, 1.57%C; quenched at 1000°C in ice brine water; black coloured γ iron ternary solid solution phase appears in ground mass of γ manganese ternary solid solution.

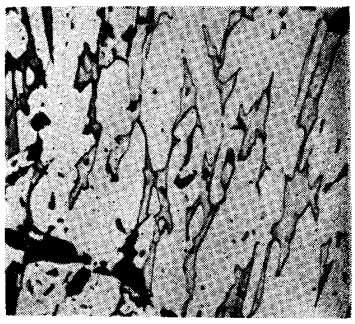

Photo. 26. ×100
59.77%Mn, 6.00%C; quenched at 1000°C in ice brine water; coloured parts are γ manganese ternary solid solution, white C ternary solid solution.

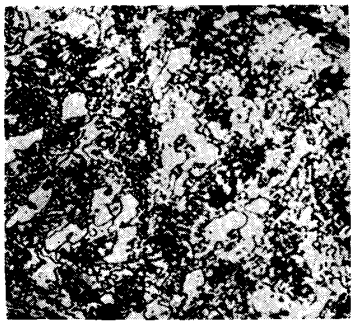

Photo. 27. ×100
78.79%Mn, 3.16%C; quenched at 1000°C in ice brine water; γ manganese ternary solid solution and βC ternary solid solution.

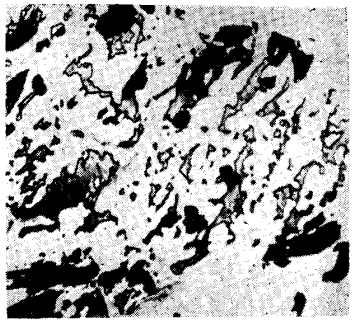

Photo. 28. ×100
78.35%Mn, 6.10%C; quenched at 1000°C in ice brine water, the most eched part is βC ternary solid solution, the white part C ternary solid solution, and the mid-coloured part αC ternary solid solution.

Photo. 29. ×400
78.35%Mn, 6.10%C; same as Photo. 28, but high magnification; the most eched part is βC ternary solid solution, white part C ternary solid solution and mid-coloured part αC ternary solid solution.

Photo. 30. ×400
68.22%Mn, 1.65%C; quenched at 1100°C in ice brine water; γ manganese ternary solid solution.

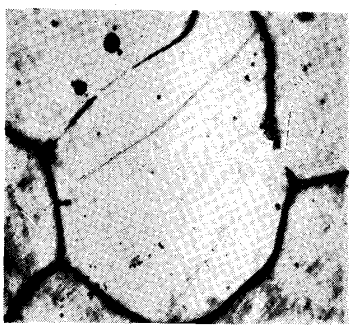

Photo. 31. ×400
70.52%Mn, 2.07%C; quenched at 1100°C in ice brine water; γ manganese ternary solid solution.

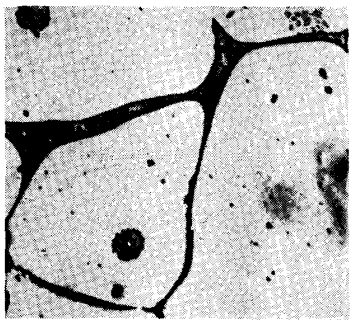

Photo. 32. ×400
68.53%Mn, 1.18%C; quenched at 1050°C in ice brine water; γ manganese ternary solid solution and γ iron ternary solid solution.

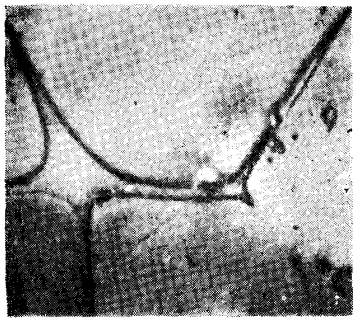

Photo. 33. ×400
70.52%Mn, 2.07%C; quenched at 1050°C in ice brine water; γ manganese ternary solid solution and γ iron ternary solid solution.

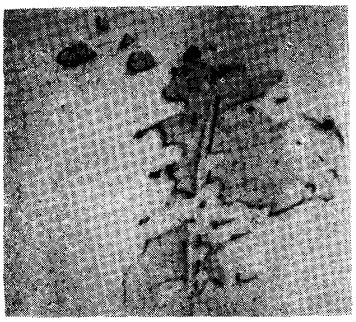

Photo. 34. ×400
70.52%Mn, 2.07%C; quenched at 900°C in ice brine water; γ iron ternary solid solution (coloured) and γ manganese ternary solid solution.

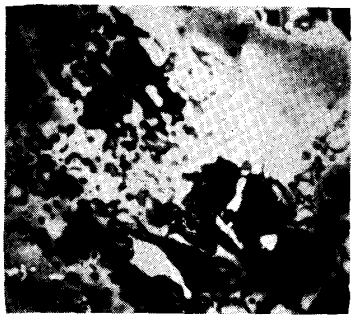

Photo. 35. ×400
68.53%Mn, 1.18%C; quenched at 900°C in ice brine water; the most coloured part is γ iron ternary solid solution, mid-coloured γ manganese ternary solid solution and β manganese ternary solid solution.

Photo. 36. ×400
89.87% Mn, 0.92%C; quenched at 700°C in ice brine water; γC ternary solid solution and ground mass of α manganese ternary solid solution.

Photo. 37. ×400
71.29 % Mn, 3.17% C ; quenched at 1000°C in ice brine water ; primary crystal of γ manganese ternary solid solution and white part is C ternary solid solution.

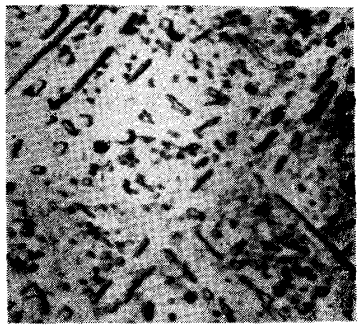

Photo. 38. ×400
70.65 % Mn, 2.56 %C ; quenched at 900°C in ice brine water; larg amount of ground mass is γ manganese ternary solid solution and a small amount of black coloured γ iron ternary solid solution and of white C ternary solid solution.

Photo. 39. ×1000
70.52 % Mn, 2.07 % C ; quenched at 700°C in ice brine water ; ternary eutectoid structure, α manganese ternary solid solution, γ iron ternary solid solution and C ternary solid solution.

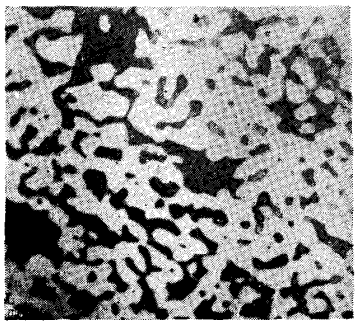

Photo. 40. ×400
70.95 % Mn, 3.58% C ; quenched at 700°C in ice brine water, the white part is C ternary solid solution, the coloured part α manganese ternary solid solution and a small amount of black coloured γC ternary solid solution.

Photo. 41. ×400
69.09 % Mn, 4.55 % C ; quenched at 1050°C in ice brine water ; the white part is C ternary solid solution, black part βC ternary solid solution and mid-coloured part γ manganese ternary solid solution.

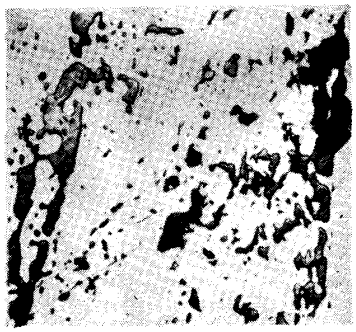

Photo. 42. ×400
70.05 % Mn, 6.14 % C ; quenched at 1050°C in ice brine water ; the coloured part is βC ternary solid solution and the white part C ternary solid solution.

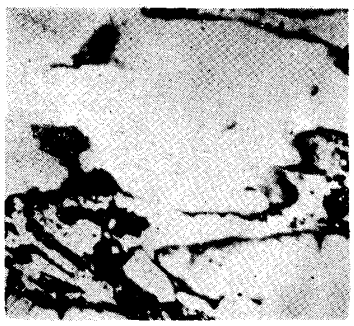

Photo. 43. ×400
71.03 % Mn, 6.77 % C ; quenched at 1050°C in ice brine water; white part is C ternary solid solution and black part βC ternary solid solution and the amounts of αC ternary solid solution is the least.

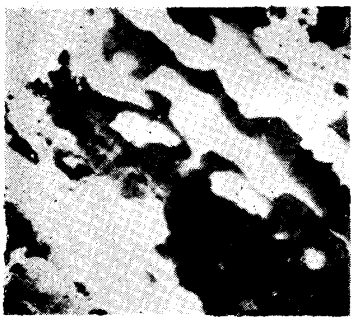

Photo. 44. ×400
71.12 % Mn, 7.34% C ; quenched at 1050°C in ice brine water ; the black part is βC ternary solid solution, white part C ternary solid solution and gray part αC ternary solid solution.

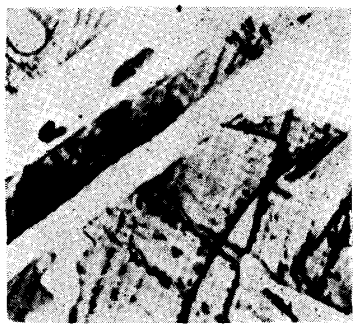

Photo. 45. ×400
67.31% Mn, 4.66 % C ; quenched at 900°C in ice brine water ; the white part is C ternary solid solution, and the coloured part γ manganese ternary solid solution and very small amount of black part is γC ternary solid solution.

Photo. 46. ×400
70.88% Mn, 5.61 % C ; quenched at 900°C in ice brine water ; the black part is γC ternary solid solution, the white part C ternary solid solution and mid-coloured part γ manganese ternary solid solution.

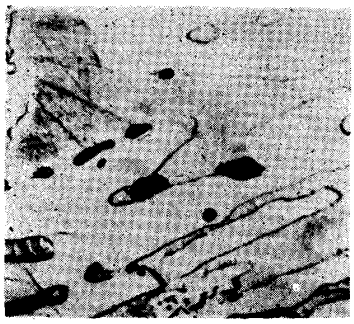

Photo. 47. ×400
70.58 % Mn, 4.92% C ; quenched at 700°C in ice brine water ; the black coloured part is γC ternary solid solution and its amount is the least, the white part C ternary solid solution and mid-coloured part α manganese ternary solid solution.

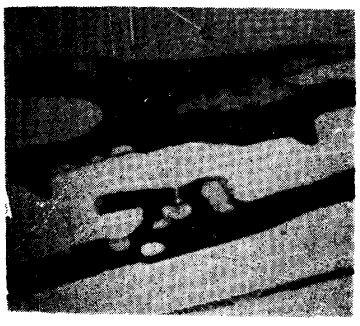

Photo. 48. ×400
70.88 % Mn, 5.61% C ; quenched at 700°C in ice brine water ; the black part is γC ternary solid solution and the white part C ternary solid solution and small amount of α manganese ternary solid solution.

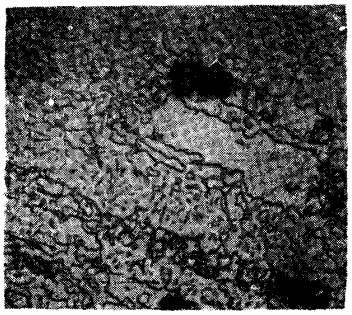

Photo. 49. ×400
70.05% Mn, 6.14% C; quenched at 700°C in ice brine water; the primary crystal of C ternary solid solution and binary eutectic structure of γC ternary solid solution and C ternary solid solution.

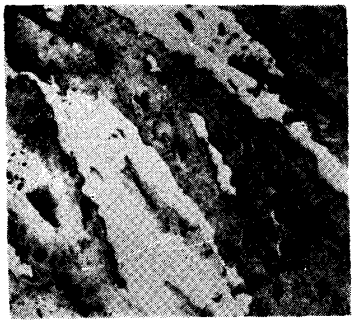

Photo. 50. ×400
71.03% Mn, 6.77% C; quenched at 700°C in ice brine water; the black part is γC ternary solid solution and white part C ternary solid solution and αC ternary solid solution is scarcely observable.

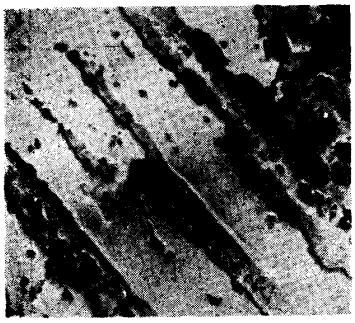

Photo. 51. ×400
74.12% Mn, 7.34% C; quenched at 700°C in ice brine water; the white part is C ternary solid solution and mid-coloured part αC ternary solid solution and a very small amount of black coloured is γC ternary solid solution.

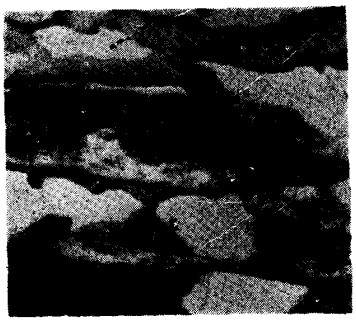

Photo. 52. ×1200
74.84% Mn, 4.54% C; quenched at 900°C in ice brine water; the ternary eutectoid structure, the black part is γC ternary solid solution, the gray part γ manganese ternary solid solution and the white part C ternary solid solution.

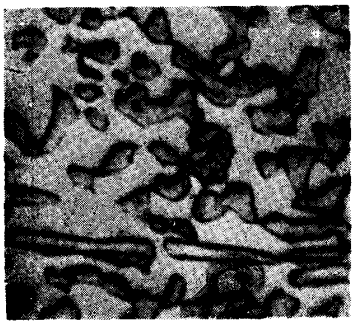

Photo. 53. ×1000
84.23% Mn, 3.57% C; quenched at 900°C in ice brine water; the binary eutectoid structure, the coloured part is γC ternary solid solution and the white part γ manganese ternary solid solution.

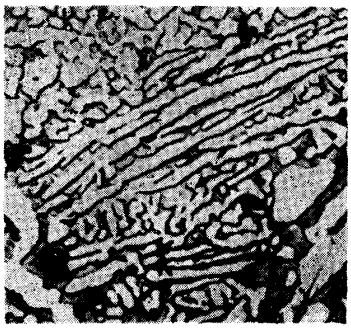

Photo. 54. ×400
96.87% Mn, 3.13% C; quenched at 900°C in ice brine water; eutectoid structure of binary system.

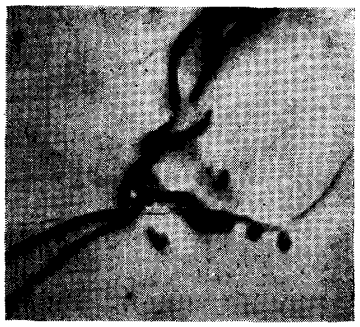

Photo. 55. ×800
89.59% Mn, 4.74% C; quenched at 900°C in ice brine water; γC ternary solid solution.

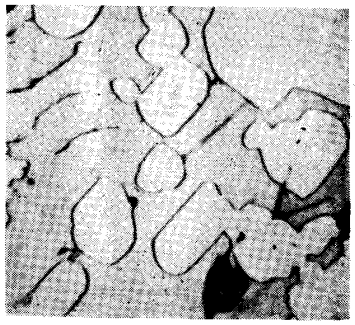

Photo. 56. ×800
74.56% Mn, 5.91% C; quenched at 900°C in ice brine water; the white part is C ternary solid solution and the gray part γC ternary solid solution.

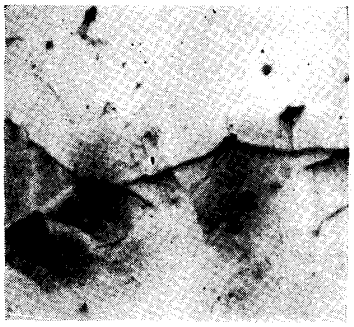

Photo. 57. ×800
87.01% Mn, 8.07% C; quenched at 900°C in ice brine water; uniform αC ternary solid solution.

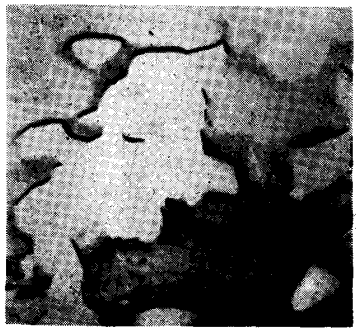

Photo. 58. ×800
72.86% Mn, 8.04% C; quenched at 900°C in ice brine water; αC ternary solid solution and C ternary solid solution.

Photo. 59. ×800
59.72% Mn, 7.62% C; quenched at 900°C in ice brine water; uniform C ternary solid solution.

Photo. 60. ×1000
70.52% Mn, 2.07% C; quenched at 700°C in ice brine water; ternary eutectoid structure, the white part is C ternary solid solution, the gray part α manganese ternary solid solution and the black part γ iron ternary solid solution.

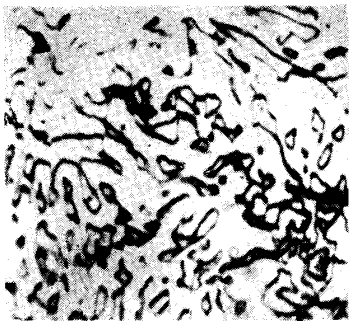

Photo. 61. ×1000
73.25% Mn, 2.26% C; quenched at 700°C in ice brine water; α manganese ternary solid solution and C ternary solid solution and a small amount of γ iron ternary solid solution.

Photo. 62. ×1000
84.75% Mn, 2.40% C; quenched at 700°C in ice brine water; the black part is γC ternary solid solution and the ground mass α manganese solid solution, the eutectoid structure.

Photo. 63. ×800
79.43% Mn, 2.49% C; quenched at 700°C in ice brine water; ternary eutectoid structure, the black part is γC ternary solid solution, mid-coloured part α manganese ternary solid solution and white part C ternary solid solution.

Photo. 64. ×1000
75.07% Mn, 2.46% C; quenched at 700°C in ice brine water; the white part is C ternary solid solution and the gray part α manganese ternary solid solution and the amount of γC ternary solid solution is very small.

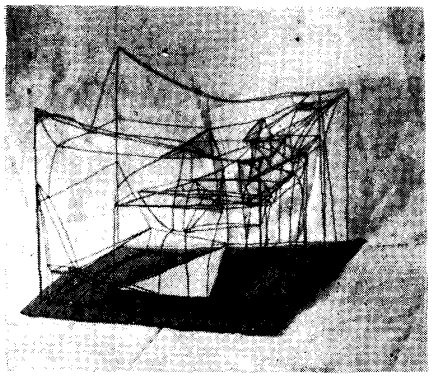

Diagram model viewed from iron-manganese alloy side.

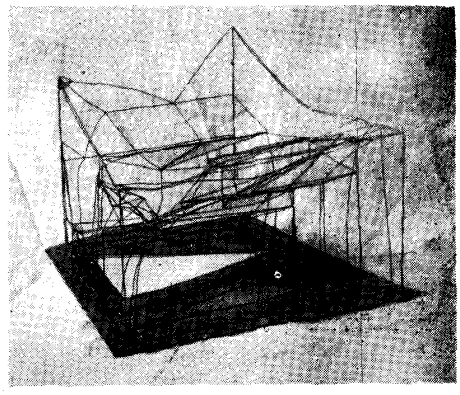

Diagram model viewed from manganese-carbon alloy side.

Photo. 66. Model of ternary diagram.

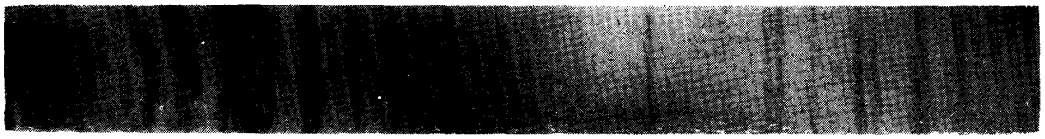

Cementite.

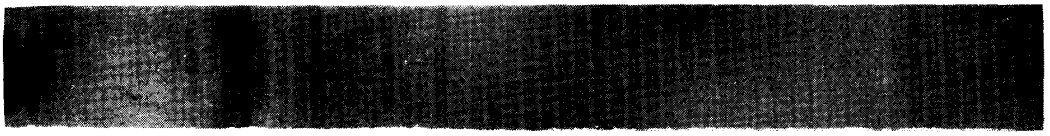

63.98% Mn, 7.47% C ; annealed.

68.14% Mn, 7.53% C ; annealed.

72.86% Mn, 8.04% C ; annealed.

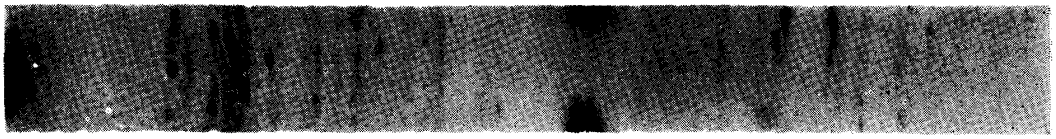

77.22% Mn, 8.29% C ; annealed.

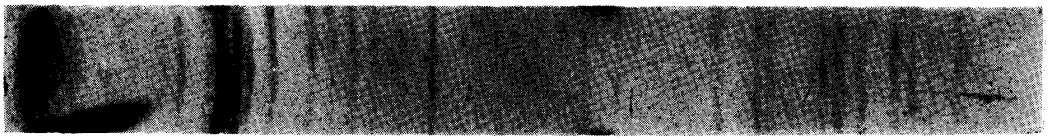

87.01% Mn, 8.07% C ; annealed.

Photo. 65. X-ray examination.

side of high manganese and high carbon did not form uniform solid solution in any proportion; in other words, some heterogeneous structures must exist in the neighbourhood of 70 per cent of manganese.

Some results of X-ray examination of respective alloys are arranged in Table 12, and some examples are shown in Photo. 65, from which a satisfactory explanation of the above sectional diagrams could also be obtained.

Table 12. X ray examination.

Specimen number	Mn %	C %	Quenching temperature °C and its structure			
			1100	1000	900	600
6005	56.57	1.02	A	A+γ		
6505	62.02	1.11	A+γ	A+γ		
7005	62.50	1.01	A+γ	A+γ	A	
7505	68.53	1.18	A+γ	A+γ	A+γ+β	
8005	72.97	1.12	γ	A+γ	γ+β+(α)	
8505	79.32	1.14	γ	γ	γ+β+(α)	
9005	84.66	1.36	γ	γ	γ+β+(α)	
9505	89.87	0.92	γ	γ	γ+β	
9705	90.33	1.34	γ	γ	γ+β+(γC)	
775075	69.35	1.02				A+α
800075	78.45	0.91				α
825075	75.42	1.13				α+(A)+(C)
850075	76.40	0.72				α
5510	52.95	1.52	A+γ			
6010	57.43	1.53	A+γ			
6510	61.58	1.57	A+γ			
7010	66.61	1.65	A+γ			
7510	68.22	1.65	A+γ			
8010	75.79	1.78	γ			
8510	78.99	1.87	γ			
9010	84.11	1.92	γ			
9510	87.16	1.93	γ			
5015	48.45	2.01	A			
5515	51.95	1.94	A+γ			
6015	58.30	1.88	A+γ			
6515	62.20	2.03	A+γ			
7015	65.83	2.05	A+γ			
7515	70.52	2.07	A+γ			
8015	73.25	2.26	γ			
8515	82.47	2.21	γ			
9015	84.75	2.40	γ			
9515	87.30	2.38	γ			
5060	48.79	5.90	A+C			
5560	53.27	6.13	γ+C			
6060	59.77	6.00	γ+C			
6560	64.26	5.89	βC+C			
7060	68.48	5.85	βC+C			
7560	74.56	5.91	βC+C			
8060	78.35	6.10	βC+αC+C			
8260	79.90	5.68	βC+C			
8560	82.75	6.14	βC+αC+C			
8950	86.21	5.24	βC+αC			

Note: A=austenite, γ iron ternary solid solution
γ=γ manganese ternary solid solution
β=β manganese ternary solid solution
α=α manganese ternary solid solution
C=C ternary solid solution
αC=αC ternary solid solution
βC=βC ternary solid solution
γC=γC ternary solid solution

VII. Complete equilibrium diagram

Fig. 54 is the complete diagram of the ternary alloy system obtained by the present experiments. In the figure, the meanings of various notations are the same as that explained before and those of phases, lines and points are given below, and arrows show the directions of respective reactions.

surface $P_7'\alpha\delta P_9P_7'$ — the solubility surface of αC ternary solid solution in βC ternary solid solution

surface $P_7''P_9''\delta_2\alpha_1P_7''$ — the solubility surface of βC ternary solid solution in αC ternary solid solution

surface $\alpha\beta_1e_7\delta\alpha$ — the solubility surface of C ternary solid solution in βC ternary solid solution

surface $\alpha_2\beta_2\varepsilon_2\delta_3\alpha_2$ — the solubility surface of βC ternary solid solution in C ternary solid solution

surface $P_6''\beta_1e_7e_6P_6''$ — the solubility surface of γ manganese ternary solid solution in βC ternary solid solution

surface $P_6'\beta\varepsilon e_6'P_6'$ — the solubility surface of βC ternary solid solution in γ manganese ternary solid solution

surface $P_9\delta e_7e_6P_9$ — the solubility surface of γC ternary solid solution in βC ternary solid solution

surface $P_9'\delta_1\varepsilon_1e_6''P_9'$ — the solubility surface of βC ternary solid solution in γC ternary solid solution

surface $P_9'\delta_1fgP_9'$ — the solubility surface of αC ternary solid solution in γC ternary solid solution

surface $P_9''\delta_2f'g'P_9''$ — the solubility surface of γC ternary solid solution in αC ternary solid solution

surface $\delta_1\varepsilon_1\eta_2c'f\delta_1$ — the solubility surface of C ternary solid solution in γC ternary solid solution

surface $\delta_3\varepsilon_2\eta_3c''f''\delta_3$ — the solubility surface of γC ternary solid solution in C ternary solid solution

surface $P_8''\alpha_1\delta_2f'hP_8''$ — the solubility surface of C ternary solid solution in αC ternary solid solution

surface $P_8'\alpha_2\delta_3f''iP_8'$ — the solubility surface of αC ternary solid solution in C ternary solid solution

surface $e_6'\varepsilon\eta e_5e_6'$ — the solubility surface of γC ternary solid solution in γ manganese ternary solid solution

surface $e_6''\varepsilon_1\eta_2e_5''e_6''$ — the solubility surface of γ manganese ternary solid solution in γC ternary solid solution

surface $\beta\gamma_1e_8\eta\varepsilon\beta$ — the solubility surface of C ternary solid solution in γ manganese ternary solid solution

surface $\beta_2\gamma_2\theta_2\eta_3\varepsilon_2\beta_2$ — the solubility surface of γ manganese ternary solid solution in C ternary solid solution

surface $P_3''\gamma_1 e_8 \sigma e_9 P_3''$ — the solubility surface of γ iron ternary solid solution in γ manganese ternary solid solution

surface $P_3'\gamma\theta\sigma_1 e_9'' P_3'$ — the solubility surface of γ manganese ternary solid solution in γ iron ternary solid solution

surface $M_2 e_9 \sigma P_{10} M_2$ — the solubility surface of β manganese ternary solid solution in γ manganese ternary solid solution

surface $M_2 e_9' \sigma_2 P_{10}' M_2$ — the solubility surface of γ manganese ternary solid solution in β manganese ternary solid solution

surface $P_{10}\sigma e_8 \eta e_5 P_{10}$ — the solubility surface of α manganese ternary solid solution in γ manganese ternary solid solution

surface $P_{10}''\sigma_3\theta_1\eta_1 e_5' P_{10}''$ — the solubility surface of γ manganese ternary solid solution in α manganese ternary solid solution

surface $e_5'\eta_1 c d e_5'$ — the solubility surface of γC ternary solid solution in α manganese ternary solid solution

surface $e_5''\eta_2 c' d' e_5''$ — the solubility surface of α manganese ternary solid solution in γC ternary solid solution

surface $\eta_1\theta_1 bc\eta_1$ — the solubility surface of C ternary solid solution in α manganese ternary solid solution

surface $\eta_3\theta_2 b''c''\eta_3$ — the solubility surface of α manganese ternary solid solution in C ternary solid solution

surface $e_{10}'\sigma_3\theta_1 bae_{10}'$ — the solubility surface of γ iron ternary solid solution in α manganese ternary solid solution

surface $e_{10}''\sigma_1\theta e_x a' e_{10}''$ — the solubility surface of α manganese ternary solid solution in γ iron ternary solid solution

surface $M_1 P_{10}''\sigma_3 e_{10}' M_1$ — the solubility surface of β manganese ternary solid solution in α manganese ternary solid solution

surface $M_1 P_{10}'\sigma_2 e_{10} M_1$ — the solubility surface of α manganese ternary solid solution in β manganese ternary solid solution

surface $e_9'\sigma_2 e_{10} e_9'$ — the solubility surface of γ iron ternary solid solution in β manganese ternary solid solution

surface $e_9''\sigma_1 e_{10}'' e_9''$ — the solubility surface of β manganese ternary solid solution in γ iron ternary solid solution

surface $e'\gamma\theta e_x e_4 e_3' e'$ — the solubility surface of C ternary solid solution in γ iron ternary solid solution

surface $e''\gamma_2\theta_2 b''\pi e_3'' e''$ — the solubility surface of γ iron ternary solid solution in C ternary solid solution

surface $A_3 e_3 e_4 P_{11} A_3$ — the solubility surface of α iron ternary solid solution in γ iron ternary solid solution

surface $A_3 e_3'\pi_1 P_{11}'' A_3$ — the solubility surface of γ iron ternary solid solution in α iron ternary solid solution

Besides these, there are respective equilibrium surfaces between the following solid solutions; α iron ternary solid solution and h ternary solid solution; α iron ternary solid solution and C ternary solid solution; h ternary solid solution and

C ternary solid solution; h ternary solid solution and α manganese ternary solid solution.

Eutectoid lines, conjugate lines and their reactions are as follows:

line $\beta_1 e_7$ — βC ternary solid solution → γ manganese ternary solid solution + C ternary solid solution

line $e_6 e_7$ — βC ternary solid solution → γ manganese ternary solid solution + γC ternary solid solution

line δe_7 — β Cternary solid solution → γC ternary solid solution + C ternary solid solution

line $e_5\eta$ — γ manganese ternary solid solution → α manganese ternary solid solution + γC ternary solid solution

line ηe_8 — γ manganese ternary solid solution → α manganese ternary solid solution + C ternary solid solution

line $e_9\sigma$ — γ manganese ternary solid solution → β manganese ternary solid solution + γ iron ternary solid solution

line $e_{10}\sigma_2$ — β manganese ternary solid solution → α manganese ternary solid solution + γ iron ternary solid solution

line σe_8 — γ manganese ternary solid solution → α manganese ternary solid solution + γ iron ternary solid solution

Table 13.

Point	Reaction	Reaction temperature	Reaction surface
e_1	liquid + αC ternary solid solution → βC ternary solid solution + C ternary solid solution	1260°C	$e_1\alpha\alpha_1\alpha_2 e_1$
e_2	liquid + βC ternary solid solution → γ manganese ternary solid solution + C ternary solid solution	1105°C	$e_2\beta\beta_1\beta_2 e_2$
E	liquid → γ iron ternary solid solution + γ manganese ternary solid solution + C ternary solid solution	1090°C	$\gamma\gamma_1\gamma_2\gamma$
δ	βC ternary solid solution + αC ternary solid solution → γC ternary solid solution + C ternary solid solution	990°C	$\delta\delta_1\delta_2\delta_3\delta$
e_7	βC ternary solid solution → γ manganese ternary solid solution + γC ternary solid solution + C ternary solid solution	925°C	$\varepsilon\varepsilon_1\varepsilon_2\varepsilon$
η	γ manganese ternary solid solution → α manganese ternary solid solution + γC ternary solid solution + C ternary solid solution	780°C	$\eta_1\eta_2\eta_3\eta_1$
σ	γ manganese ternary solid solution + β manganese ternary solid solution → α manganese ternary solid solution + γ iron ternary solid solution	850°C	$\sigma\sigma_1\sigma_2\sigma_3\sigma$
e_8	γ manganese ternary solid solution → γ iron ternary solid solution + α manganese ternary solid solution + C ternary solid solution	730°C	$\theta\theta_1\theta_2\theta$
e_4	γ iron ternary solid solution + α iron ternary solid solution → h ternary solid solution + C ternary solid solution	150°C	$e_4\pi\pi_1\pi_2 e_4$
e_x	γ iron ternary solid solution → h ternary solid solution + α manganese ternary solid solution + C ternary solid solution	<0°C	$bb'b''b$

Table 14. Chemical compositions of respective points.

Point	Manganese %	Carbon %	Iron %	Temperature of reaction °C
e_1	80.0	6.3	13.7	1260
α	86.0	6.6	7.4	
α_1	87.0	7.6	5.4	
α_2	71.0	7.2	21.8	
e_2	61.0	3.8	35.2	1105
β	73.0	3.35	23.65	
β_1	73.0	4.15	22.85	
β_2	60.0	6.8	33.2	
E	48.5	4.0	47.5	1090
γ	47.0	1.8	51.2	
γ_1	69.5	2.55	27.95	
γ_2	47.0	6.7	46.3	
δ	82.0	4.8	13.2	990
δ_1	87.0	5.2	7.8	
δ_2	89.0	7.85	3.15	
δ_3	64.0	7.5	28.5	
e_7	76.0	4.2	19.8	925
ε	75.0	2.5	22.5	
ε_1	84.0	4.75	11.25	
ε_2	57.5	7.25	35.25	
σ	71.5	2.15	26.35	850
σ_1	50.0	1.0	49.0	
σ_2	73.0	0.35	26.65	
σ_3	78.0	1.0	21.0	
η	75.0	2.35	22.65	780
η_1	80.0	1.25	18.75	
η_2	84.0	4.40	11.60	
η_3	53.0	7.15	39.85	
e_8	71.5	2.4	26.10	730
θ	36.0	1.1	62.9	
θ_1	78.0	1.25	20.75	
θ_2	47.0	7.0	46.0	
e_4	15.0	0.3	84.7	150
π	10.0	0.2	89.8	
π_1	2.0	0.15	97.85	
π_2	15.0	6.8	78.2	

line $\gamma_1 e_8$ — γ manganese ternary solid solution → C ternar ysolid solution + γ iron ternary solid solution

line $\gamma\theta$ — γ iron ternary solid solution → γ manganese ternary solid solution + C ternary solid solution

line θe_x — γ iron ternary solid solution → α manganese ternary solid solution + C ternary solid solution

line $e_3 e_4$ — γ iron ternary solid solution → α iron ternary solid solution + C ternary solid solution

line $\alpha\delta$ — βC ternary solid solution → C ternary solid solution + αC ternary solid solution

Peritectoid lines and their reaction are as follows:

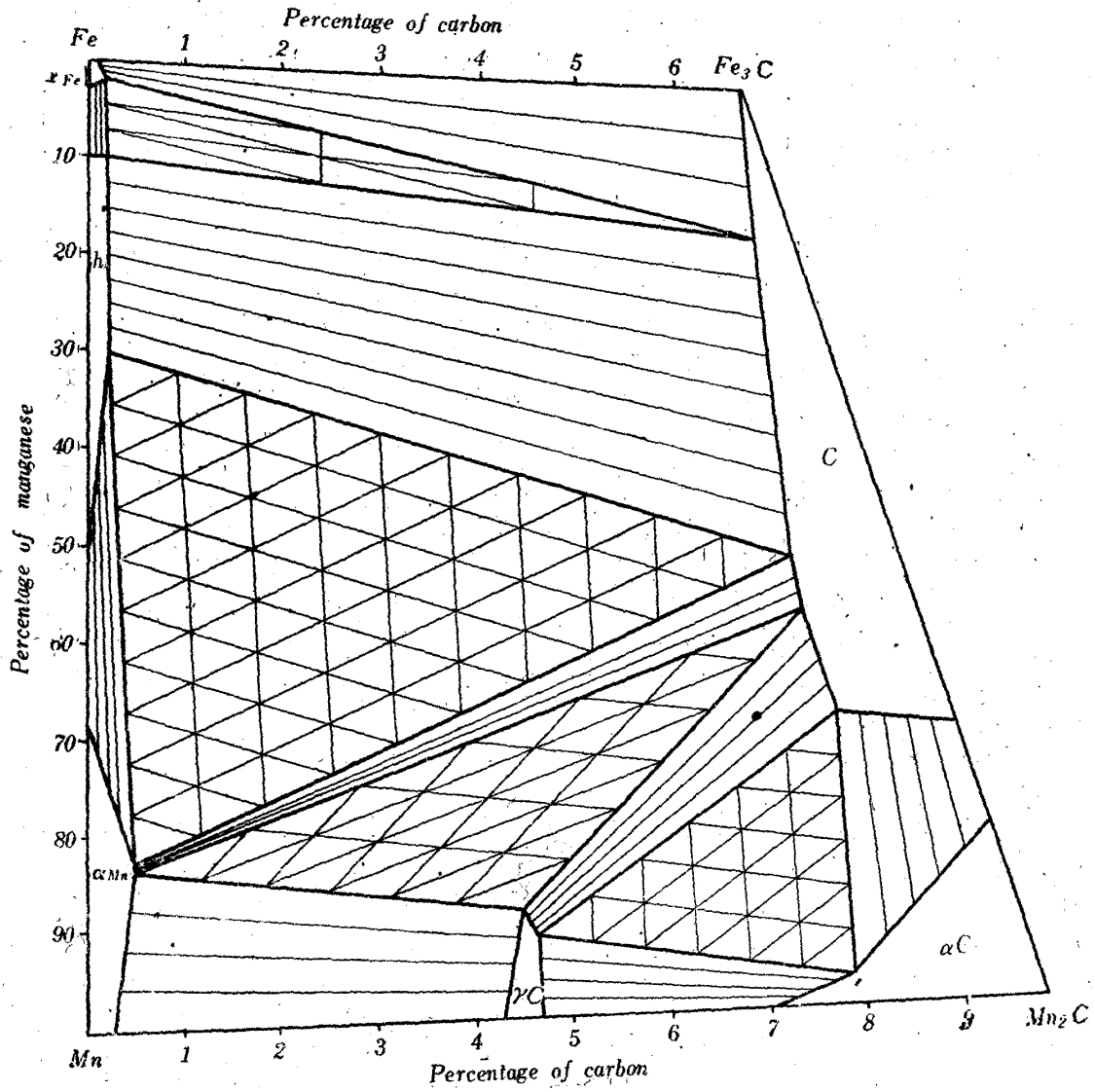

Fig. 55. Structural diagram of iron-manganese-carbon ternary alloy at room temperature, in the neighbourhood of which the reactions have made a complete progress. Blanks, conjugates and meshes are the one-,two- and three-phase regions, respectively.

line $P_9\delta$ — βC ternary solid solution + αC ternary solid solution → γC ternary solid solution

line $P_{10}\sigma$ — γ manganese ternary solid solution + β manganese ternary solid solution → α manganese ternary solid solution

line $P_{11}e_4$ — γ iron ternary solid solution + α iron ternary solid solution → h ternary solid solution

Peritecto-eutectoid points and their reaction are as follows:

point δ — βC ternary solid solution + αC ternary solid solution → γC ternary solid solution+C ternary solid solution

point σ — γ manganese ternary solid solution + β manganese ternary solid solution → α manganese ternary solid solution + γ iron ternary solid solution

point e_4 — γ iron ternary solid solution + α iron ternary solid solution → h ternary

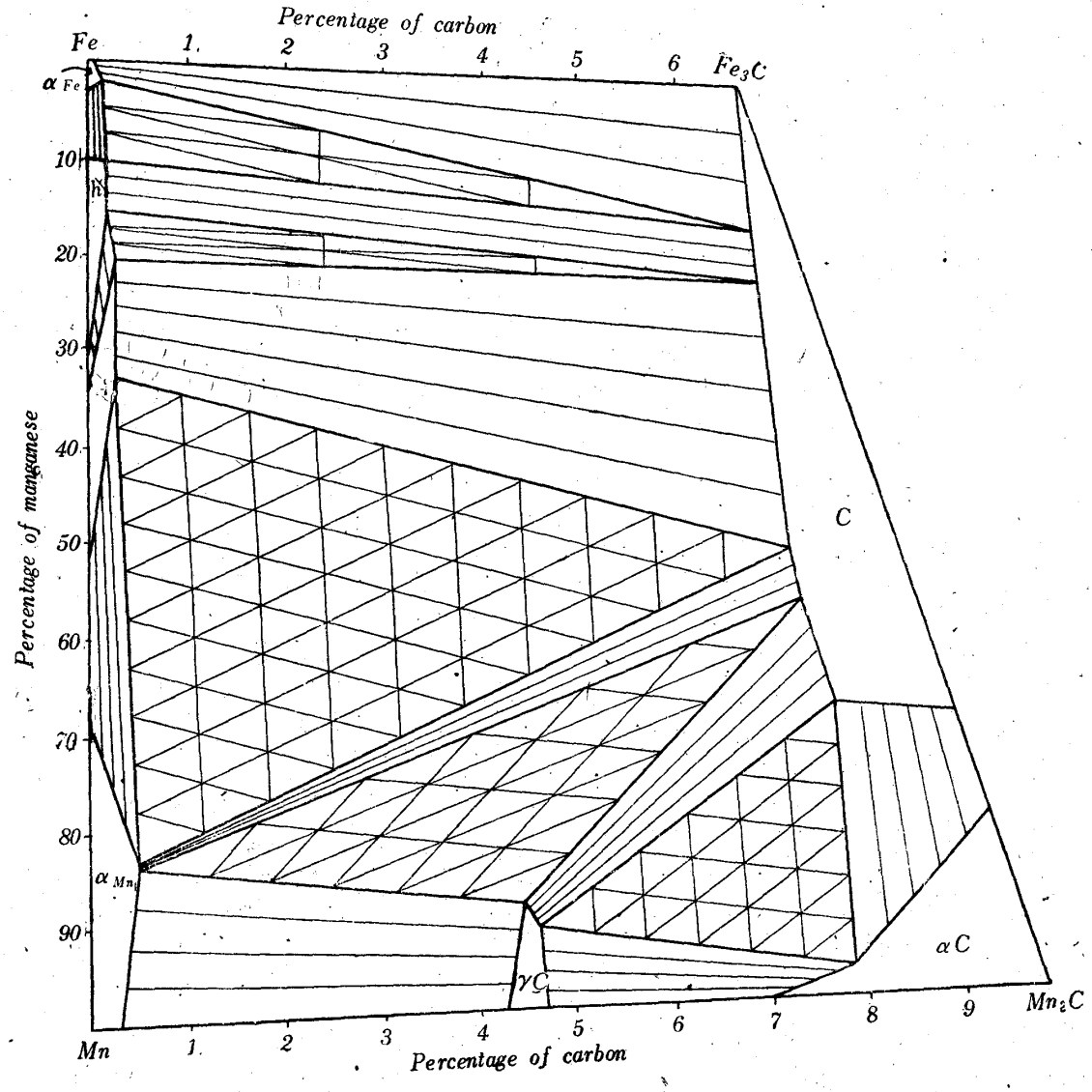

Fig. 56. Structural diagram of iron-manganese-carbon ternary alloy at room temperature when slowly cooled. Blanks, conjugates and meshes are show the one-, two- and three- phase regions, respectively.

solid solution + C ternary solid solution

Ternary eutectoid points and their reactions are as follows:

point e_7 — βC ternary solid solution → γ manganese ternary solid solution + γC ternary solid solution + C ternary solid solution

point η — γ manganese ternary solid solution → α manganese ternary solid solution + γC ternary solid solution + C ternary solid solution

point e_8 — γ manganese ternary solid solution → α manganese ternary solid solution + γ iron ternary solid solution + C ternary solid solution

point e_x — γ iron ternary solid solution → h ternary solid solution + α manganese ternary solid solution + C ternary solid solution

Surfaces at which non-variant reactions take place, and the temperature and nature of the reaction, and the components of each point which takes part in the equilibrium are shown in Table 13.

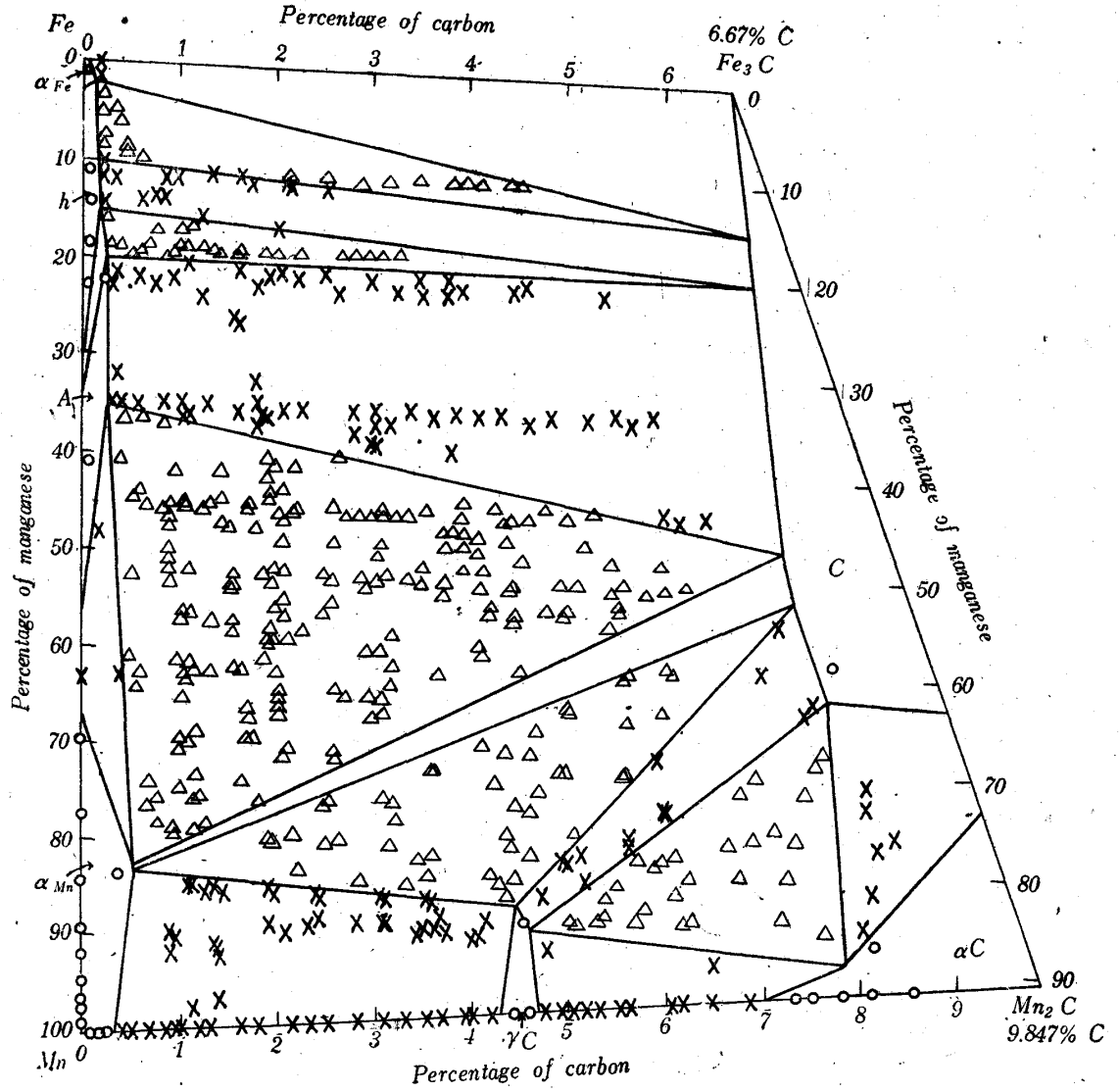

Fig. 57. Structural diagram of iron-manganese-carbon ternary alloy at room temperature. White small circle show uniform one-phase, cross mark two-phase and deltoid three-phase region, which was determined microscopically.

The composition of the points at which the above reactions occur are shown in Table 14.

Fig. 55 shows the structural diagram at room temperature at which the reactions shown in Fig. 54 are considered to have completed. It was, however, difficult to find actually that the reaction had fully advanced at the point e_x. Practically speacking, it was inevitable that a small amount of γ iron ternary solid solution remained at room temperature in the alloy containing about 30 per cent of manganese. Accordingly, it may be considered that the isothermal surfaces at somewhat higher temperatures than that shown in Fig. 55 are the structural diagram in actual case at room temperature as shown in Fig. 56, in which conjugate lines of two-phase equilibrium and meshes of three phase equilibrium are given. Fig. 57 shows the results of microscopic examination and the structural diagram at room temperature of ternary system, in which white small circle shows uniform phase and cross mark two-phase and deltoid three-phase regions.

Photo. 66 is the cubic pattern of iron-manganese-carbon ternary diagram viewed from the side of manganese and carbon, and of iron and manganese, respectively, which will be convenient to understand the outline of the ternary diagram.

Summary

The present investigation may be summarized as follows:

The ternary diagram of iron, manganese and carbon was completely determined, by using electrolytic iron, distilled manganese and sugar charcoal as alloying materials. The diagrams of binary alloys of this system determined by the present author were based upon.

It was succeeded to make clear the cause of weathering of high manganese and high carbon alloys in air. The weathering was caused by the decomposition of γC ternary solid solution or of αC ternary solid solution attacked by moisture in air. The same alloy, however, suffered no weathering and was kept safe when its structure was changed into βC ternary solid solution by quenching at high temperatures.

In conclusion, the author express his deepest gratitude to Dr. T. Ishiwara, the ex-Director of the Research Institute for Iron, Steel and Other Metals, for his kind guidance, and also offers his best thanks to the members of Dr. A. Osawa's laboratory for their efficient aid in X-ray analyses, and to the members of the analysis laboratory for their sincere cooperation in chemical analyses of the specimens. Lastly he wishes to express his hearty thanks to Mr. Toshio Numata for his friendly help of the present work.